Title

The Effects of Environmental Stressors and Stressor Interactions on the Evolutionary Dynamics of Bacterial Population and Gene Epistasis

Author

Kang, Manzhu

Publication Date

2019

Peer reviewed|Thesis/dissertation

UNIVERSITY OF CALIFORNIA

Los Angeles

The Effects of Environmental Stressors and Stressor Interactions on the Evolutionary Dynamics of Bacterial Populations and Gene Epistasis

A dissertation submitted in partial satisfaction of the requirements for the degree

Doctor of Philosophy in Biology

by

Manzhu Kang

2019

ABSTRACT OF THE DISSERTATION

The Effects of Environmental Stressors and Stressor Interactions on the Evolutionary Dynamics of Bacterial Population and Gene Epistasis

by

Manzhu Kang

Doctor of Philosophy in Biology

University of California, Los Angeles, 2019

Professor Pamela J Yeh, Chair

Environmental stressors come in many different forms and affect every level of ecological organization. In a natural environment, organisms experience mixtures of stressors at various doses or strengths of exposure that could be constantly changing, both temporally and spatially. Complex environmental regimes and interactions among multiple stressors can have a profound effect on both the short-term fitness of organisms and their long-term evolutionary dynamics. This dissertation uses a bacterium-drug system to study drug-drug, drug-temperature, and gene-gene interactions. The first question we ask is how bacteria evolve to combat new stressors. Through an interaction network clustering approach followed by transcriptomic analysis, we show that *Escherichia coli* may have co-opted its cellular response to temperature stress for antibiotic stress because these stressors share similar physiological effects. We also found that antibiotic stress modifies the thermal response of *E. coli* by altering both its optimal growth temperature and

temperature breadth. Next, we ask how we can identify and quantify dose-dependent drug interactions, including interactions among more than two components, i.e., higher-order interactions. To do this, we introduce a novel visual representation termed interaction landscape to directly map local dose-dependent interactions and the transitions between different interaction classes. Finally, we ask how gene-gene interactions change in fluctuating environments. We showed that changes in the type and magnitude of environmental fluctuations could affect fitness due to the differences in epistatic interactions of mutations. We quantify structural features of fitness landscapes by calculating the ruggedness across broad concentration gradients of various antibiotics. We show that fluctuating environments frequently lead to epistasis sign switches (from negative to positive or vice versa) on the pairwise level, as a potential mechanism to either promote specialization or maintain genetic variation. Overall, this dissertation combines experimental, mathematical, and computational biology to identify and understand the structures and patterns of interactions at different scales and their effects on the fitness and eco-evolutionary dynamics of bacterial populations.

The dissertation of Manzhu Kang is approved.

Peter Nicholas Nonacs

Van Maurice Savage

Jeffrey H Miller

Pamela J Yeh, Committee Chair

University of California, Los Angeles

2019

TABLE OF CONTENTS

LIST OF FIGURES

Chapter 2

Chapter 3

Chapter 4

Chapter 5

LIST OF TABLES

Chapter 2

Chapter 3

Chapter 4

Chapter 5

ACKNOWLEDGEMENTS

I want to thank my mentor, Pamela J Yeh, for driving me to push through all the difficult times with the utmost trust and support.

I thank the rest of my committee members: Jeffrey H Miller, Van Savage, and Peter Nonacs for your suggestions, criticisms, help, and guidance. Especially, Jeffrey Miller, I would not be where I am today without your support throughout the years.

I thank my friends, colleagues and lab members, Bjørn Østman, Natalie Lozano, Portia Mira, Rina Watanabe, Jasmine Kuo, Mauricio Cruz-Loya, Elif Tekin, Alex Brummer, Cynthia White, Jack Mao, Maral Sakayan, Nina Singh, Crystal Gianvecchio and Ian Boucher for your feedback and comments, for contributing to this work, and for sharing the laughers and tears of my PhD years.

I thank Tessa Villasenor for being my grad school encyclopedia.

I thank Bryan France, Bobby Tofig, Jackie Song, and Robert Damoiseaux for the assistance and guidance at MSSR and for contributing to this work.

I want to thank my parents. You have given me everything that you have. I am beyond grateful for having you as parents, friends, and my biggest supporters.

Finally, I thank Yangyang Jiang, for your endless support, patience, and encouragement. Thank you for being my biggest source of inspiration.

Chapter 2 is a reprint of Cruz-Loya M, Kang T. M, Lozano N. A, Watanabe R, Tekin E, Damoiseaux R, Savage V. M, and Yeh P. J (2019). “Stressor Interaction Networks Suggest Antibiotic Resistance Co-opted from Stress Response to Temperature”, Interactional Society for Microbial Ecology. Jan;13(1):12-23. Mauricio Cruz-Loya and the dissertation author were the

primary authors and contributed equally to this work. Natalie Ann Lozano, Rina Watanabe and Elif Tekin contributed to collecting, analyzing and visualizing the data. Robert Damoiseaux, Van M Savage and Pamela J Yeh were the senior authors of the paper that oversaw the conceptualization, writing and editing of the paper.

Chapter 3 is a version of Cruz-Loya M, Tekin E, Kang T. M, Rodriguez-Verdugo A, Savage V. M, and Yeh P. J. "How Antibiotic Shift Temperature Responses of *E. coli*". The manuscript is currently under preparation for submission. Mauricio Cruz-Loya, Elif Tekin and the dissertation author were the primary authors and contributed equally to this work. Alejandra Rodriguez-Verdugo, Van M. Savage and Pamela J. Yeh were the senior authors that oversaw the project and edited the manuscript.

Chapter 4 is a version of Kang T. M, Østman B, Cruz-Loya Mauricio, Lozano N. A, Damoiseaux R, Savage V. M, and Yeh P. J. "Transitions in Interaction Landscapes of Multidrug Combinations". The manuscript is currently under review in the journal of *PLOS Computational Biology*. The dissertation author and Bjørn Østman were the primary authors and contributed equally to this work. Mauricio Cruz-Loya and Natalie Ann Lozano contributed to the analysis, data visualization and editing the manuscript. Robert Damoiseaux, Van M Savage and Pamela J Yeh were the senior authors of the paper that oversaw the conceptualization, writing and editing of the paper.

Chapter 5 is a version of Kang T. M, Østman B, Damoiseaux R, Savage V. M, and Yeh P. J. "Fitness Landscape across Environmental Gradients Reveal Changes in the Direction and Magnitude of Epistasis". The manuscript is under preparation for submission. The dissertation author was the primary author of the paper. Bjørn Østman contributed to the conceptualization,

data analysis, and editing of the paper. Damoiseaux R, Savage V. M, and Yeh P. J were the senior authors that oversaw the project and edited the manuscript.

VITA

EDUCATION

2013 – 2014: University of California, Los Angeles, M.S.

2008 – 2011: California State University, Los Angeles, B.S.

PROFESSIONAL EXPERIENCE

2014 – 2015: Research Assistant in Dr. Hayoun Lee's Lab at USC

2012 – 2013: Research Assistant in Dr. Jeffrey H. Miller's Lab at UCLA

PUBLICATIONS

8. Cruz Loya*, M., Kang*, TM, Watanabe, R., Tekin, E., Savage, VM., Yeh, P. Stressor interaction networks suggest antibiotic resistance coopted from stress response to temperature. *The international society of microbial ecology*. 2019

7. Tekin, E., White, C., Kang, TM., Singh, N., Cruz Loya, M., Damoiseaux, R., Savage, VM., Yeh, P. Prevalence and Patterns of Higher-order Interactions. *NPJ systems biology and applications*. 2018

6. Park, SY., Love, TMT., Reynell, L., Yu, C., Kang, TM., Anasto, K., DeHovitz, J., Liu, C., Kober, KM., Cohen, M., Mack, WJ., Lee, HY. The HIV Genomic Incidence Assay Meets False Recency Rate and Mean Duration of Recency Infection Performance Standards. *Scientific Report*. 2017.

5. Tse, L., Kang, TM., Yuan, J., Mihora, D., Becket, E., Maslowska, KH., Schaaper, RM., Miller, JH. Extreme dNTP Pool Changes and Hypermutability in *dcd ndk* strains. *Mutation Research*. 2016.

4. Song, LY., D'Souza, S., Lam, K., Kang, TM., Yeh, P., Miller, JH. Exploring Synergy between Classic Mutagens and Antibiotics to Examine Mechanisms of Synergy and Antibiotic Action. *Antimicrobial Agents and Chemotherapy*. 2015.

3. Zhou, A., Kang, TM., Yuan, J., Beppler, C., Nguyen, C., Mao, ZY., Nguyen, MQ., Yeh, P., Miller, JH., Synergistic Interaction of Vancomycin with Different Antibiotics in Escherichia coli: Trimethoprim and Nitrofurantoin Potentiate Vancomycin in Wild-type E. coli. *Antimicrobial Agents and Chemotherapy*. 2015.

2. Kang, TM., Yuan, J., Zhou, A., Beppler, C., Miller, JH., Deoxycytidine Deaminase-Deficient Escherichia coli Strains Display Acute Sensitivity to Cytidine, Adenosine, and Guanosine and Increased Sensitivity to a Range of Antibiotics, Including Vancomycin. *Journal of Bacteriology*. 2014.

1. Kang, TM., Yuan, J., Nguyen, A., Becket, E., Yang, H., Miller, JH., The Aminoglycoside Antibiotic Kanamycin Damages DNA bases in Escherichia coli: Caffeine Potentiates the DNA-damaging Effects of Kanamycin while Suppressing Cell Killing by Ciprofloxacin in Escherichia coli and Bacillus anthracis. *Antimicrobial Agents and Chemotherapy*. 2012.

CHAPTER 1

Introduction

Environmental traits can be critical drivers in many ecological and evolutionary processes such as niche differentiation [1, 2], biodiversity [3-5], adaptation [2, 6], and extinction [7, 8]. Within a specific environmental condition, a stressor can be defined as any factor that reduces the fitness of an organism [9]. Organisms likely experience a myriad of stressors simultaneously. Sensing, responding, and adapting to various stressors and mixtures of stressors present a great evolutionary challenge [10, 11].

Microorganisms inhabit almost every environment on Earth [12]. For example, cyanobacteria can survive in extreme temperatures from Antarctic ice to continental hot springs [13]. Most foodborne pathogens such as *Escherichia coli* can persist in diverse environments both inside and outside of the host [14]. These microbes are constantly challenged by a combination of various stressors, such as antibiotics, changes in temperature, varying pH, or starvation [14]. From the public health standpoint, bacteria that evolve antibiotic resistance have caused a widespread public health care crisis. Each year in the United States alone, antibiotic resistance is related to roughly 2 million infections and 23,000 deaths [15]. For ecologists and microbiologists, microorganisms can be ideal systems to examine diversity and function. For example, soil microbes are vital for regulating productivity and nutrient cycling [16, 17], and the gut microbiota is now recognized as a crucial factor for the health and even behavior of the host [18-20].

The laboratory strain of *E. coli* is one of the most studied model organisms widely used in molecular biology and microbiology studies [21]. It is also the subject of an ongoing study in experimental evolution led by Richard Lenski since 1988 [22]. There are many advantages to using

bacterial populations to study evolution [23]. They are clonal organisms that can be grown in the laboratory with highly controlled and replicable experiments. Their small genome sizes allow easy and low cost for genetic manipulation and genomic analysis. The short replication time and small culture volume allow the researchers to maximize the throughput with the help of automated platforms. Taken together, studies of microorganisms have proven to be highly applicable and valuable in answering some of the most fundamental questions in ecology and evolutionary biology [23-28].

This dissertation exploits these advantages, using a bacterium-drug system to understand how the external environment, especially with the presence of various types (different drugs) and intensities (different concentrations of drugs) of stressors, affects the fitness and eco-evolutionary dynamics of bacterial populations. Chapter 2 focuses on revealing the potential evolutionary strategy of *E. coli* to combat novel stressors based on the interaction properties between antibiotics and stressful temperatures. Chapter 3 examines the overall physiological effect of combined exposure to antibiotic and temperature stress by quantifying the thermal response and emphasizes the important implication for a general understanding of how ecological systems adapt to environmental challenges on shorter timescales. Chapter 4 aims to understand dose-dependent interactions, focusing on the prevalence, strength, and structure of interactions based on the intensity of the drug dosage. Finally, chapter 5 uses fitness landscapes to show how the magnitude or severity of environmental change affects phenotypic fitness due to their effect on gene-gene interaction or epistasis.

CHAPTER 2

Stressor Interaction Networks Suggest Antibiotic Resistance Coopted from Stress Response to Temperature

2.1 Introduction

Organisms encounter and respond to myriad stressors [29, 30]. Stresses to bacteria can come in many different forms, such as use of antibiotics [31, 32], changes in temperature [33], variations in salt concentration or pH [34], or a lack of nutrients [35]. Cellular responses to these stressors vary but can range from specific subcellular mechanisms such as efflux pumps that pump out toxic compounds [36, 37] and outer membrane porins that regulate osmolarity [38] to more global modulation that includes dormancy or quiescence under nutrient limitation [39].

Temperature is one of the stressors that living organisms have needed to contend with since life first evolved [40-43]. Indeed, phylogenetic evidence based on ribosomal RNA sequences places the emergence of hyperthermophiles near the root of the tree of life [44, 45], so sensing, responding, and adapting to temperature must constitute some of the oldest adaptations in nature. The heat-shock response machinery, which is a mechanism for cells to combat the noxious effects of high temperatures, is present across all domains of life and is highly conserved [46-49]. In contrast, the first antibiotics are thought to have arisen more recently in evolutionary history, between 2 billion and 40 million years ago [50]. Consequently, it seems likely that adaptive responses to variations in environmental temperature evolved before responses to antibiotics. It seems possible that some of the mechanisms that confer resistance to variations in temperature have been co-opted to resist antibiotic stress as well, especially since temperature and drugs impact

many of the same cellular components. In addition to functional overlap, there are compelling reasons for cells to evolve a relatively small suite of stress responses to multiple types of stressors. Developing a novel stress response requires investment in terms of genetic material (i.e., information), protein production, time to evolve, and energy to support simultaneous responses. Thus, it is highly inefficient therefore unlikely for a cell or organism to evolve an independent response for every single stressor it encounters.

For example, in response to two different types of stressors—drugs and heavy metal—many Gram-negative bacteria, such as *Pseudomonas aeruginosa*, evolved an efflux pump that actively pumps out all toxic molecules [51]. Another example of a general response machinery to different stressors in bacteria is the alternative sigma factor σ^S, a transcription factor that regulates the expression of more than 70 genes that confer resistance against stresses as diverse as temperature change, starvation, pH, and DNA damage [52-54]. Together, these studies suggest bacteria have similar responses to multiple types of stress that harm the same cellular components (e.g., DNA, protein, cell membrane, or cell wall).

It is natural to ask which response mechanisms evolved first, whether these original responses were co-opted to respond to other stressors, and how much overlap exists among how stressors affect bacteria. For instance, both temperature and antibiotics can harm similar cellular functions: high temperatures and antibiotics (e.g., macrolides and aminoglycosides) both affect protein synthesis and folding [55, 56]. Heat shock proteins can be induced by some antibiotics [57], and that resistance to antibiotics can be temperature dependent [58]. Furthermore, heat-adapted Escherichia coli could require resistance to rifampicin, despite the drug being absent during the selection process [59]. Additionally, overexpression of heat-shock proteins increases short-term survival of bacteria exposed to aminoglycosides [60]. Other stress responses, such as

those for nutrient starvation and oxidative stress, have also been linked to the emergence of antibiotic resistance [61].

Typically, this overlap between cellular responses to stress has been studied by isolating subcellular parts and attempting to piece together the information involved to understand stress responses at a whole-cell level. Despite these intriguing, isolated subcellular studies, we are unaware of any systematic, comprehensive study of these overlaps and co-opting. The lack of such a study is partly because obtaining direct data is extremely challenging in terms of the cellular pathways that need to be dissected, the evolutionary time scales that must be used, and the differing selection pressures that need to be manipulated and observed.

Here, we take a reverse and complementary approach: by studying the effect of perturbations on the whole system, we gain more insights into the mechanisms of its specific parts. It is now feasible to accomplish this because of recent progress on high-throughput data collection and on methods that reveal the mechanisms of antibiotics using network clustering [62, 63]. For these clustering methods, interactions are characterized based on growth assays of bacteria exposed to antibiotic combinations. Interaction networks can then be constructed by collecting the full factorial of interactions among several antibiotics. Clustering this network according to interaction profiles (a procedure called monochromatic clustering) yields groups of drugs with the same mechanisms of action [63]. This relationship between mechanism and interactions likely arises because the mechanism of action corresponds to functional impacts on the cell that map with high fidelity to the effective interactions among the antibiotics. The interaction profile of a drug can thus reveal its effect in the cell and its mechanism of action. A great benefit of this approach is that it does not require as much time or resources as molecular studies. In these studies, interactions between drugs are typically characterized in one of three ways: additivity (drugs have

independent effects on growth), synergy (combined effect of the drugs is greater than expected based on single-drug effects), or antagonism (combined effect is smaller than expected) [64]. We will follow the same nomenclature in this paper to describe interactions between temperatures and drugs.

Here we generalize and extend the ideas of monochromatic clustering. We develop a clustering method for stressor interaction networks (SINs) to categorize non-drug stressors that affect bacterial growth, and to further reveal information about the shared effects of temperature and antibiotics on the cell.

Here, we derive for the first time how to accomplish this for the case of non-optimal or extreme temperatures. We collect comprehensive data on bacterial growth in the presence of each stressor separately, and when pairs of stressors are present simultaneously. We analyze these data to identify groups of antibiotics that have similar physiological effects to low and high temperature stress. This physiological similarity is inferred by grouping stressors that interact similarly with other stressors, as revealed through the SIN clustering analysis, and grounded in the original intuition of monochromatic clustering. In this way, we systematically analyze overlap between stress responses to temperature and antibiotics to assess the extent that cellular responses to drugs co-opt and mimic the responses to temperature, an ancient stressor. More specifically, we quantify to what extent the physiological effects of temperature in the cell are shared across a wide range of temperatures or if there is more nuanced variation. Finally, we use these results to identify common functional aspects of stressors that we use to help develop a classification system for stress responses.

Intriguingly, our results are consistent with low and high temperature stress responses having been co-opted through evolution to combat multiple classes of antibiotics. Because the

monochromatic clustering methodology depends only on the existence of an interaction network, it seems possible to apply a similar methodology to broader types of interactions among multiple types of stressors.

2.2 Materials and Methods

Bacterial strain

The study primarily used BW25113, a derivative of the F-, λ-, *E. coli* K-12 strain BD792 (CGSC6159) [65]. For each bacterial strain, a single colony was inoculated into 2 mL of LB media (10 g/L tryptone, 5 g/L yeast extract, and 10 g/L NaCl) and grown overnight followed by resuspension in 25% glycerol, then aliquoted into 50μL and frozen at -80°C. Cultures used for daily experiments were started by adding 20μL of thawed aliquots into 2mL of LB media. The culture was incubated at 37°C until it reached exponential growth phase and diluted to maintain 10^4 cells per experimental condition.

Compounds and Materials

A total of 12 antibiotics were included in the study as representatives of all major drug classes. Gentamycin (GEN), levofloxacin (LVX), tetracycline (TET), tobramycin (TOB), erythromycin (ERY), ampicillin (AMP), clindamycin (CLI), streptomycin (STR), nitrofurantoin (NTR), cefoxitin (FOX), and trimethoprim (TMP), all from Sigma (St Louis, Mo); and ciprofloxacin (CPR) from MP Biomedicals (Santa Ana, Ca). Stock solution at 20 mg/mL of each antibiotic was stored in 50μL aliquot at −20°C and each aliquot was only frozen and thawed once to preserve potency.

2.2.3 Growth experiment

Drug concentrations were selected to partially inhibit bacterial growth (10% to 50% inhibition) that were first determined by a twelve step concentration series of 2-fold at each step in 96-well plates (Costar). A 5 ml stock solution of each drug in LB media was made at 10-fold of their respective concentrations (Table 2-1). For drug pair experiments, 10μL of each component drug was mixed into 96-well plates followed by the addition of 80μL cell inoculum; while 10μL of LB media was added in replacement of a second drug for single drug experiments. Replicate plates were prepared from the same antibiotic stock solution to minimize variation and incubated at 300 rpm in parallel at various temperatures (*E. coli:* 22°C, 25°C, 30°C, 37°C, 41°C, 44°C, 46°C). OD600 measurements for cell density were taken after 4-hour, 8-hour, 12-hour and 24-hour growth for *E. coli*. To examine the drug interaction clustering of *E. coli* in a different external environment, we used LB media without salt. The media was prepared with 10 g/L tryptone, 5 g/L yeast extract in every liter.

Table 2-1 Antibiotics and doses used for the antibiotic-temperature SIN clustering experiments

Compound	Abbreviation	Class/cellular target	Dose (μg/mL) *E. coli*	Dose (μg/mL) *E. coli* LB no salt
Ampicillin	AMP	Cell wall synthesis inhibitor	1.2	1.4
Cefoxitin	FOX	Cell wall synthesis inhibitor	1.2	1.2
Levofloxacin	LVX	Fluoroquinolone, DNA gyrase inhibitor	0.01	0.015
Ciprofloxacin	CPR	Fluoroquinolone, DNA gyrase inhibitor	0.005	0.005
Nitrofurantoin	NTR	DNA damaging, multiple mechanisms	2	1.6
Trimethoprim	TMP	Folic acid synthesis inhibitor	0.1	0.17
Tobramycin	TOB	Aminoglycoside	1.5	0.45
Gentamycin	GEN	Aminoglycoside	1	0.2
Streptomycin	STR	Aminoglycoside	2	0.6
Clindamycin	CLI	Protein synthesis inhibitor, 50S	40	25
Erythromycin	ERY	Protein synthesis inhibitor, 50S	50	20
Tetracycline	TET	Protein synthesis inhibitor, 30S	0.25	0.25

Gene expression profile

We measured expression of about 2000 genes in *E.coli* using the promoter library of transcriptional fusion of *gfp* to each promoters [66]. Strains were maintained in 15% glycerol at -80°C before inoculating and grown overnight in LB medium with 25 μg/mL of kanamycin in 384 well plates. Cultures were then transferred and pinned into 50 μL of LB medium per well, followed by a 4-hour incubation at 37°C to allow growth up to exponential phase. To measure differential expression at high temperature, cultures were moved to 44°C where optical density of 595 nm and GFP fluorescence (excitation, 480 nm; emission, 535 nm) were measured every 2 hours for 24 hours using a programmable robotic system (Thermo Cytomat). For expression profile with antibiotic treatments, cultures were pinned into 30 μL of LB medium before 4-hour incubation, and another 30 μL of LB medium with 2X concentration of antibiotics (STR at 4 μg/mL and TET at 1 μg/mL) were added into the plates. Controls were carried out at 37°C without temperature shift or addition of antibiotics. Antibiotics and control conditions were measured using the same robotic system and time frame.

Drug sensitivity profile for heat adapted strains

We profiled antibiotics sensitivity for 10 high temperature adapted lines collected and described by Rodriguez-Verdugo *et al.* [67]. In addition, we compared their sensitivity profiles with the ancestral strain of *E. coli* B (genotype *REL1206*). IC 50 for 12 drugs was determined by a 11-step concentration series of 2-fold in 3 replicates, method described in previous sections under Growth experiment.

Relative growth and interactions

The relative growth under stressor x (presence of a drug or a non-optimal temperature) is defined as $w_x = \frac{g_x}{g_\varphi}$, where g_x is the growth of the bacterial culture under stressor x and g_φ is the growth

of the culture at reference state φ —the culture at its optimal temperature for growth in the absence of antibiotics. Under the Bliss Independence criterion [64], an interaction is additive if $w_{xy} = w_x w_y$, where $w_{xy} = \frac{g_{xy}}{g_\varphi}$ is the relative growth when stressors x and y are both present. The deviation from additivity is defined as $\varepsilon_{xy} = w_{xy} - w_x w_y$. When this measure is significantly nonzero, it signifies an interaction exists. The sign of this measure determines the interaction type ($\varepsilon_{xy} < 0$ corresponds to synergy and $\varepsilon_{xy} > 0$ to antagonism). The raw ε_{xy} is then rescaled by appropriate reference values (as in [63]) to yield a rescaled measure, $\tilde{\varepsilon}_{xy}$. Its magnitude can be interpreted as the strength of interaction.

Statistics

With the experimental procedure detailed above, four measurements of the OD600 were taken at every time point, each one corresponding to a different growth curve, for each stressor and all possible pairwise combinations. The OD (optical density) values were used as a proxy that is proportional to the absolute growth ($g_x, g_y, g_{xy}, g_\varphi$). We chose the point estimate $\hat{g}_x$ to be the sample mean of the four measurements of absolute growth under condition x. The point estimate for each relative growth was taken to be $\widehat{w}_x = \frac{\hat{g}_x}{\hat{g}_\varphi}$ and the point estimate for the interaction $\hat{\tilde{\varepsilon}}_{xy} = \tilde{\varepsilon}(\widehat{w}_x, \widehat{w}_y, \widehat{w}_{xy})$. We followed a parametric bootstrap approach for constructing a confidence interval for the interaction, with the assumption that the absolute growth (i.e., OD) measurements under each condition follow a log-normal distribution. The maximum likelihood estimators (which correspond to the sample mean and variance of the logarithm of the observations) were used to estimate the parameters of the underlying distribution for the absolute growth under each condition. We then took 20000 parametric bootstrap samples of $n = 4$ observations from the log-normal distribution with the estimated parameters. The mean of each one of these samples was used to

construct a bootstrap sample for the mean relative growth values ($\widehat{w}_x^{(i)}, \widehat{w}_y^{(i)}, \widehat{w}_{xy}^{(i)}$), and the interactions $\hat{\tilde{\varepsilon}}_{xy}^{(i)} = \tilde{\varepsilon}(\widehat{w}_x^{(i)}, \widehat{w}_y^{(i)}, \widehat{w}_{xy}^{(i)})$, where $i = 1, \ldots, 20000$. A 95% confidence interval for $\tilde{\varepsilon}_{xy}$ was constructed by taking the 2.5 and 97.5 percentiles of its bootstrap sample.

Network of antibiotic and temperature effects

We construct an interaction network where nodes represent the stressors (i.e., drugs or temperatures), and colored edges represent non-additive interactions, with the edge color corresponding to interaction type (red for synergy and green for antagonism). In general, exact additivity ($\tilde{\varepsilon}_{xy} = 0$) is rare, but there is nevertheless an important qualitative distinction between approximate additivity (i.e., $|\tilde{\varepsilon}_{xy}| \leq \tilde{\varepsilon}_{ref}$), where $\tilde{\varepsilon}_{ref}$ is a threshold below which an interaction is considered approximately additive) and strong synergistic and antagonistic interactions. Since the observed interactions are subject to measurement error and population variability, we only assign edges for which the confidence interval ($\tilde{\varepsilon}_{2.5}, \tilde{\varepsilon}_{97.5}$) for $\tilde{\varepsilon}_{xy}$ excludes the critical value $\tilde{\varepsilon}_{ref}$. We thus define the discretized interaction (i.e., color) of an edge to be

$$c(\tilde{\varepsilon}_{2.5}, \tilde{\varepsilon}_{97.5}) = \begin{cases} 1 & \text{(green)} & \tilde{\varepsilon}_{2.5} > \tilde{\varepsilon}_{ref} \\ -1 & \text{(red)} & \tilde{\varepsilon}_{97.5} < \tilde{\varepsilon}_{ref} \\ 0 & \text{(no edge)} & \text{otherwise} \end{cases}$$

The higher this critical value, the stronger an interaction needs to be to be assigned as an edge in the network. Thus, with values that are too low, weak effects can be assigned as interactions, and with values that are too high, there may not be enough assigned interactions (i.e., edges) in the network for the clustering algorithm to be effective. We chose $\tilde{\varepsilon}_{ref} = 0.2$ because empirically this yielded a good compromise between the two. With this definition, the discretized nonzero value of c corresponds to a statistically significant interaction, with $c = -1$ (red edges) corresponding to synergy and $c = 1$ (green edges) to antagonism. When $c = 0$, we either cannot reject additivity or there is missing data.

Monochromatic clustering

The stressors in the interaction network were clustered into monochromatic classes using a newly developed modification of the Prism 2 algorithm [63]. The algorithm was implemented in the Python programming language. Each node starts in a different cluster, and at each iteration of the algorithm, the pair of clusters (X, Y) that minimizes the penalty

$$F(X,Y) = k_D D(X,Y) + k_S(\Delta S(X,Y) + \alpha(1 - p_{XY}))$$

is merged. This procedure is repeated until a single cluster remains, containing all nodes in the network. The first two terms in $F(X,Y)$ are identical as in the previous version of the algorithm [63]. Their function is to penalize merging clusters that have dissimilar interactions to each other (represented by the weighted distance term: $D(X,Y)$) and that result in non-monochromatic clusters (through the entropy term: $\Delta S(X,Y)$), respectively.

A new aspect of the algorithm, which is not present in previous versions, is the term $\alpha(1 - p_{XY})$, where, p_{XY} is the proportion of shared edges between clusters X and Y, and α is an arbitrary tuning constant. The purpose of this term is to penalize the entropy term so that joining clusters with more shared interactions is favored with respect to clusters with no or few shared edges. Without this term, it is always possible to form monochromatic clusters by simply merging clusters with member nodes that have no or few shared edges. However, these clusters need not have similar overall interactions, and thus lack any physiological information. Our modified algorithm avoids this problem and outcome.

Note that in this formulation we also chose to write $\Delta S(X,Y)$ with an opposite sign as in [63], to be consistent with the usual convention that positive values mean increases and negative values mean decreases. Within the penalty $F(X,Y)$, each term is multiplied by a constant that affects the relative weight of each term. We chose the weights $k_D = 1$ and $k_S = 0.1$ as in [63]. The tuning

constant, $\alpha = 0.1$, is new to this work, and was chosen to be of roughly the same order of magnitude, but smaller than the change in entropy $\Delta S(X,Y) \in [0,1]$. This choice of α gives clusters that better separate antibiotics according to mechanism of action for networks with a small number of edges. Another difference with respect to the previous algorithm is that we use the mean distance between the antibiotics (known as average linkage) as the metric for distance between clusters $D(X,Y)$. This choice is less sensitive to outliers than the previous choice of the minimum distance.

2.3 Results

Clustering of an antibiotic and temperature interaction network reveals overlap in their physiological effects

To find groups of stressors (i.e., antibiotics and/or temperatures) that have similar effects on *E. coli* physiology, we first evaluate the interactions—synergy, additivity, or antagonism—between each pair of antibiotics, and between each antibiotic within a range of growth temperatures (22°C, 25°C, 30°C, 37°C, 44°C, 46°C) (Figure 2-1a, b). The maximum growth in the absence of antibiotic was observed at 41°C: this optimum growth temperature was chosen as the unstressed reference state for evaluating the relative growth in the presence of each stressor. We evaluate the interactions based on the 24-hour growth of *E. coli* after exposure to the corresponding stressors. We then construct a stressor interaction network (SIN) (Figure 2-1c) where nodes represent the stressors and colored edges represent interaction type (discretized based on a hypothesis test, see Figure 2-1c and Methods 2.2). The resulting network is clustered to find

monochromatically interacting groups, which correspond to similar interaction profiles, using our modified Prism 2 algorithm (Figure 2-1d, see Methods 2.2 for details of the algorithm).

Figure 2-1 Schematic illustration of the approach taken in this work. a Growth is measured in the following conditions: reference growth g_φ at the optimal temperature (T_{opt} = 41 °C) in the absence of drug, g_x at optimal temperature with drug, g_y at experimental temperature T_{exp}, but no drug, and g_{xy} at non-optimal temperature with drug. b The growth of each experimental condition is converted to proportions w_x, w_y, w_{xy} by dividing by the reference growth. The difference between w_{xy} (observed growth) and the product of w_x and w_y (expected growth under independence) is then used to classify the interaction between drugs and temperatures into three cases: synergistic (red line), additive (white or not shown), and antagonistic (green line), c which can be represented as an interaction network. d Drugs and temperatures can then be clustered into a functional class based on the mono- chromaticity of interactions with a different class. This example shows a drug-temperature interaction, but drug–drug interactions are obtained similarly, by replacing the growth with no drug at T_{exp} with the growth under a second drug at T_{opt}.

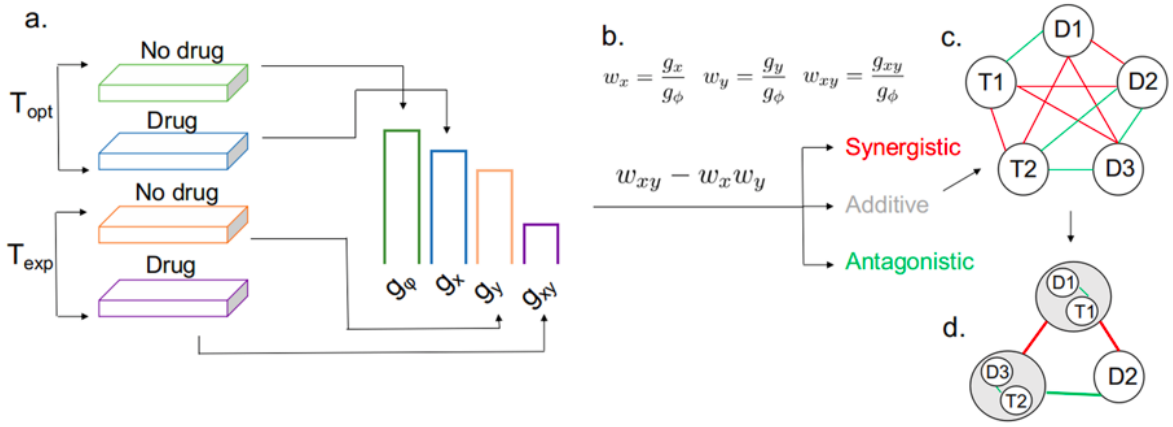

Consistent with overlap in the mechanism of action of specific drugs and the physiological effect of non-optimal temperatures, we find that the evaluated temperatures cluster with antibiotics in the following three groups (Figure 2-2): (1) All temperatures lower than the temperature for peak growth cluster together, along with the fluoroquinolones (LVX, CPR), which are DNA gyrase inhibitors, and with the 30S protein synthesis inhibitor tetracycline (TET). (2) The temperature 44°C clusters with the DNA-damaging drug nitrofurantoin (NTR) and with trimethoprim (TMP),

an inhibitor of the folic acid biosynthesis pathway that is responsible for generating an essential DNA precursor. (3) The highest evaluated temperature, 46°C, clusters with the aminoglycosides (GEN, STR, TOB), antibiotics that affect protein translation proofreading [68]. We thus conclude that monochromatic clustering successfully separated the antibiotics according to their mechanism of action and/or grouped with temperatures that have similar physiological effects.

Figure 2-2 Monochromatic clustering of the interaction network. a Unclustered interaction network. The nodes that correspond to drugs are color-coded by their mechanism of action (Table 1), and the nodes that correspond to temperatures are colored in a gradient from blue (low) to red (high). The edges correspond to discretized interaction type: synergy (red), antagonism (green), additive or unknown (no edge). b Network clustered into monochromatic classes by the modified Prism2 algorithm.

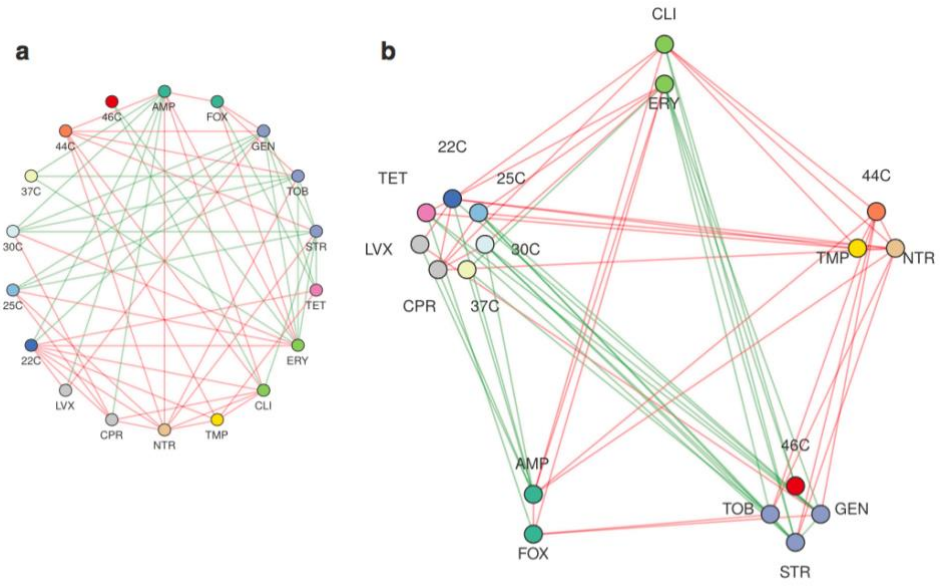

To evaluate the robustness of our clustering results, we also measure interactions in a different condition: LB medium with no salt (Figure 2-3). As before, we find that high temperatures cluster with aminoglycosides (GEN, STR, TOB) and TMP, but now they cluster in a

single group. Low temperatures cluster in a single group with CLI, a 50S protein synthesis inhibitor, instead of TET, LVX, CPR.

Figure 2-3 Interactions and clustering under no salt conditions. The interaction effect ($\tilde{\varepsilon}$) values are color coded in a gradient, from synergy (red) to additive (grey) and antagonism (green). (a) Matrix heatmap of the mean interaction effects. Antibiotics with the same mechanism of action show similar interaction patterns. (b) Matrix heatmap of the discretized interaction types used for constructing the edges of the interaction network. (c) Network clustered into monochromatic classes by the modified Prism2 algorithm.

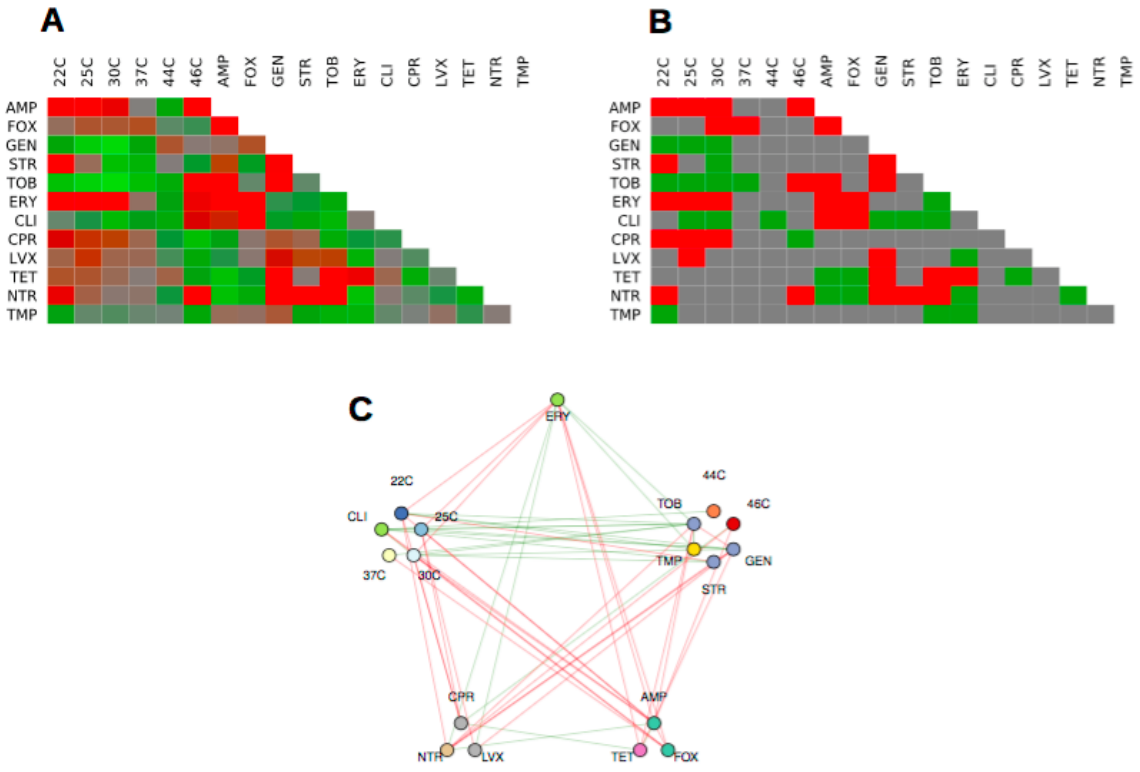

Patterns in antibiotic and temperature interactions

We find that the distribution of the interactions between all pairs of stressors at 24-hour growth is trimodal (Figure 2-4a), with peaks that correspond to synergy ($\tilde{\varepsilon}_{xy} \approx -1$), additivity ($\tilde{\varepsilon}_{xy} \approx 0$) and antagonism ($\tilde{\varepsilon}_{xy} \approx 1$), similar to previous work [63]. Ampicillin (AMP) and the

aminoglycosides (GEN, STR, TOB) are mostly antagonistic with temperatures lower than the optimum (41°C), and synergistic or additive with higher temperatures (Figure 2-4b).

Figure 2-4 Interaction effects between antibiotics and temperature based on growth after 24-h. The interaction effect (~ε) values are color-coded in a gradient, from synergy (red) to additive (gray) and antagonism (green). a. Overall distribution of the mean estimated interaction effects across all treatments. The distribution shows three clear peaks, corresponding to strong synergy, additivity, and antagonistic buffering. b Matrix heatmap of the mean interaction effects. Antibiotics with the same mechanism of action show similar interaction patterns. c Matrix heatmap of the discretized interaction types used for constructing the edges of the interaction network.

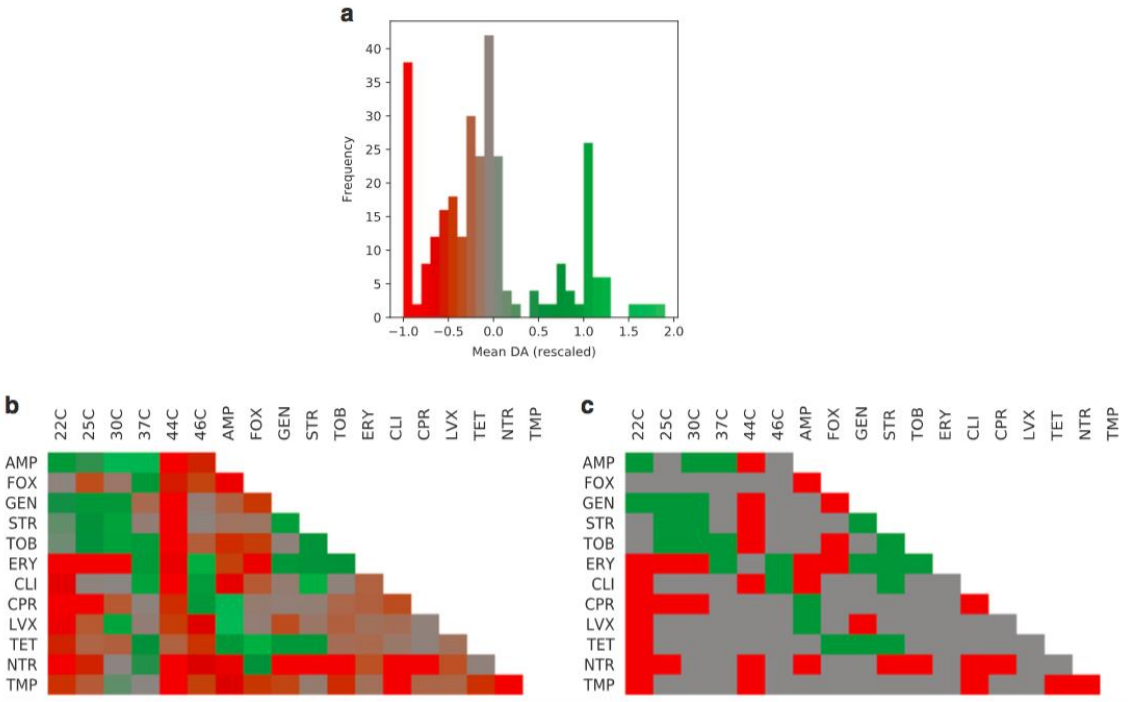

Erythromycin and clindamycin (ERY, CLI) exhibit the opposite pattern: they are mostly synergistic with lower temperatures and antagonistic with temperatures near the optimum or higher, except for 44°C. Furthermore, fluoroquinolones (LVX, CPR), tetracycline (TET), nitrofurantoin (NTR), and trimethoprim (TMP) are more synergistic with both low and high temperature

extremes, and they are either additive or slightly antagonistic with intermediate temperatures. All interactions were calculated using the mean growth under each condition (see Methods 2.2).

Gene expression dynamics after exposure to antibiotics and high temperatures

Next, we explore the molecular mechanisms involved in the response to antibiotics by evaluating genome-wide transcriptional dynamics after exposure to high temperature (44°C) and two representative drugs that clustered with temperatures: TET (22–37°C, cold cluster) and STR (46°C cluster). To do this, we measure fold changes in gene expression compared to a control condition (37°C) with a library of *E. coli* strains containing GFP fused to more than 1800 promoters [66]. Consistent with the drug-temperature clusters, we find that the overall gene expression at 44°C is more similar to the response to STR than to TET (Figure 2-5a).

We also look at the expression of some canonical genes from the heat-shock and cold-shock responses (Figure 2-5b). We find that *cspA* and *cspG*, main regulators of the cold-shock response, are over-expressed only in response to TET, while *cspB* and *cspI* are under-expressed. We find that *rpoH*, the main regulator of the heat-shock response is over-expressed compared to control only in the 44°C condition and is under-expressed upon exposure to TET. However, chaperones involved in the heat-shock response (*dnaJ*, *dnaK*, *groE*, *grpE*) show increased expression under both STR and TET. This indicates that components of the heat-shock response are being activated in response to both antibiotics, while the cold-shock response is activated only for TET (a drug from the low temperature cluster). Analysis of gene ontology terms shows that genes involved in the response to unfolded proteins, which is a well-known effect of high-temperature stress, are induced in response to STR (Figure 2-5c).

Figure 2-5 Gene expression of E. coli after exposure to antibiotics and high temperature. The gene

expression response of *E. coli* was evaluated with a library of 1870 fluorescent transcriptional reporters. a Mean absolute gene expression distance between experimental conditions. Lower numbers indicate conditions with more similar gene expression profiles. b Gene expression of representative heat-shock and cold-shock genes relative to control (37°C) in response to experimental conditions (44°C, STR, TET). c Gene ontology terms in the biological process category over-represented in the set of over-expressed and under-expressed genes in each experimental condition relative to control. Terms that are in bold occur in more than one treatment.

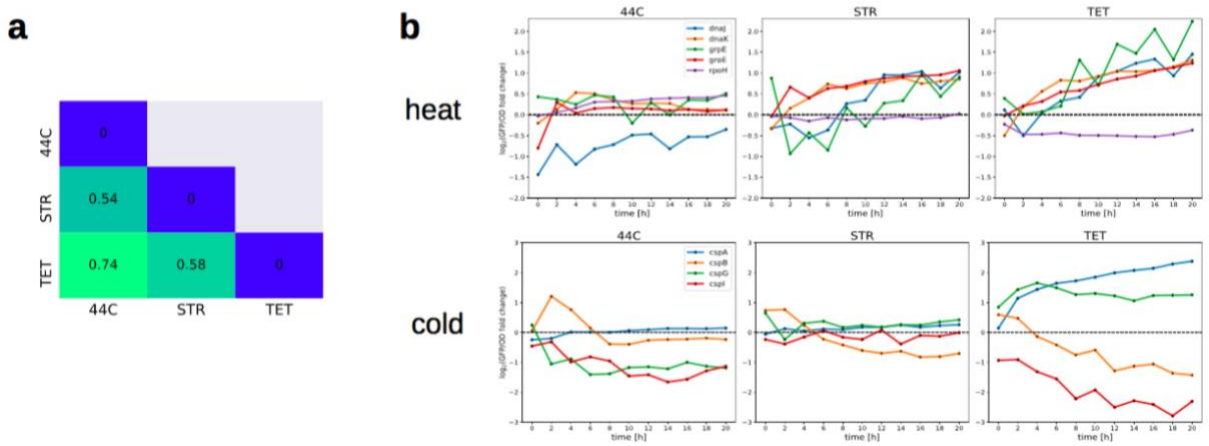

c

Over-Expressed Biological Process GO Terms		
44°C	**STR**	**TET**
pentose catabolic process	chaperone cofactor-dependent protein refolding	glutathione metabolic process
fatty acid beta-oxidation	negative regulation of transcription, DNA-templated	**folic acid-containing compound metabolic process**
bacterial-type flagellum-dependent cell motility	tricarboxylic acid cycle	phospholipid biosynthetic process
carbohydrate transport	positive regulation of transcription, DNA-templated	peptide catabolic process
tetrahydrofolate biosynthetic process	cellular response to sulfate starvation	
extracellular polysaccharide biosynthetic process	translesion synthesis	
	maltodextrin transport	
	cellular response to unfolded protein	
	pyrimidine nucleobase catabolic process	
	folic acid-containing compound metabolic process	
	cellular response to nutrient levels	

Under-Expressed Biological Process GO Terms		
44°C	**STR**	**TET**
deoxyribonucleotide biosynthetic process	purine nucleoside catabolic process	**glutamine biosynthetic process**
positive regulation of transcription, DNA-templated	response to acidic pH	metabolic process
arginine catabolic process	sulfur compound metabolic process	putrescine catabolic process
response to cold	cellular amino acid catabolic process	**nitrogen compound metabolic process**
	L-cysteine catabolic process to pyruvate	transcription, DNA-templated
	glutamine biosynthetic process	
	nitric oxide catabolic process	
	pyrimidine nucleobase catabolic process	
	uracil catabolic process	
	nitrogen utilization	
	putrescine catabolic process	
	nitrogen compound metabolic process	
	carbohydrate metabolic process	

Changes in antibiotic sensitivity for heat-adapted *E. coli* strains

Our above experiments evaluate the overlap between the existing responses of wild-type *E. coli* to antibiotics and temperature. It is also of interest to evaluate if there is cross-resistance between temperature-adapted strains and antibiotics. Previously, Rodríguez-Verdugo *et al.* [67] adapted an *E. coli* strain for over 2000 generations at 42.2°C and showed the heat-adapted strains acquired resistance to rifampicin. The resistance phenotype was mapped to mutations in the *rpoB* gene [67]. We profile 10 of the heat-adapted strains, their ancestor strain, and 3 different *rpoB* mutants exposed to the antibiotics used in the clustering experiment. As predicted from our clustering analysis, most heat-adapted strains are as or more resistant to antibiotics (NTR and TMP) that mimic the effects of high temperatures (44°C) (Figure 2-6a, b). Resistance to aminoglycosides (which clustered with 46°C, a much higher temperature to the one the heat-adapted strains were evolved on) was higher in some temperature-adapted strains and lower in others. Moreover, compared with the ancestor strain, most heat-adapted strains are more sensitive to antibiotics that mimic the effects of cold temperatures such as protein synthesis inhibitors (CLI, ERY, TET)

(Figure 2-6a, b). These results are based on changes in IC50, the antibiotic concentration that results in 50% growth.

Figure 2-6 Antibiotic sensitivity of high-temperature-adapted *E. coli* strains. a Absolute change in the IC50 (μg/mL) relative to the ancestral strain. Heat-adapted strains (red), *rpoB* mutant strains (purple). Error bars represent 95% credible intervals (CIs). Gray region represents the 95% CI of ancestral strain. Drugs are grouped according to the clusters of antibiotics and temperature in (Figure 2.2). Conditions where the model fit was poor were removed from the plots. b Heatmap of log2 fold changes from the ancestral IC50. Heat-adapted strains are denoted by HA, while *rpoB* mutant strains are denoted by M. Positive numbers (yellow) indicate increased IC50 (more resistance), while negative numbers (blue) indicate a decreased IC50 (higher sensitivity). Drugs are grouped in the same way as in a. Missing conditions are shown in white.

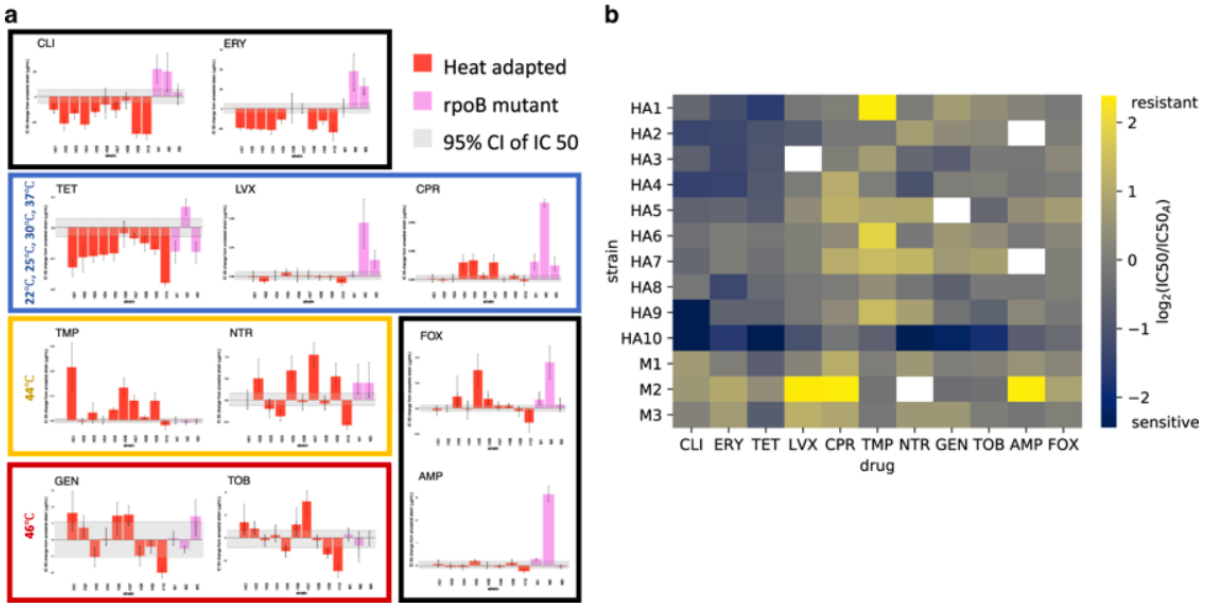

Intriguingly, the same patterns were not observed for the *rpoB* mutants exposed to some drugs (e.g., for ERY, CLI). These mutants were not adapted at high temperature, suggesting that there are additional adaptive mutations in the heat-adapted strains besides *rpoB*.

2.4 Discussion

In this paper, we cluster interactions among drugs and temperatures to infer that there are shared physiological responses of *E. coli* to these stressors. Our SIN analysis suggests that the stress responses to low temperatures overlap with those of antibiotics that affect DNA gyrase and a 30S protein synthesis inhibitor. In addition, the stress responses to high temperatures overlap with those of drugs that affect protein translation proofreading and drugs that damage DNA. Due to this overlap, we conclude that cellular responses to temperature stress have likely been evolutionarily co-opted to also respond to many classes of antibiotic stress. Because pressure and pH are also ancient stressors, we expect that responses to them may have also been co-opted to deal with antibiotic stress. Our approach provides a powerful basis for asking similar questions about other environmental, chemical, or physical stressors that affect the population growth of an organism.

We show that monochromatic clustering successfully separates antibiotics and temperatures into groups that have similar effects on bacterial physiology (Table 2-2).

Table 2-2 Effects of temperature and antibiotics in cellular physiology

	Temperature		**Antibiotics**
	High	**Low**	
DNA	Decreased negative supercoiling	Increased negative supercoiling	CPR, LVX: DNA gyrase inhibitors NTR, TMP: DNA damage
Protein	Misfolding and aggregation	Translational block	ERY, CLI, TET: inhibition of translation GEN, STR, TOB: increased errors in translation
Cell membrane	Increased membrane fluidity, damage to membrane due to aggregation of membrane proteins	Decreased membrane fluidity and altered fatty acid composition	GEN, STR, TOB: damage to membrane due to incorporation of misfolded membrane proteins

First, all temperatures (22°C, 25°C, 30°C, 37°C) lower than the optimum (41°C, which results in the highest growth) cluster with antibiotics that either affect the early stages of protein synthesis (TET prevents the association of aminoacyl tRNAs with the ribosome [69]) or are DNA gyrase inhibitors (LVX, CPR). This is consistent with the known effects of low temperature. One of the main effects of cold shock is translational block, which is thought to most likely occur at the translation initiation step [70]. Some previous reports have also shown that cold-shock induces the expression of DNA gyrase and a transient increase of negative supercoiling of DNA in E. coli [70-72]. Second, the highest evaluated temperature (46°C) clusters with the aminoglycosides, antibiotics that affect protein translation proofreading [68]. This leads to misfolding and aggregation of defective proteins that mimic the well-known effects of high temperatures on protein stability and folding [49]. Finally, 44°C clusters separately from 46°C, with antibiotics that either damage nucleic acids or inhibit their synthesis. This intriguing finding suggests the main physiological effect of this temperature (compared to 41°C) could be due to effects on nucleic acids. This connection to nucleic acids is suggestive given that the heat-shock protein Hsp70 enhances repair of UV-induced DNA damage [73]. We speculate that this specific temperature clustering separately from the aminoglycosides may be due to the heat-shock response being able to partially combat protein unfolding at 44°C, but not 46°C.

An important feature of the monochromatic clustering framework is that it implicitly assumes each node (i.e., stressor) in the SIN belongs to a single cluster. This single cluster assumption is likely a good approximation for antibiotics as they tend to bind to specific cellular targets. However, physical or environmental stressors, such as temperature, can affect many cellular processes simultaneously. Because of this, the clusters in our study correspond to consensus effects: these are informative summaries of the dominant effects of the environmental

stressor, but could miss secondary effects that are not shared with the other members of the cluster. Further theoretical and computational work could focus on relaxing the single cluster assumption of monochromatic clustering to allow temperatures to be grouped with multiple, potentially dissimilar classes of antibiotics. This updated methodology could allow a more nuanced approach, capable of breaking down the effects of an environmental stressor in terms of more targeted perturbations such as antibiotics, chemical inhibitors, or gene deletions that are deleterious to different cellular subsystems.

Indeed, some of the evaluated temperatures do have similar interactions to antibiotics in different clusters (Figure 2-7). Examples are the lowest temperatures evaluated (22°C, 25°C). These temperatures have similar interaction profiles to both the 30S (TET) and 50S (ERY, CLI) protein synthesis inhibitors, while higher temperatures that are still below the optimum (30°C, 37°C) are only similar to the 30S inhibitors. This is reflected in (ERY, CLI) being in a separate cluster from the low temperatures. Interestingly, low temperatures cluster with CLI under no salt conditions (Figure 2.3), and a previous report has shown cold-shock proteins are induced in response to CLI [74].

Figure 2-7 Dissimilarity of interactions. A heatmap with the dissimilarity between the interactions of each pair of conditions (see Methods 2.2) is shown. The dissimilarities are color coded in a gradient from white (more similar) to dark blue (more dissimilar). From these results, it is apparent that temperatures can be similar to multiple classes of antibiotics.

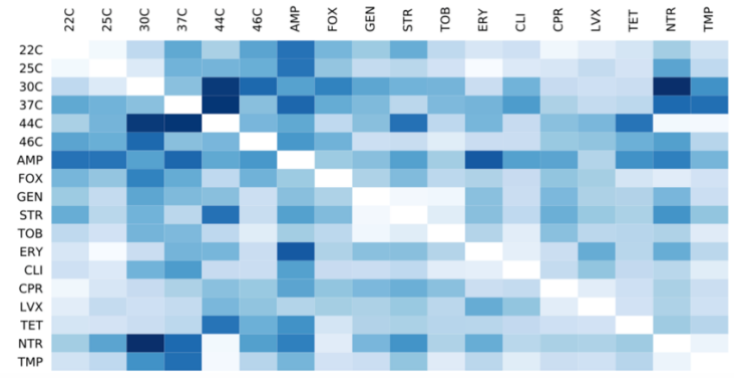

Clinically, the impact of temperature on the effects of antibiotics is also of interest because it suggests some antibiotics could have increased or reduced effectiveness in patients with fever or hypothermia. Previous work has shown there is increased resistance to gentamicin (GEN) in *Francisella tularensis*, *Listeria monocytogenes*, and *Klebsiella pneumoniae* at 26°C when compared to 37 °C [58]. This increased resistance seems to be mediated by reduced drug uptake. It has also been reported that streptomycin (STR), tetracycline (TET), ampicillin (AMP), and cefoxitin (FOX) have increased effectiveness at 46°C compared to 37°C in *Pseudomonas aeuriginosa* [75]. Our results are consistent with both reports, as we found: (1) aminoglycosides (GEN, STR, TOB) are mostly synergistic with high temperatures and antagonistic with low temperatures, (2) synergy of beta-lactams (AMP and FOX) with high temperatures, and (3) synergy of TET with 46°C (but, interestingly, with 22°C as well). Some other antibiotics (LVX, NTR, and TMP) also exhibit this curious pattern of being synergistic with both temperature extremes and either additive or slightly antagonistic with less stressful temperatures. Further work is needed to obtain a more detailed understanding of these interaction patterns.

Our transcriptional analysis shows that the overall expression patterns of *E. coli* exposed to high temperature are more similar to those induced by STR than those induced by TET (Figure 2-5a). We find that *cspA* and *cspG*, main cold-shock response regulators in *E. coli*, have increased expression in response to TET, but not STR or high temperature (Figure 2-5b). Other cold-shock regulators (cspB, *cspI*) show decreased expression. It has been shown that cold-shock genes are differentially induced depending on the severity of the cold stress. In particular, *cspA* expression is induced between 20–30°C, while *cspI* is induced between 10 and 15°C [76]. These gene expression results are in agreement with our drug/temperature clusters, since the low temperature cluster contains temperatures between 22 and 37°C. We find that genes involved in the response

to unfolded protein (as determined by gene ontology annotations), which commonly results from heat stress, are overrepresented in the genes induced by STR, a representative antibiotic that clustered with heat (Figure 2-5c). Interestingly, some heat-shock response genes that combat unfolded protein stress (*dnaK*, *dnaJ*, *groE*, *grpE*) have increased expression in response to both STR and TET. However, the main heat-shock response regulator *rpoH* is not over-expressed in response to either antibiotic (in fact, is under-expressed in response to TET). Together, these results suggest heat-shock genes participate in the response to both antibiotics. However, they may be activated in a different way than the canonical heat-shock response.

Our clustering and gene expression results show that multiple antibiotics (particularly aminoglycosides, TET, DNA gyrase inhibitors, and DNA-damaging antibiotics) have similar overall effects in *E. coli* physiology to specific low or high temperatures. This is consistent with components of the stress response to temperature having been co-opted over evolutionary time to deal with antibiotics that disrupt similar cellular structures or functions to those affected by low- and high-temperature stress. Moreover, we show that this overlap between stress responses can be related to the acquired cross-resistance of temperature-adapted strains to specific groups of antibiotics.

Typically, the overlap between cellular responses to stress has been studied by isolating subcellular parts and attempting to piece together this information to understand stress responses at the whole-cell level. Here, we take a reverse, yet complementary approach: by studying the effect of perturbations on the whole system, we gain more insights into the mechanisms of its specific parts. Importantly, no aspect of this methodology is specific to antibiotics and temperature. Our SIN clustering method can be used to evaluate shared responses among any combination of physical, chemical, and/or biological stressors that affect organismic growth.

In conclusion, we evaluate if the overlap between antibiotic and temperature stress responses is predictive of the cross-resistance of high-temperature-adapted strains to antibiotics (Figure 2-6). We find that high-temperature-adapted strains become more sensitive to protein synthesis inhibitors (CLI, ERY, TET), drugs that either clustered with or are similar to low temperatures. In contrast, the temperature-adapted strains become more resistant to drugs that clustered with 44°C (NTR, TMP), but not necessarily to drugs that cluster with 46°C (GEN, STR, TOB). Overall, these results strongly suggest that seemingly novel drug resistance is conferred to strains via adaptations they acquired while being evolved at extreme temperatures. Specifically, strains adapted to heat (42.2°C) are more resistant to drugs that damage DNA (which cluster with 44°C, a similar temperature), while also being more sensitive to drugs that mimic the effect of cold. However, this pattern is not universal, since the strains do not become more sensitive to fluoroquinolones (LVX, CPR), which also cluster with cold. Interestingly, the *rpoB* mutants do not follow the same antibiotic resistance patterns as the temperature-adapted strains, suggesting there may be more adaptive mutations to temperature besides *rpoB*.

2.5 Acknowledgements

We thank Bobby Tofig for the laboratory assistance at the facility of Molecular Screening Shared Resource at UCLA.

CHAPTER 3

How Antibiotics Shift Temperature Response of *E. coli*

3.1 Introduction

Many environments experience daily and seasonal temperature fluctuations that affect rates of physiological processes. These changes in turn affect biological and ecological traits and ultimately impact the behavior of communities [77-85]. In this manner, temperature fluctuations can drive the evolution of organisms through variation in thermal sensitivity—the ability to function and survive at different temperatures [81, 86-91].

At a cellular level the performance of an organism across different temperatures can lead to various genetic and physiological adaptation mechanisms. For example, in bacteria thermal sensitivity is related to many physiological and genetic modulations in metabolism, including outer membrane rigidity [92, 93], chemotaxis [94, 95], enzymatic thermo-stability [96, 97], and other general adaptive responses [49, 98]. Moreover, the heat shock response—a cellular mechanism to deal with the deleterious effects of high temperatures, such as protein misfolding and aggregation—is highly conserved in both prokaryotes and eukaryotes [49, 99]. Understanding responses to temperature changes is important to infer general patterns of how organisms, species, communities, and ecosystems are adapting to fluctuations in climate patterns and different environmental conditions.

Thermal sensitivity patterns and the performance of organisms across different temperatures are classically represented by the optimal temperature at which the organism performs best (i.e., attains its maximum growth) and the thermal breadth (sometimes referred to

as performance breadth), which describes the temperature range at which the organism can exhibit some level of functioning (Figure 3-1a). These two key parameters are fundamental to grasping the variability of physiological and ecological traits in response to temperature changes in different taxonomic groups and habitats. Because shifts in the thermal response curves are representative of average fitness performance and temporal niches [100], optimal temperature and thermal breadth are indicative of evolution and acclimation patterns based on how species' performance contributes to survivorship or fecundity [89]. For instance, seasonal variation in temperature could lead to an evolution of different attack and escape speeds that would allow individuals to perform best when they are predator or prey [101].

Figure 3-1 Temperature response curves change under antibiotic stress. (a) An example of a left shift of optimal temperature with antibiotic GEN. (b) An example of a right shift of optimal temperature with antibiotic ERY. (c) Optimal growth temperature (middle dot) and temperature niche (thin line joining the half-maximal growth temperatures, left and right dots) observed under each antibiotic used in this study. Point estimates for the optimal and half-maximal growth temperatures are shown as dots. To show the uncertainty in the estimates, 95% credible intervals (CIs, see Materials and Methods) are drawn as thick lines. The CIs for the no drug condition are shaded in the plot to facilitate comparison.

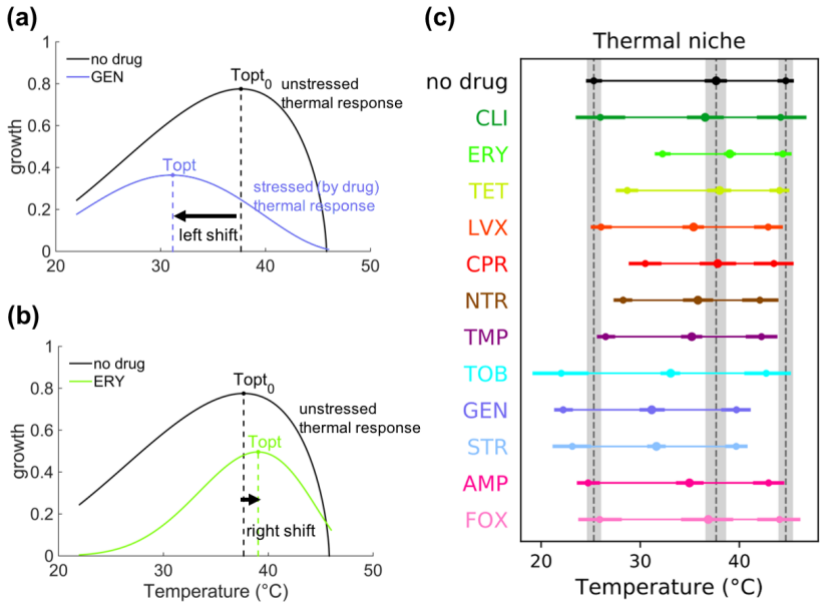

Temperature can interact with other environmental stressors such as light, precipitation, pH, and salinity. Exposure to different stressor types and intensities can lead to a phenotypic variation in an organism's ability to respond to temperature changes [102, 103]. Nevertheless, how the effects of environmental stressors interact with temperature responses is not well understood. Therefore, insights on whether temperature responses—as described by optimal temperatures and temperature breadths—can change rapidly and plastically in the presence of other environmental stressors have been lacking. In fact, it has been commonly assumed that thermal responses are not altered in the presence of other stressors [104-106]. A systematic approach that informs how optimal temperatures and temperature breadths are shifted by stressors (Figure 3-1) is needed to uncover these ambiguities and provide additional insights on fitness trade-offs and thermal adaptation strategies.

Here, we use a combined empirical-theoretical approach to study if the characteristics of thermal response curves change in response to additional environmental stressors. In particular, we use an experimental system of *Escherichia coli* and antibiotics as stressors in order to investigate how a physiological trait—growth of the bacterium—responds to variation in temperature in the presence of different stressor conditions. We obtain temperature response data for *E. coli* in 12 single-drug and 66 two-drug combination environments, where antibiotics are chosen to cover a wide range of mechanisms of action (Table 3-1). We then quantify both the optimal temperature and the temperature breadth of *E. coli* in the presence of these different environments.

Table 3-1. List of antibiotics. The antibiotics used are listed with their abbreviation, mechanism of action, dose, and our color scheme throughout the paper. Similar colors are chosen for drugs belonging to the same class for mechanism of action. For example, colors of blue tones are chosen for aminoglycosides.

Antibiotic	*Abbreviation*	*Color*	*Mechanism of Action*	*Dose (μg/mL)*
Ampicillin	AMP		cell wall synthesis inhibitor	1.2
Cefoxitin	FOX		cell wall synthesis inhibitor	1.2
Levofloxacin	LVX		fluoroquinolone, DNA gyrase inhibitor	0.01
Ciprofloxacin	CPR		fluoroquinolone, DNA gyrase inhibitor	0.005
Nitrofurantoin	NTR		DNA damaging, multiple mechanisms	2
Trimethoprim	TMP		folic acid synthesis inhibitor	0.1
Tobramycin	TOB		aminoglycoside	1.5
Gentamycin	GEN		aminoglycoside	1
Streptomycin	STR		aminoglycoside	2
Clindamycin	CLI		protein synthesis inhibitor, 50S	40
Erythromycin	ERY		protein synthesis inhibitor, 50S	50
Tetracycline	TET		protein synthesis inhibitor, 30S	0.25

We first show that individual stressors can have a substantial impact on the optimal temperature and temperature breadth. Next, we evaluate if the directions of the shifted thermal responses are related to the mechanism of action of the antibiotics. Previously, we determined that some specific classes of antibiotics have similar physiological effects to either heat or cold stress in *E. coli* [107]. We find that in most cases the direction of the shifts in the thermal responses under antibiotic stress can be explained through these groups. Lastly, we investigate how pairs of stressors move optimal temperatures in different directions as compared to the optimal temperatures under single-stressor conditions. In particular, we evaluate the extent to which the optimal temperatures result from integrated effects of both stressors, or whether a single stressor is the key driver of the temperature response. We infer from our results that a single drug often plays a dominant role in determining the optimal temperature response of a combined treatment.

Our experimental and theoretical framework on temperature response curves of *E. coli* presented here allows us to better understand how thermal sensitivities change in response to stressors. Therefore, our analysis will shed light on fundamental features shaping the ecological and evolutionary responses of organisms facing complex environmental conditions. By using antibiotics as stressors and a bacterium as a model organism, our study system is particularly valuable for its experimental tractability and reproducibility.

3.2 Materials and Methods

Bacterial strain and growth medium

The study used BW25113, a derivative of the F-, λ-, *E. coli* K-12 strain BD792 (CGSC6159) [65]. Bacterial cultures were grown in LB broth (10 g/L tryptone, 5 g/L yeast extract, and 10 g/L NaCl) and maintained in 25% glycerol at -80°C. Fresh cultures were started by adding 20μL of thawed bacterial glycerol stock into 2 mL of LB followed by incubation at 37°C. Cultures were grown to exponential growth phase and diluted to maintain 10^4 cells per experimental condition.

Antibiotics

A total of 12 antibiotics were included in the study as representatives of all major drug classes. Ciprofloxacin (CPR) from MP Biomedicals (Santa Ana, CA) and Gentamycin (GEN), levofloxacin (LVX), tetracycline (TET), tobramycin (TOB), erythromycin (ERY), ampicillin (AMP), clindamycin (CLI), streptomycin (STR), nitrofurantoin (NTR), cefoxitin (FOX), and trimethoprim (TMP)—all from Sigma (St Louis, MO)—were used. Stock solution at 20 mg/mL

of each antibiotic was stored in 50μL aliquots at −20°C. Each aliquot was only frozen and thawed once to preserve potency.

Growth experiments

Antibiotics used in all experiments inhibited bacterial growth at sub-lethal concentrations (50% to 90% growth). The desired concentrations were first determined by a twelve step concentration series of 2-fold at each step in 96-well plates (Costar). Antibiotic stock solutions were prepared in a total volume of 5 mL at 10-fold of their respective concentrations (Table 3-1). Experiments of pairwise drug combinations were prepared by adding 10μL of each component drug followed by the addition of 80μL cell inoculum. 10μL of LB medium was added in replacement of a second drug for single drug experiments. Each experimental condition was conducted in 4 replicates from the same antibiotic stock solution. The plates were incubated at various temperatures (22°C, 25°C, 30°C, 37°C, 41°C, 44°C, 46°C) with aeration at 300 rpm. Cell density was measured at 4-hours, 8-hours, 12-hours and 24-hours by reading at OD600 nm. The optical density measurements (used as a proxy for bacterial growth) at 24-hours were used to infer the temperature curves.

Extended Briere model for characterizing temperature response curves

Briere [108] defines a simple model for the temperature dependence of a trait, such as growth, denoted by $g(T)$ as follows:

$$g(T) = c(T - T_{min})(T - T_{max})^{\frac{1}{2}}$$

where T_{min}, T_{max} are the minimum and maximum temperature of growth. This equation can be solved analytically to show that the optimal temperature yielding maximum growth is always attained at $T_{opt} = \frac{2}{3}T_{max} + \frac{1}{3}T_{min}$. This model is not flexible enough to describe the antibiotic

growth curves we found empirically. As a more general alternative, we propose an extended Briere model

$$g(T) = c(T - T_{min})^a (T - T_{max})^b$$

where $a, b \geq 0$ are parameters that determine the shape of the curve. In this extended Briere model of temperature dependence of a trait, we have $T_{opt} = \alpha T_{max} + (1 - \alpha) T_{min}$. In this model the optimum temperature can lie anywhere between T_{min} and T_{max} depending on the value of the fraction $\alpha := \frac{a}{a+b}$.

The extended Briere model can be reparametrized as

$$g(T) = g_{max} \left[\left(\frac{T - T_{min}}{\alpha} \right)^{\alpha} \left(\frac{T_{max} - T}{1 - \alpha} \right)^{1-\alpha} \left(\frac{1}{T_{max} - T_{min}} \right) \right]^s$$

where g_{max} is the maximum value of the trait, i.e. growth, and $s = a + b$ is a parameter that determines the smoothness of the temperature response curve. We use this parametrization for parameter fitting of temperature response curves of the bacterium across different drug combination treatments (see Table 3-1 for chosen drugs in our study).

Bayesian parameter fitting

The extended Briere model was fitted to the temperature growth curve for the bacterium under all conditions through a Bayesian methodology with the pymc3 library of the Python programming language [109]. The following methodology is used for obtaining Bayesian estimates for the model parameters. Let y_i be the ith observed data point for growth after 24 hours and let T_i be the temperature at which it was observed. The observed values were assumed to be Gamma distributed with

$$y_i | \, g(T_i), \sigma_{T_i} \sim \text{Gamma}\big(\mu = g(T_i), \;\; \sigma = \; \sigma_{T_i}\big)$$

where the Gamma distribution is parametrized in terms of the mean, μ, and standard deviation, σ. The data are clearly heteroskedastic, and multiple measurements were taken at the same temperature enabling estimates of the standard deviation at each measured temperature. Because of this, a different standard deviation was modeled for each measured temperature. The following hierarchical model was used for the standard deviation:

$$\sigma_{T_i} \mid \beta \sim halfCauchy(\beta)$$

$$\beta \sim halfCauchy(0.3)$$

A variational method (full-rank ADVI) [110] was used to obtain approximate posterior distributions for the model parameters. These posterior distributions were used to construct point estimates—the expected value of the posterior distribution—and 95% credible intervals for all parameters to evaluate the uncertainty in the estimates. Credible intervals are the Bayesian analog to confidence intervals. A credible interval contains the true value of the parameter of interest with the specified (e.g. 95%) probability, given the observed data.

Models for predicting optimal temperatures for multi-drug responses

We denote single drugs as *X* and *Y*, and the combination of drugs as *XY*. We use these drug notations as a subscript for the corresponding optimal temperatures, i.e. $T_{opt,X}$, $T_{opt,Y}$, and $T_{opt,XY}$. For predicting the optimal temperature of multi-drug combination treatments, we define five different models by the choice of simple yet biologically meaningful scenarios (Figure 3-2).

(i) A single drug is playing a major role in determining the optimal temperature of the bacterial response. The optimal temperature of the combination is given by either of

the two individual stressors (*min* or *max* model). $T_{opt,XY} = \min(T_{opt,X}, T_{opt,Y})$ or $T_{opt,XY} = \max(T_{opt,X}, T_{opt,Y})$.

(ii) The optimal temperature of the bacterium in the presence of drug combinations is shifted to lower or higher temperatures than both single drugs' optimal temperature values. Along the lines of these extreme behaviors, we define *attenuated* and *elevated* optimal temperature models $T_{opt,XY} \ll \min(T_{opt,X}, T_{opt,Y})$ or $T_{opt,XY} \gg \min(T_{opt,X}, T_{opt,Y})$.

(iii) Temperature tolerance is determined by both of the drugs in the combination. To uncover such cases, we define our fifth model, namely the *mean* optimal temperature model. This model expresses the optimal temperature of the combined treatment as the average of the two single drug optimal temperatures (Fig 3.1). In other words, the *mean* model is equivalent to $T_{opt,XY} = \frac{(T_{opt,X}+T_{opt,Y})}{2}$.

Figure 3-2 The optimal growth temperature under stressor combinations is often determined by a single stressor. (a) Schematic illustration of models to determine the optimal growth temperature under two stressors ($T_{opt\ XY}$) given the single stressor optimal temperatures ($T_{opt\ X}, T_{opt\ Y}$). (b) The frequency at which each model is the best fit, across all drug combinations. (c) Proportion of time each antibiotic is the main driver of the optimal temperature when combined with other antibiotics, based on the individual models: min, max, attenuated, and elevated.

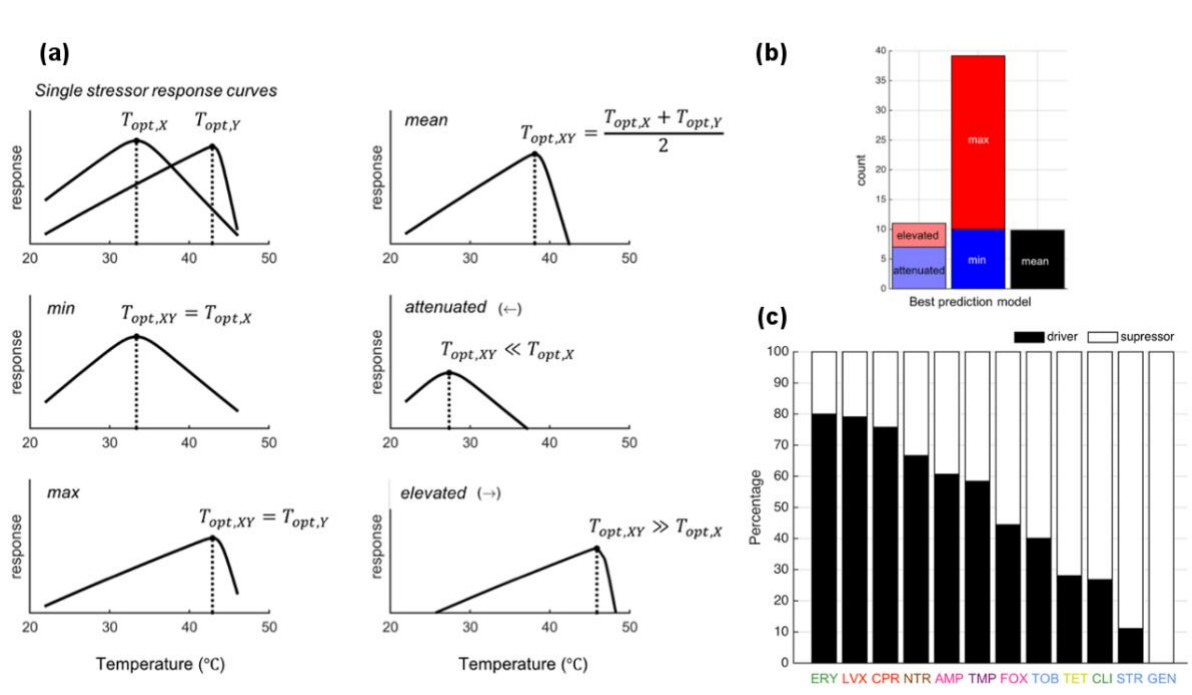

To determine the best optimal temperature model, we measured the difference between the actual value and the predicted value of each of the *min*, *mean*, and *max* models. We considered the best-fit model as the one with the smallest absolute difference between actual and predicted values. When this absolute difference is greater than the cutoff value of 2.20°C (Figure 3-3), then the best model is determined to be either the *attenuated* or *elevated* model depending on the direction of the optimal temperature shift.

Figure 3-3 Threshold for distinguishing single-driver models (*min* versus *attenuated* or *max* versus *elevated*). The distribution of model prediction errors across the *min*, *mean*, and *max* models is plotted to decide a cutoff to determine if the optimal temperature shift of a pairwise combination is large enough to decide the attenuated or elevated models are a better fit. When the prediction error (as defined by an absolute value of difference of optimal temperature prediction and actual optimal temperature) is higher than 2.20 °C, the best model is either the attenuated model or elevated model based on the direction.

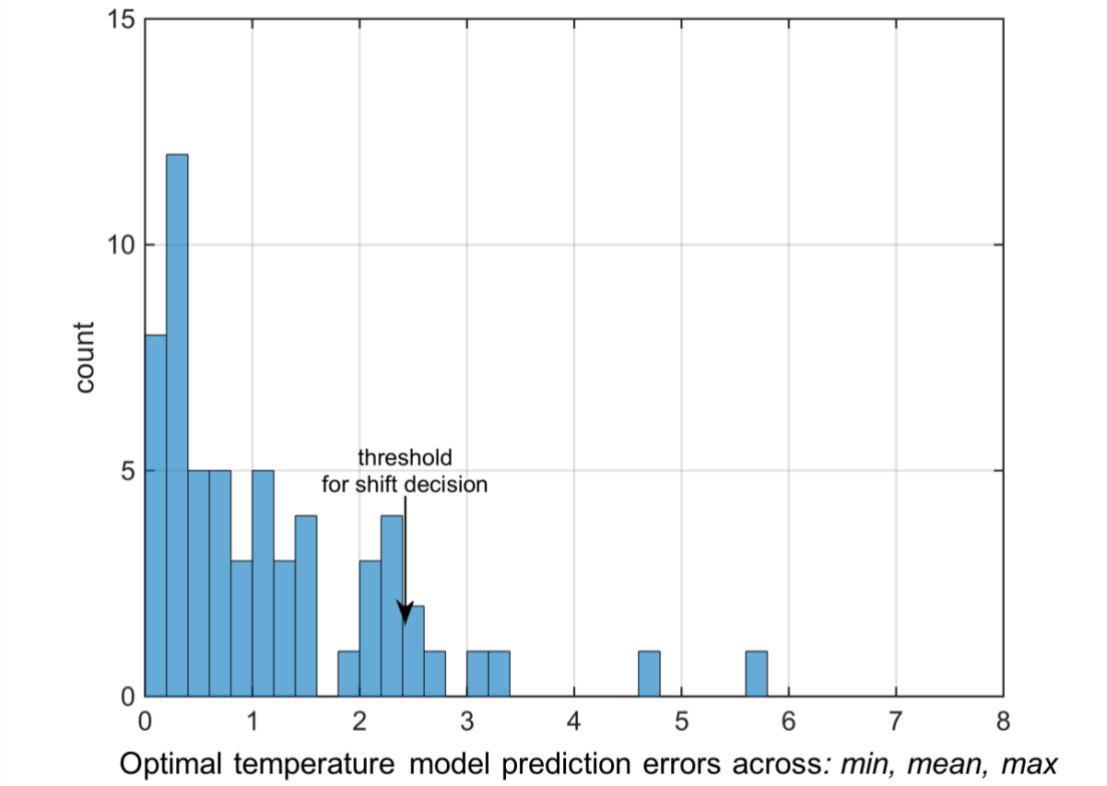

3.3 Results

In this paper, we investigate how different stressors (antibiotics) alter an organism's response to temperature, both in isolation and in combination. To do this, we determine the temperature optimum and temperature niche/breadth of *E. coli* by fitting the extended Briere model (see Materials and Methods 3.2) to experimental data of bacterial growth collected under different (unstressed and stressed) growth environments across multiple temperatures (22°C, 25°C, 30°C, 37°C, 41°C, 44°C, 46°C). The entire dataset and model fits are shown in Figure 3-4.

Figure 3-4 Full dataset and model fits. Lower half: The growth data for all antibiotic combinations (blue dots), as well as the fitted extended Briere model (black lines), are shown, as well as 95% credible intervals for the extended Briere model. The upper left corner corresponds to the no drug case. Upper half: The fitted curves corresponding to each drug combination are shown in black, and the fits corresponding to each single drug are shown in their corresponding color. In the uppermost row, the growth curve in the absence of antibiotics is shown in black and the single drug curves are shown in the corresponding color.

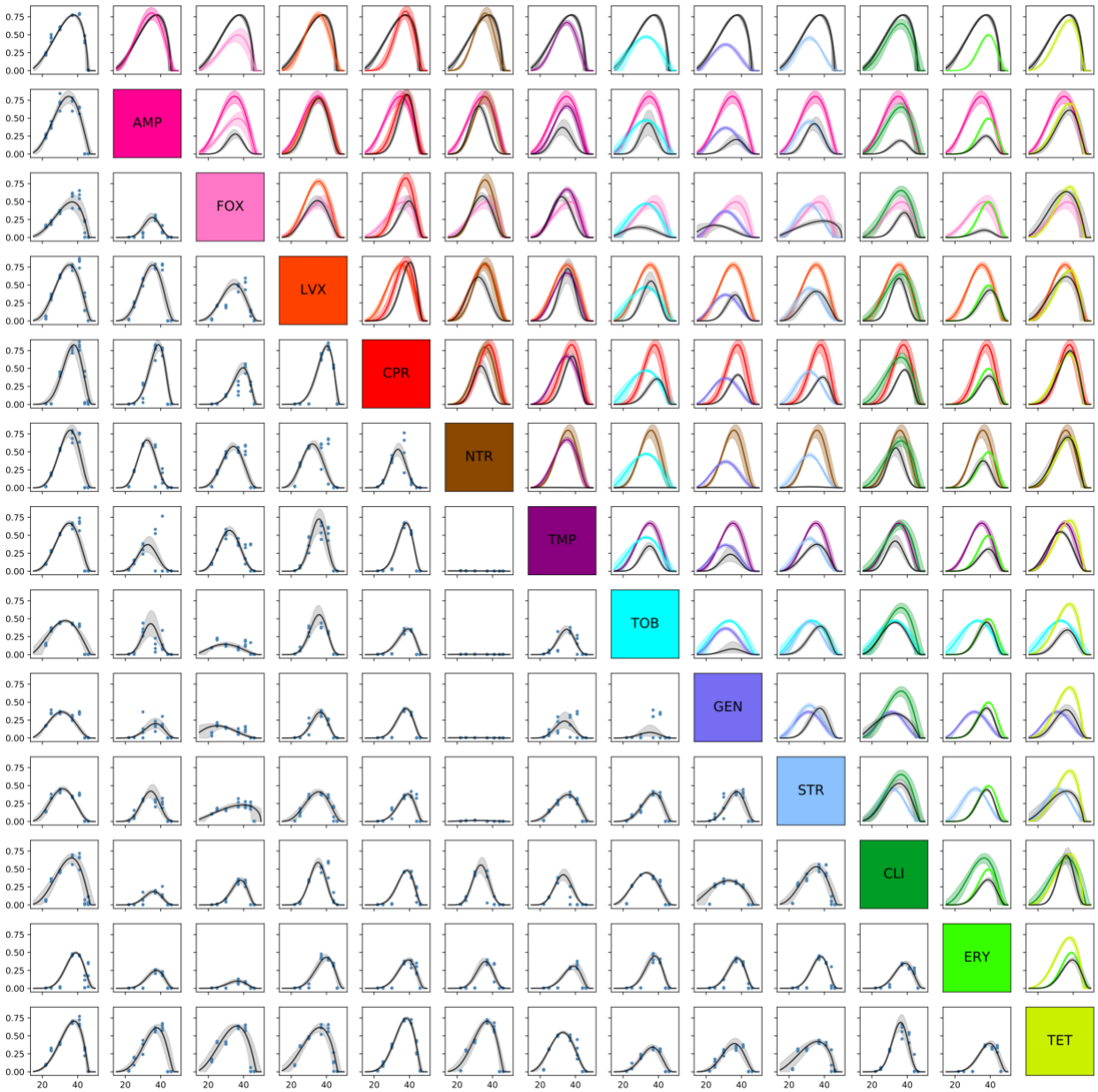

First, we explore how the optimal growth temperature and temperature breadth of *E. coli* change under single-stressor conditions (Figures 3-1a, b). We find that the majority of the single-drug environments exhibit left shifts—meaning the optimal temperature is lower — (Figure 3-1c) compared to the no-drug condition, $T_{opt} = 37.7℃$, CI: $(36.7℃, 38.6℃)$. Right shifts are both less common and of lower magnitude than the observed left shifts. We also find that the thermal niche breadth typically becomes narrower under antibiotic stress.

Next, we investigate whether the physiological effects of antibiotics bear any relation to the direction of the observed shifts in the temperature responses (Figure 3-5). To do this, we group the antibiotics according to the similarity of their physiological effects to those of low or high temperatures, as determined previously [111]. We observe the direction of the shifts for both single drugs (Figure 3-5a, left panels) and drug combinations that contain one or more of the antibiotics in the group (Figure 3-5a, right panel). We find that—for both single drugs and combinations—cold-similar antibiotics (i.e., with effects on bacteria similar to those caused by low temperatures) tend to either leave the optimal temperature unchanged or shift it slightly to the right (i.e., to higher optimal temperatures). In contrast, heat-similar antibiotics (i.e., with effects on bacteria similar to those caused by high temperatures) tend to result in unchanged optimal temperatures or shifts to the left (i.e. to lower optimal temperatures). In fact, bacteria exposed to aminoglycosides (TOB, GEN, STR), which induce misfolding of membrane proteins and have similar physiological effects to very high temperatures (Figure 3-5), show the greatest shifts towards the left. This is not the case for other protein synthesis inhibitors such as ERY or CLI that are similar to cold. Interestingly, beta-lactams shift the temperature curves in a similar way to heat-similar drugs when used in combinations, despite them having a different mechanism of action (inhibition of cell wall synthesis) that was not found to be heat-similar.

We then compare the optimal temperature and temperature niche—the range between the temperatures that result in half-maximum growth—for bacteria under all antibiotic combinations to the single drug conditions (Figure 3-5b). For some antibiotics (e.g. ERY, CPR) the optimal temperature and the thermal niche range are similar to those of the single drug when combined with most other antibiotics. In contrast, there are other antibiotics for which these features show much more variation when combined with others (e.g. GEN, STR, TOB, FOX). This suggests that some antibiotics may act as the main drivers of the temperature response curve of antibiotic combinations.

Figure 3-5 Physiological effects of antibiotics predict the direction of shifts in the optimal temperature. (a) Left: The fitted temperature response curve in the presence of single antibiotics is compared to the unstressed growth condition. Drugs are grouped according to the similarity of their effects to temperature [111], as shown in the top of the plots, except beta-lactams which did not show similarity to temperature. Right: Histogram of shifts in the optimal temperature under all pairwise drug combinations involving the drugs in the group. The individual estimates are shown as lines in the bottom. The unstressed optimal temperature is shown as a dotted line in both sets of plots. For both single drugs and combinations, the direction of the optimal temperature shifts depends on whether the drug is similar to cold or heat. (b) Optimal growth temperature and temperature niche observed under each antibiotic combination used in this study. The first drug in the combination is shown at the top of the plot. The second drug is shown in the y-axis using its assigned line color. The CIs for the single drug conditions are shown with shaded 95% credible intervals to facilitate comparisons. Conditions where the maximum growth was too small to estimate parameters reliably were removed.

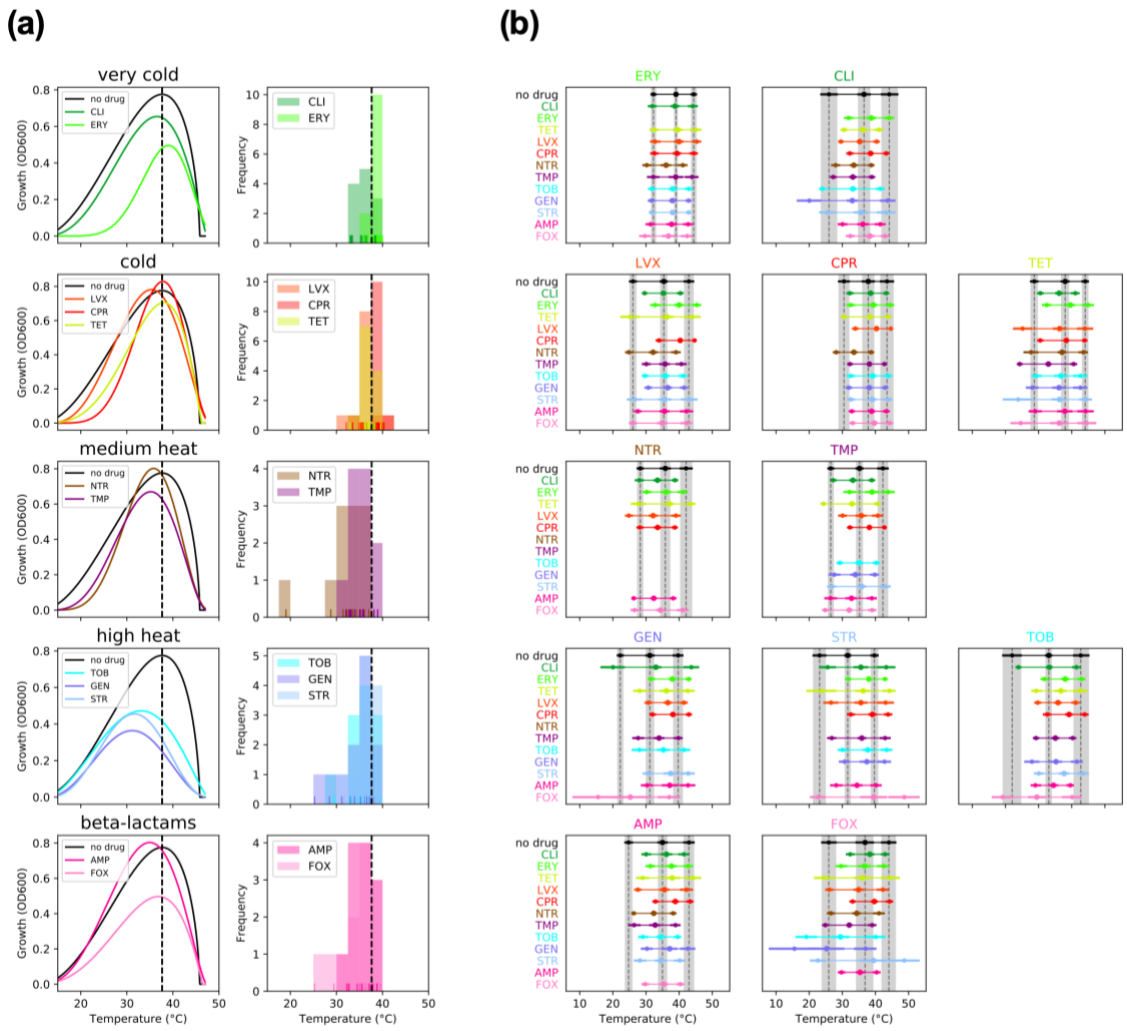

Following this idea, we further explored how the optimal growth temperature is determined under combinations of stressors relative to the optimal temperature under single stressor conditions. We contrast the observed optimal temperatures with the predictions of five candidate models of how the combination optimal temperature could be determined from that of the single stressors (see Material and Methods 3.2, Figure 3-2a). The *min* and *max* models assume that the optimal temperature of the combination is determined by the optimal temperature of a single drug (the minimum or the maximum of the pair, respectively). These models best describe most (65%)

multi-drug combinations (Figure 3-2b). The *attenuated* and *elevated* models assume that the optimal temperature of the combination is either lower or higher, respectively, than for both single drugs. These models best describe 18% of the combinations. Lastly, the *mean* model assumes that the temperature of the combination is determined by the average of the single drug optimal temperatures. This model best described only 17% of the drug combinations. These results suggest that the optimal temperature of antibiotic combinations is often determined by a single drug.

Finally, we explore cases where single-driver models (*min*, *max*, *attenuated* and *elevated*) represent the best optimal temperature model over the *mean* model, where both stressors compromise to result in the optimal temperature of an organism in the presence of combined stressors (Figure 3-2c). Interestingly, we rarely observe aminoglycosides (GEN, STR, TOB), antibiotics similar to high-heat, being drivers. In contrast, some cold-similar drugs (ERY, LVX, CPR), but not others (CLI, TET), frequently drive the optimal temperature of the combination. To account for the possibility that some antibiotics appear to be a driver more often than others purely by chance, we used a permutation test to evaluate our data against the null model that all drugs are equally likely to be a driver. This test provides strong evidence ($p=0.002$) that some antibiotics have a greater tendency to be drivers than others by testing the entire dataset simultaneously. We also tested if specific antibiotics are drivers more often than expected by chance. However, we did not obtain statistically significant results for individual drugs, after correcting for multiple comparisons. We believe this may be due to a lack of statistical power to detect differences due to the smaller number of observations for individual antibiotics when compared to the full dataset.

3.4 Discussion

Through a systematic analysis of growth response curves of bacteria across different temperatures and under different stressor environments, we investigate the effects of stressors on the phenotypic variation in temperature response traits—optimal temperature and temperature niche breadth. We see that stressors often decrease the temperature breath and shift the optimal temperature in a direction that depends on their physiological mechanism of harm. In addition, our results suggest that left shifts—where the optimal temperature in a stressed environment is lower than the optimal temperature in unstressed environmental conditions—are more common and dramatic as opposed to right shifts towards higher optimal temperatures.

High temperature harms living organisms through multiple mechanisms, including misfolding and aggregating proteins, damaging nucleic acids and increasing membrane permeability [49]. The heat shock response attempts to prevent and/or repair this damage by producing chaperones that aid the correct folding of proteins [112]. It has previously been shown that certain kinds of antibiotics can activate components of the heat-shock response [111, 113]. However, adding antibiotics to heat stress is unlikely to help the cell survive high temperatures, since the heat-shock response is already induced by the high temperature alone. Thus, right shifts in the optimal temperature may be rare because it is unlikely that adding a second stressor can reduce or repair the high-temperature induced damage. In most cases where we do observe a right shift, it seems to be due to asymmetrical effects on the temperature response curve, where the left portion (i.e. below the unstressed optimal temperature T_{opt}) is more depressed by the antibiotic than the right portion (Figure 3-4, Figure 3-5a).

In contrast, cold temperatures predominantly slow down cell growth by suppressing DNA replication or protein translation [114, 115]. Since the effects of low temperature seem to be primarily mediated by slowing down metabolism and growth rather than the accumulation of physical damage, it seems more likely that stressors can shift the optimal temperature to the left, especially when the stressor is more harmful at higher temperatures. In some cases, cold temperatures might allow cells to sustain antibiotic killing because certain antibiotics are only effective against actively growing cells [116]. Low temperatures have also been shown to alter the structural stability [117] or the global uptake of some antibiotics such as gentamicin, thus impairing killing efficiency [118].

Based on network clustering methods [63, 119], we previously found that certain antibiotic classes have similar physiological effects to either heat or cold in *E. coli* [111]. These temperature-drug groups were also shown to correlate with changes in drug sensitivity of high-temperature adapted strains obtained by Rodríguez-Verdugo *et al* [67]. Interestingly, here we find that in most cases the direction of the shifts in the optimal temperature can be predicted from these groups. Cold-similar drugs tend to either leave the optimal temperature unchanged, or to shift it slightly to the right. In contrast, heat-similar drugs tend to result in larger shifts to the left or leave the optimal temperature unchanged (Figure 3-5). Similar trends are exhibited by antibiotic combinations containing drugs in these groups. We propose that this phenomenon can be explained in the following way: the overlap in the physiological effect of the drugs and the corresponding temperature stress (heat or cold) causes increased damage to similar cellular functions (e.g. aminoglycosides and high temperatures simultaneously present will result in more misfolded proteins than either stressor on its own). When a drug is added, this could "overload" the stress-response machinery of the cell at less extreme temperatures, causing a greater reduction in growth

when the temperature damage overlaps with that of the drug. The cases with the most pronounced shifts in optimal temperature tend to have lower peak growth (Figure 3-5a). This suggests that perhaps these shifts become more pronounced when increasing the antibiotic concentration. Hence, we hypothesize that increasing the concentration of heat-similar drugs will result in greater shifts to the left and that doing so for cold-similar drugs will result in greater shifts to the right.

Notably, although the aminoglycosides (TOB, GEN, STR) share the same cellular target—the ribosome—as the other protein synthesis inhibitors (CLI, ERY, TET) used in our study, they result in distinct effects on the thermal response. Previously, differences in the effects of aminoglycosides and other protein synthesis inhibitors at different growth rates have been attributed to the reversibility of ribosomal binding [120]. In that study, the authors found that STR is more effective when the growth rate is lower, which does not agree with our results at low temperatures. This discrepancy may be because the reduction in growth was previously manipulated by nutrient limitation as opposed to the temperature variation in our study. Instead of binding reversibility, we could explain the different effects of these drugs by their mechanisms of action being qualitatively different, with the aminoglycosides being heat-similar and the other protein synthesis inhibitors being cold-similar. This is because aminoglycosides, unlike other protein synthesis inhibitors, induce mistranslation by the ribosome that decreases translational accuracy and causes protein misfolding [121]. Cold temperatures may counteract this effect by slowing down ribosomal activity and increasing accuracy [74], thus causing aminoglycosides to be less effective when bacterial growth is suppressed at lower temperatures, as we observe. Reduced drug uptake at low temperatures could also play a role [118]. Interestingly, beta-lactams have a similar effect in the temperature response as heat-similar drugs. We speculate that this may be due to increased effectiveness at high temperatures due to a synergy between the cell wall

damage caused by the antibiotic and the increased membrane permeability caused by high temperatures. Further disentangling these processes in future studies will help to understand the connection between antibiotic susceptibility and bacterial physiology.

We find that the breadth of the temperature niche is typically reduced in the presence of antibiotics, both in isolation and in combination. The lower and upper limits of growth are believed to be set by chemical and physical limits on the biological processes necessary for bacterial physiology, growth and cell division [81]. As such, this result is perhaps expected, since it is unlikely that adding a second stressor can increase this temperature range. However, we see the range can be reduced if the stressor is more harmful at either temperature extreme.

The optimal temperature of *E. coli* in the presence of antibiotic pairs often moves in a direction that is mostly determined by a single antibiotic. In a work on green algae, growth response to multiple environmental drivers has been shown to be dominated by the response to a single driver [122]. That study showed growth could be predicted for environments with a high number of interacting stressors if a severely detrimental driver was present. Environments with a smaller number of factors that involve temperature, CO_2, and pH suggested that specific interactions between responses determined overall growth rather than the response to an overriding factor. In contrast, we see effects on optimal growth temperature due to both a dominating driver and the interaction between drivers. For example, aminoglycosides (TOB, GEN, STR) show the largest degree of downshifting of the optimal temperature. However, when a second drug is added, this downshifting tends to be alleviated. Thus, in combinations of stressors, aminoglycosides are not the dominant driver for changing optimal temperature despite their large effects when used alone. Therefore, identifying a dominant environmental driver can be a simplified approach to

understanding organismal response to a complex system, but it needs to be done with care since interactions between drivers can be a contributing factor as well.

Our findings on single-stressor effects on thermal responses are surprising, especially in terms of optimal temperatures. Most models for the thermal optimum—the temperature at which the maximum growth is attained—posit that the optimum is below the mean environmental temperature by an amount determined by temperature variability in the environment [104-106]. It is tacitly assumed that the optimum temperature of individuals is thus either genetically hardwired or set through development to closely align with these predictions and thus be determined by environment in which the individual has been reared and the species has evolved. For this reason, the optimal temperature could be expected to be static when experiencing other stressful conditions. Nevertheless, against these expectations, in our data we observe that stressors can substantially change the optimal temperature for growth. On the other hand, organisms experiencing selection for greater adaptability traits to temporal changes could exhibit physiological plasticity with broader temperature breadth to adjust with various environmental stressors [100].

Although there has been substantial interest in understanding thermal response curves because of their potential to predict responses to climate change [101, 123, 124], the implications might be even broader. For example, an intriguing recent study showed that increased local temperatures were associated with increasing antibiotic resistance [125]. This may be because temperature or seasonality effect environmental growth of resistant strains [126, 127] and horizontal gene transfer—one method of facilitating resistance transmission [128, 129]. Another study showed the impact of chronic or long-term temperature changes unexpectedly coincided with spontaneous mutations against rifampicin resistance, an antibiotic that impairs RNA polymerase [67]. Climate change has also been linked to the impact on host-parasite dynamics that

alters the frequency and severity of many infectious diseases [130, 131]. Our work here and elsewhere shows that certain classes of antibiotics are more effective at different temperatures, and that there is substantial overlap in the response mechanisms to temperature and some kinds of antibiotics. This suggests the hypothesis that climate change might favor the evolution of resistance of specific (e.g. heat-similar) antibiotics indirectly by their resistance to high temperature stress.

From our results it appears that drugs can be used to modify temperature response curves in predictable ways. A temperature-drug system could perhaps be used to examine scenarios for biological responses to climate change via a variety of thermal responses. These experiments could be performed in a laboratory setting, which would enable the use of high-throughput platforms and a large number of replicates. Going forward, our system could serve as a simplified model for examining changes in response to temperature across seasons, geographic gradients, and climate change.

Temperature is one of the fundamental drivers of biological processes. By using antibiotics as stressors, our study system is particularly valuable for its tractability, reproducibility, and potential to study temperature-stressor interactions beyond the pairwise level. Our results on temperature response curves under combinations of antibiotics provide insights into the evolutionary adaptation of organisms to changes in temperature and what drives these adaptations. Investigating stressor effects on the physiological and ecological trait responses to temperature changes under this framework could lead to future research directions in exploring other environmental stressors that may aid in predicting the stability and diversity of ecological systems.

3.5 Acknowledgements

We thank Nina Singh for comments on the manuscript. We thank Rina Watanabe for laboratory assistance.

CHAPTER 4

Transitions in Interaction Landscapes of Multidrug Combinations

4.1 Introduction

Combination therapy is widely used to treat a number of chronic health issues such as cancer [132, 133], HIV [134, 135], hypertension [136], or multidrug resistant bacterial infections [137, 138]. Understanding the effects of these drug combinations and interactions among drugs is a major clinical concern and active research area [139-147] . Effectively leveraging interactions of drug combinations can be a promising strategy for combatting the evolution of drug resistance. However, a detailed understanding of how multiple drugs interact in a dose-specific manner is challenging to examine and visualize. Gaining this understanding is critical both for devising optimal treatments and for leveraging selection pressures to combat evolution of resistance.

Measures for interactions are often evaluated based on a coarse-grained categorization of three interaction types: additive (no interaction), synergistic (combined effect greater than expected based on single-drug effects), and antagonistic (combined effect less than expected based on single-drug effects). Synergistic drug combinations—in which combining drugs enhances the effects of the individual drugs—are commonly prescribed for patients because they maximize efficacy at lower doses. However, previous work indicates that antagonism may be more beneficial for slowing down the rate of resistance evolution to the component drugs [141, 144]. Thus, simply knowing how interactions deviate from additivity towards synergy or antagonism is potentially a powerful indicator to anticipate effects of a specific drug combination on treatment and resistance development.

Nevertheless, in practice it becomes challenging to use this interaction categorization to optimize treatment strategy and leverage evolution of resistance due to the complexity of dose-dependent interactions. Many empirical studies of drug interactions are conducted at a fixed dose and thus can only measure a single interaction type for each specific drug combination (i.e., Bliss Independence) [141, 142, 148]. The Bliss independence model is one of the most commonly used measures of drug interactions because it is intuitive, simple to calculate, readily expandable to numerous interacting components, and experimentally less demanding because it only requires four measurements—the control with no drug, drug x, drug y, and drug x, y combined—to classify a pairwise interaction.

When interaction type changes as drug dose is varied [149], the common interaction definitions based on single-dose measurements break down because it is incorrect to apply a single interaction type to that specific drug combination. Changes in interactions based on doses is well known for combinations of antibiotics, antifungal, and chemotherapeutic agents [148, 150-153]. This suggest interactions are not properties of drug combinations but drug concentrations. But our question is: Is this dose-dependency a second-order correction of slight importance, or does it represent substantial and significant deviations that would be difficult to capture by a nonlinear (but monotonic) null model? Moreover, does this depend on the particular drugs used, the extremeness of the concentrations, or net versus emergent interactions? More systematic studies are needed to find and understand general patterns and thus to avoid adverse effect that promote development of resistance and disease relapse. Such cases could occur when the interaction of a drug combination is defined at a specific dose combination and is extrapolated into a region of drug doses where the interaction is neither what is expected nor what is desirable. Until now, there have been no direct and intuitive visualizations of high-dimensional drug spaces to help verify and

more deeply understand the range of complexities in transitions among interaction types and whether drug interactions "switch" type or have a "phase transition" in type or whether they smoothly transition.

In this paper, we describe a new approach to visualize and analyze interaction data--interaction landscapes and various companion methods—and to present results on higher-order drug-interactions in a pathogenic *Escherichia coli* strain by examining all possible three-drug combinations among 8 antibiotics, each varied across a range of 7 concentrations. We specifically focus on changes in interaction type, precisely because we are looking for substantial and significant changes—not second-order corrections—that are more qualitative than quantitative and are thus likely to be found by most any null model. We introduce a new and direct visual representation of dose-dependent drug interactions that we term "interaction landscapes". This approach is placed directly within the space of drug interactions where general inferences about consequences of interactions can be made quickly with extremely efficient use of the information in the data. Interestingly, because interactions are calculated from fitness differences, the interaction landscape is a visual representation that partly captures directions and strengths of selection pressures. Therefore, these interaction landscapes will help to analyze how drug-dose combinations affect treatment strategies, regions of positive or negative selection pressures, and evolution of resistance.

Interaction landscapes, which are based on our high-throughput data and calculated from our mathematical framework, provide direct visualizations of local synergy or antagonism embedded within a larger interaction space and thus enable quantification and assessment of the directionality, pervasiveness, organization, and transition between regional synergy and antagonism. Consequently, we can use these landscapes to carefully investigate and answer the

questions above. We expect broad implications of this general approach and ideas, including in environmental pollution and risk assessment of toxic chemical mixtures where the exposure is rarely a uniform dose.

4.2 Materials and Methods

Bacterial Strain

We used *E. coli* CFT073, a highly virulent pyelonephritis strain isolated from human clinical specimen, obtained from ATCC (designation number 700928). The strain was grown in 2 mL of LB media (10 g/L tryptone, 5 g/L yeast extract, and 10 g/L NaCl) and streaked onto LB agar plates to isolate single colonies. Then a single colony was inoculated into 2 mL of LB and grown for 24 hours. Following the incubation, the culture was mixed with 2 mL of 50% glycerol and aliquoted into 50 μL to generate bacterial cell stocks with 25% glycerol for storing at -80°C. Each experiment was started with a thawed aliquot stock by inoculating 20 μL into 2 mL of LB media. The culture was incubated at 37°C until it reached exponential growth phase (an OD of 0.5) and diluted to maintain 10^4 cells per experimental condition.

Antibiotics

Antibiotics used include erythromycin (ERY), ampicillin (AMP), clindamycin (CLI), streptomycin (STR), nitrofurantoin (NTR), cefoxitin (FOX), and trimethoprim (TMP), all from Sigma (St Louis, Mo), and ciprofloxacin (CPR) from MP Biomedicals (Santa Ana, Ca). All antibiotics were dissolved and sonicated in 100% DMSO (Sigma) except for STR which was

dissolved in 50% DMSO, due to limited solubility in 100% DMSO. Experiments for IC50 and drug interactions (below) were conducted in clear flat bottom 384-well plates from Greiner BioOne.

IC50 determination

A 20-step two-fold serial dilution was prepared for each antibiotic. The source plate was made by preparing each drug with a total volume of 70 μL at 10 mM as the starting concentration, or the first step, filled into a 384 well plate. The following dilution steps were conducted by a robotic liquid handling system with a transfer volume of 35 μL per step. Meanwhile, 25 μL of LB per well were prefilled into a second 384-well plates using the Multidrop 384 (Thermo Scientific). Next, 500 nL from the source plate were delivered into the prefilled plate using the Biomek FX (Beckman Coulter) with a pin tool (V&P Scientific). Then, 25 μL of bacteria inoculum was added to each well to reach a final 50 μL per well with 1% DMSO. Each plate included negative controls (media alone), vehicle controls (media with 1% DMSO), and positive controls (media with 1% DMSO and cells). The plates were incubated at 37°C with OD_{595} measurement for cell density at 4-hour intervals for 24 hours. IC50s were determined by fitting a sigmoidal dose-response curve using the software Graphpad Prism. This is only used to analyze the preliminary results to determine the concentrations of each drug used in the drug combination experiments.

Determining drug-dosage levels from dose-response curve of single drugs

To establish reasonable resolutions of various drug doses, we designed our dilution regime to cover a wide range of dose effectiveness in terms of bacterial fitness of lethal, low, intermediate, and high. Mean dose response curves of each single drug show a sigmoidal and monophasic curve that results in the desired fitness levels. Dose indices 1 and 2 are regarded as low doses, where fitness

is between 1 and 0.8, with fitness here measured as growth rate relative to bacteria in no-drug environments. Dose indices 3 to 5 are intermediate doses that give a mean fitness around 0.4. High doses of 6 and 7 result in fitness below 0.2, except for clindamycin that has fitness well above the other drugs. We then calculated IC95 concentrations—where the dose concentration inhibits 95% of bacterial growth compared to no-drug environments—for each single drug (Table 4-1) to normalize the combined dose in triple-drug combinations in terms of combined effectiveness.

Table 4-1 List of drugs used in the study

Compound	Abbreviation	Cellular Target	Top dose (μM)	IC95 (μM)
Ampicillin	AMP	cell wall synthesis inhibitor	25	10.0
Cefoxitin	FOX	cell wall synthesis inhibitor	25	15.4
Ciprofloxacin	CPR	Fluoroquinolone, DNA gyrase inhibitor	0.5	0.1
Nitrofurantoin	NTR	DNA damaging, multiple mechanisms	250	56.7
Trimethoprim	TMP	folic acid synthesis inhibitor	10	4.8
Streptomycin	STR	Aminoglycoside	50	26.8
Clindamycin	CLI	Protein Synthesis inhibitor, 50S	500	722.3
Erythromycin	ERY	Protein Synthesis inhibitor, 50S	500	268.3

Drug combination experiment

All three-drug combinations formed from a set of eight drugs were tested, resulting in 56 unique three-drug combinations. Each drug combination was conducted in duplicate. The reproducibility is assessed in the supplemental material (Table 4-2). A source plate for each drug was prepared in seven-step, two-fold dilutions with various starting concentrations (Table 4-1), dependent on their respective IC50, with a total of 70 μL in DMSO at each dilution step. In addition, a zero dose was included into each drug gradient as the lowest concentration. A combination drug plate was

prepared by pinning from each source plate of the component drugs using a 250 nL pin tool (V&P Scientific) to restrict the DMSO concentration to be lower than 1%. Methods for cell inoculation and incubation were the same as stated above. OD measurements were taken at 12 hours.

Table 4-2 Test for reproducibility of our two experimental replicates. The table on the left shows the correlation between our two replicates. The table on the right shows the correlation between any two random experiments. Trivial refers to conditions where in a three-drug combination, the concentration of at least one of the three drugs is zero.

	all	remove trivial
DA	0.705	0.628
DA (smooth)	0.762	0.728
E3	0.648	0.398
E3 (smooth)	0.714	0.409

	all	remove trivial
DA	0.476	0.296
DA (smooth)	0.529	0.379
E3	0.443	0.196
E3 (smooth)	0.472	0.175

Measuring fitness

Optical density measurements were made with Perkin Elmer Wallace 1420. Fitness was calculated as

$$W = (OD - OD_{neg})/(OD_{pos} - OD_{neg}),$$

where OD is the optical density of the experimental condition with bacteria and drugs, OD_{pos} is the positive control without drugs, and OD_{neg} is the negative control without bacteria or drugs. Fitness is given with a precision of two decimals, and we therefore exclude fitness measurements below 0.01.

Quantifying interactions

Interactions are commonly quantified as the deviation from Bliss independence [64]. We quantify this using *deviation from additivity* (DA), which measures interactions between drugs, while additivity is defined when the presence of one drug does not affect the percent reduction of bacterial growth of another drug, using Bliss independence as a null model. If the fitness of the organisms given three drugs is W_{XYZ}, and the fitness when only given one drug is W_X, W_Y, and W_Z, for drugs X, Y, and Z, respectively, then [154].

$$DA = W_{XYZ} - W_X W_Y W_Z$$

DA incorporates both pairwise and three-way drug interactions but cannot discern between them. To measure emergent interactions that occur only when three drugs are present, we subtracted both the single-drug effects and the component pairwise effects [154].

$$E3 = W_{XYZ} - W_X W_{YZ} - W_Y W_{XZ} - W_Z W_{XY} + 2W_X W_Y W_Z$$

Pairwise effect, or *DA2*, is calculated as

$$DA2 = W_{XY} - W_X W_Y$$

To delineate boundaries and tease apart interactions as synergistic, additive, or antagonistic from the unimodal distribution of *DA* and *E3*, rescaling was applied to each measurement. *DA* was rescaled by dividing by the absolute value of *DA*, but replacing W_{XYZ} (denoted as $\widetilde{W}_{XYZ}$) by 0 if $DA \leq 0$, to account for cases of extreme lethal synergy ($W_{XYZ} = 0$) while no single drug completely

was completely lethal, and by the minimum value of W_X, W_Y, W_Z if *DA* > 0, for cases of buffering antagonism where combined drugs have the same effect as the strongest single-drug effect.

$$DA_R = (W_{XYZ} - W_X W_Y W_Z)/|\widetilde{W}_{XYZ} - W_X W_Y W_Z|,$$

where $\widetilde{W}_{XYZ} = 0$ for $DA \leq 0$ and $\min(W_X, W_Y, W_Z)$ otherwise.

Similarly, *E3* is rescaled by dividing by

$$|\widetilde{W}_{XYZ} + W_X W_{YZ} + W_Y W_{XZ} + W_Z W_{XY} - 2W_X W_Y W_Z|,$$

where $\widetilde{W}_{XYZ} = 0$ for $E3 \leq 0$ and $\min(W_X W_{YZ}, W_Y W_{XZ}, W_Z W_{XY})$ otherwise [154]. This rescaling results in values between -1 and ∞. We further discretize both DA_R and $E3_R$ based on the natural breaks in the histogram distribution of DA_R and $E3_R$. Values below -0.5 correspond to synergy, between -0.5 and 0.5 to additivity, and above 0.5 to antagonism. Values above 1 are capped at 1.

$DA2_R$, the pairwise DA is rescaled as $\widetilde{W}_{XY} = (W_{XY} - W_X W_Y)/|\widetilde{W}_{XY} - W_X W_Y|$, where $\widetilde{W}_{XY}$ = $\min(W_X, W_Y)$ for $W_{XY} > W_X W_Y$ and is 0 otherwise. For $W_{XY} > \min(W_X, W_Y)$, $\widetilde{W}_{XY} = (W_{XY} - \min(W_X, W_Y))/(1 - \min(W_X, W_Y)) + 1$.

Smoothing

To increase resolution of interaction transition with dose—given the fairly noisy OD measurements—we smoothed the data using a weighted average algorithm by considering our

dose combination matrix as a metric space. For each data point (interaction measurement at each drug-dose combination), both rescaled *DA* and *E3* were recalculated as a weighted average depending on the Euclidean distance (within the three-dimensional matrix) between the original data point and the points used for calculation. The weight is 1 for the origin, and $1/8d$ for the 26 nearest neighbors, where d is the Euclidean distance from the origin. If a neighboring value was missing, either because it lies at the boundary or because it was excluded due to low fitness, its weight was set to zero. The sum of the weights was required to comprise at least 59 percent of the original weight matrix. For smoothing, both *DA* and *E3* were truncated to values between -1 and 1, with higher values set equal to 1.

4. 3 Results

Overall, we find that interaction types are often strongly dose-dependent, and that this is true for both lower-order (two drug) and higher-order (three drug) combinations. We typically observe smooth transitions between different interaction types and subspaces within a drug combination. Furthermore, net interactions tend to transition from synergy at low dose to antagonism at high doses. For emergent interactions, higher doses often have the opposite effect and lead to more antagonism. These transitions happen quickly but smoothly. Finally, pairwise interactions can often be used to predict net three-drug interactions but not emergent three-drug interactions.

Interaction type is dose dependent and regionally confined.

Both lower-order (2-drug) and higher-order (3-drug) interactions are strongly dose dependent. To assess the effect of increasing dose on interaction in a two-drug case, we compared how one drug (at a specific dose) interacts with another drug at either a high dose or a low dose. In a three-drug combination, the interaction was examined with two drugs at a specific dose while the third drug was added at a high or a low dose. For combinations of 3 drugs, we measured interaction both at the overall net level (*DA*)—combined pairwise and three-way interactions—and at the emergent level (*E3*), where the pairwise interactions are subtracted from the net interactions so that only the truly three-way interaction part remains (Figure 4-1b). We then plotted the interaction measurements in a 3-dimensional matrix or the interaction landscape (Figure 4-1c). As shown in Figure 4-1c, the interaction landscape for the combination of AMP, CLI, and ERY presents a mixture of synergistic (red) and antagonistic (green) regions as dosage is varied. In addition, the landscapes of *DA* and *E3* are not entirely superimposable in terms of the regional interactions, meaning that a specific drug-dose combination can give rise to different landscape by including or excluding certain interacting components.

Figure 4-1 Schematic representation of experimental design. (A) For one triple-drug combination of X, Y, and Z, the drug X plate includes 7 steps of 2-fold serial dilutions (in red) plus no drug control (in white) going in the horizontal direction. Drug Y plate includes the same concentration gradient but in the vertical direction (in blue). Combining drug X and drug Y plates results in a 2-dimensional matrix of drug X+Y. Drug Z is composed of 7 plates each with one concentration across the full 7-drug gradient (in green). Each of the seven drug Z plates is transferred to a drug X+Y plate to form a matrix of X+Y+Z at one respective dose (drug X+Y+Z). Finally, a 3-dimensional matrix of all three drugs is constructed of all seven additions of Z into one plate of X+Y, plus a control where Z is zero. (B) For each drug-dose combination, the overall interaction of *DA* is calculated with the three subsets of pairwise interactions of drug X+Y, drug X+Z, and drug Y+Z with each at a specific dose denoted as n (2), and the interaction when all three drug are present (3); while emergent three way *E3* represent the interaction of only at the three drug level. (C) Construction of the interaction landscape with *DA* and *E3* measurements. Each three-dimensional matrix represents a three-drug combination, each data point is plotted with the overall interaction (*DA*) or emergent three way (*E3*). The color scale represents the degree of interaction from -1 to 1. Red and green indicate synergistic and antagonistic interactions, respectively. Additivity (i.e., no interaction) with values between -0.5 to 0.5 were not plotted. The two interaction landscapes are shown as examples for the different net (*DA*) and emergent (*E3*) interactions of the drug combination AMP/CLI/ERY.

A. Drug-dose combination experiment

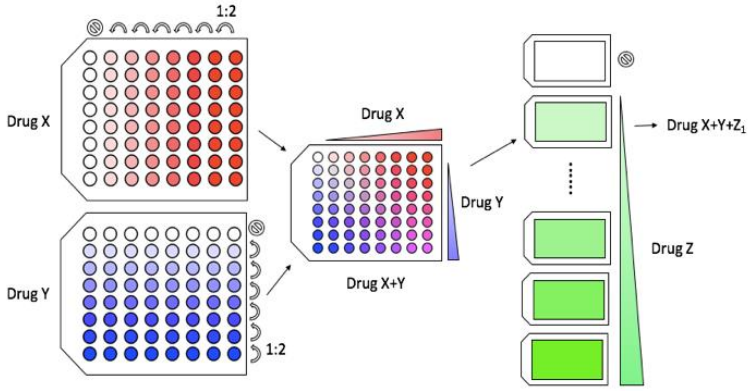

B. Characterization of interaction

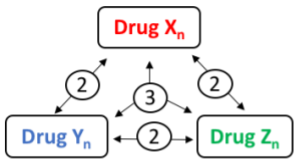

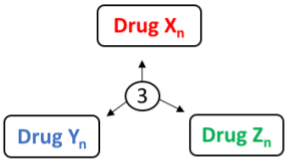

$$DA = W_{XYZ} - W_X W_Y W_Z$$

$$E3 = \underbrace{W_{XYZ}}_{\text{Observed overall effect with three drugs}} - \underbrace{W_X W_{YZ} - W_Y W_{XZ} - W_Z W_{XY}}_{\text{Component single and pairwise effects}} + \underbrace{2W_X W_Y W_Z}_{\text{Expected three drug effect}}$$

C. Construction of interaction landscape

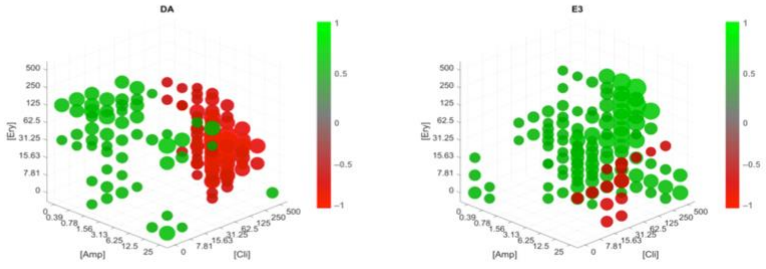

The distinction between *DA* and *E3* is intriguing. Although each is calculated from a different metric, the null model for *E3* expects no measurable interaction (in this case an empty landscape) if the overall interaction completely equates to the lower-order components so that they cancel each other. Although interactions change with dose, these changes tend to be confined to a smaller dose space, rather than being completely random. Furthermore, the pattern is not specific to certain drug combinations but more widely holds true. We also note the effect of smoothing on the landscapes as we compare them in parallel, in a representative drug combination (Figure 4-2).

Figure 4-2 Three-dimensional interaction landscapes for a representative triple drug combination. *DA* or *E3* as a function of the dose of each of three drugs. Rescaled values (top row) and smoothed values (bottom row) for *DA* (left column) and *E3* (right column) for each drug-dose combination. Markers are color coded from bright red for synergy (*DA* = –1) to bright green for antagonism (*DA* = 1). Additive interactions (–0.5 < *DA* < 0.5) have been excluded. In drug combination AMP-CLI-ERY, the smoothed values show that *DA* is predominantly antagonistic at lower doses and synergistic at higher doses. The pattern changes when we only include three-way interactions (*E3*), for which antagonism generally dominates, and there is minimal correspondence between regions of antagonism in *DA* and *E3*. In drug combination AMP-CPR-CLI, the difference between the predominantly synergistic interactions in *DA* switches to almost exclusively antagonistic in *E3*. Notably, there is no correspondence between *DA* and *E3*, indicating that *DA* is driven by the pairwise interactions while the three-way emergent interactions measured by *E3* are independent of the pairwise interactions.

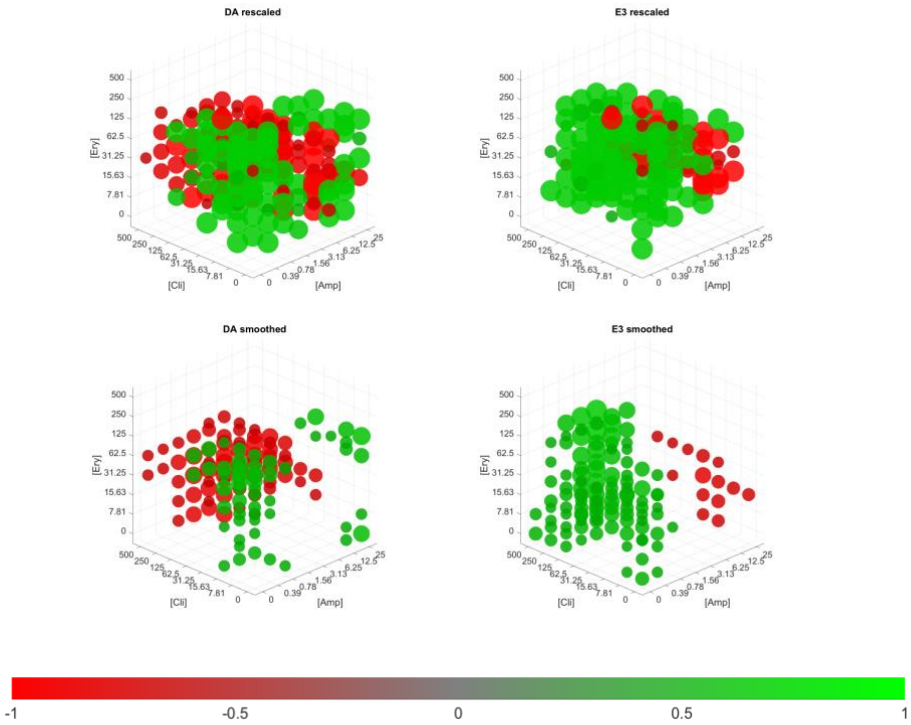

Smoothing dampens the noise by averaging out the interaction measurements with its neighboring points so the interactions are, on the whole, weakened. But the general patterns in the landscape remain (in terms of the synergistic and antagonistic regions) when the signal is above the noise level. The distributions of *DA* and *E3* among all combinations of drugs and doses are multimodal with peaks at synergy (*DA* = –1), additivity (*DA* = 0), and antagonism (*DA* = 1) (Figure 4-3a, b). Smoothing the data results in a more continuous distribution (Figure 4-3c, d). The peaks at the boundaries of synergy and antagonism are much less prominent (Figure 4-3c, d), and low drug concentrations result primarily in net interactions that are additive or antagonistic (Figure 4-3). Synergistic *DA* and *E3* interactions are mostly observed at intermediate and high concentrations with a dearth at low doses (Figure 4-3c, d).

Figure 4-3 Rescaled net (*DA*) and emergent (*E3*) interaction distributions. Panel A and C show the overall net level (*DA*) that encompasses all component pairwise and three-way interactions. Panel B and D show interaction at the emergent level (*E3*), where the pairwise interactions are subtracted from the net interactions so that only the truly three-way interaction part remains. The colors correspond to drug concentration, where IC95 were used as the maxima. Drug concentrations above IC95 were counted as the maxima. (A) Rescaled *DA*, (B) rescaled *E3*, (C) smoothed *DA*, (D) smoothed *E3*. Low drug concentrations (red) result predominantly in additive ($-0.5 < DA < 0.5$) or antagonistic interactions ($DA > 0.5$). Higher concentrations (green to purple) are more evenly distributed among interaction types.

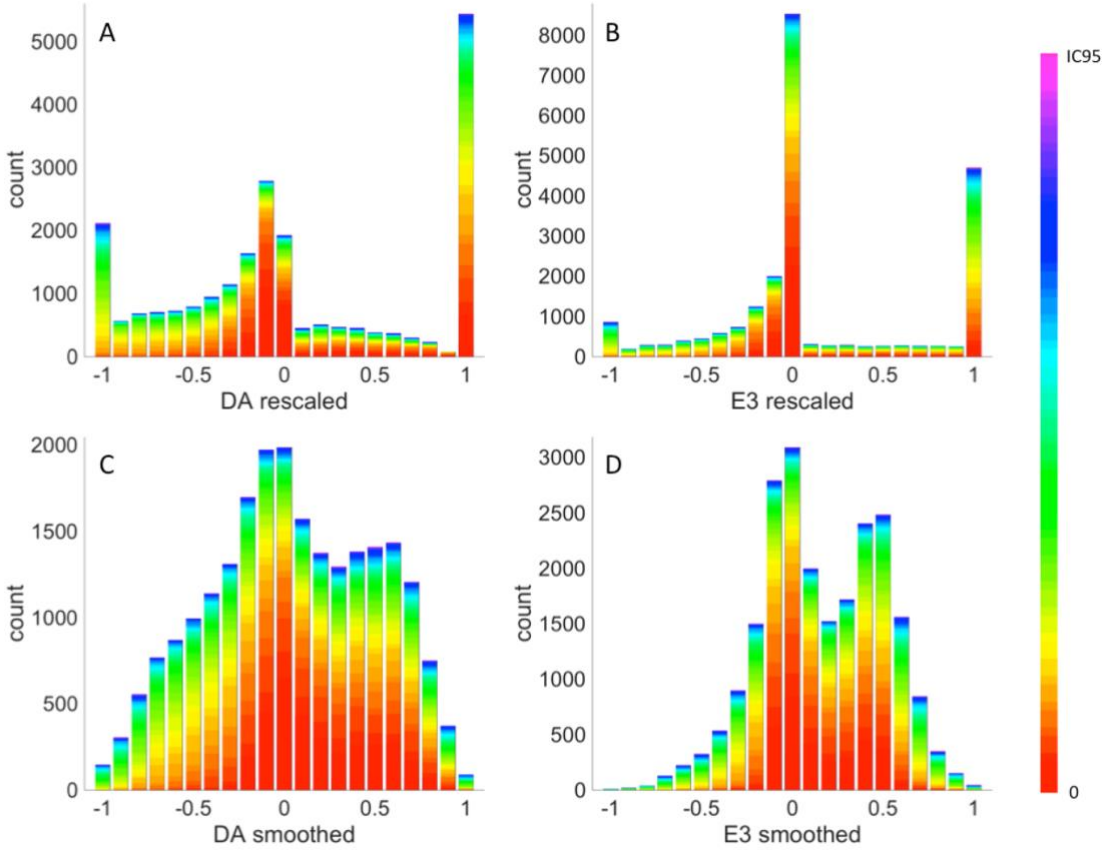

Interaction type transitions.

When interaction type changes, net interaction (DA) tends to become more synergistic as the combined dose increases, while emergent interaction (*E3*) becomes more antagonistic (Figure 4-4).

Figure 4-4 Change of interactions of three drug combination as a function of combined dose. Interaction is plotted on the y axis and characterized as synergistic (<-0.5), additive (-0.5 to 0.5), and antagonistic (>0.5). (A) Change of *DA* and (B) *E3* with dose for each interaction types of antagonistic (green) and synergistic (red). For both *DA* and *E3*, total antagonism and synergy each increase in magnitude with dose, though the effect is smallest for *DA* antagonism and strongest for *DA* synergy.
DA antagonism: Pearson's ρ = 0.396, p = 0.045.
DA synergy: Pearson's ρ = -0.883, p = 5.1e-09.
E3 antagonism: Pearson's ρ = 0.951, p = 1.0e-13.
E3 synergy: Pearson's ρ = -0.891, p = 2.4e-09.
Combined dose is the sum of 2 to the power of each of the three dose indices ($2^x + 2^y + 2^z$), and antagonistic lines include all points where *DA* (or *E3*) > 0 and < 0 for synergy.

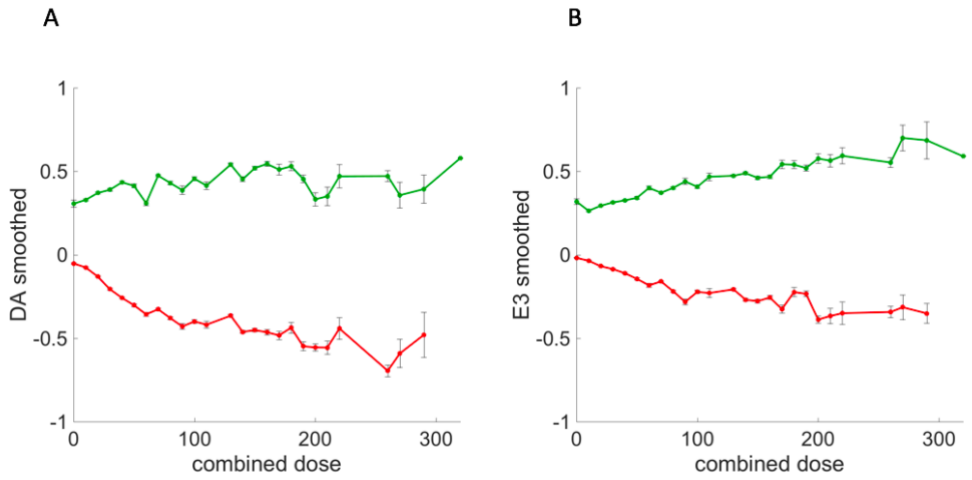

We counted the number of cases of interaction transitions based on the change in direction (e.g., antagonism to synergy) (Figure 4-5). For interaction transition to synergy from a low to high dose, we show about 20% occurrence in *DA* while *E3* has only less than 4%. Most of the transitions are from additivity (no interaction) to either synergy or antagonism. Abrupt transitions between synergy and antagonism are extremely rare, occurring less than 4% for *DA* and less than 1% for *E3*. Antagonistic interactions remain antagonistic or becomes additive 26% of the time for 2-drug combinations and 17% for 3-drug combinations. Emergent interactions (*E3*) are rarely synergistic. We did not see any emergent synergy at the low dose, while at high dose there is about 4% (Figure 4-5).

Figure 4-5 Distributions of transitions between interaction types from a low dose (index 1) to a high dose (index 6). To assess the effect of increasing dose on interaction in a two-drug case, we compared drug interaction of drug A at a sub-inhibitory concentration and drug B at either a high dose and a low dose. In a three-drug combination, the interaction was examined with a third drug at a high and low dose. Pairwise interactions (*DA2*, i.e. overall pairwise interaction) are dominated by antagonism and additivity at the low dose (green and gray, 99%), while a total of 10% are synergistic at the high dose (left). Three-way (*DA)* interactions are mostly additive at the low dose (gray, 76%) and antagonistic (green, 22%), but change from additivity to antagonism (16%) and from additivity or antagonism to synergy (21%) at the high dose. The emergent three-way interactions measured by *E3* are mainly additive at the low dose (gray, 89%) with the rest being antagonistic and result in very few synergistic interactions at the high dose (3%), with some being antagonistic (22%) and a majority being additive (75%).

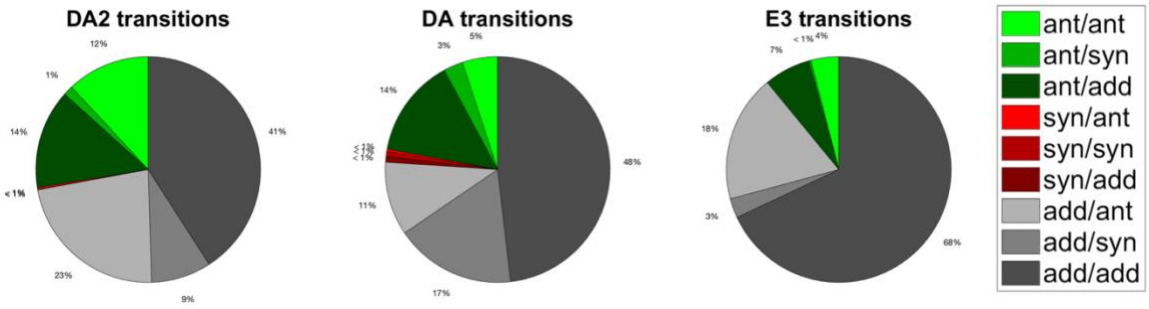

Interaction transitions are summarized for each drug combination with both the sum and absolute change in *DA* (Figure 4-7).

Figure 4-6 Changes of interaction from low to high dose in each drug combination. Interaction is calculated at both the *DA* (overall net interaction) and *E3* (emergent three way) at each dose combination from lowest to highest and the changes are summarized as both the absolute change (top panel) and the overall change (bottem panel). (A) Absolute *DA* changes (top) and total *DA* change (bottom). (B) Absolute *E3* changes (top) and total *E3* change (bottom). Blue is rescaled data, and red is smoothed data. The total *DA* changes between doses 1 and 6 are positive when the majority changes to become more antagonistic, while those that primarily change to synergy are negative. The sum of *E3* transitions are nearly all positive, showing that three-way interactions almost exclusively change to more antagonism as the dose is increased.

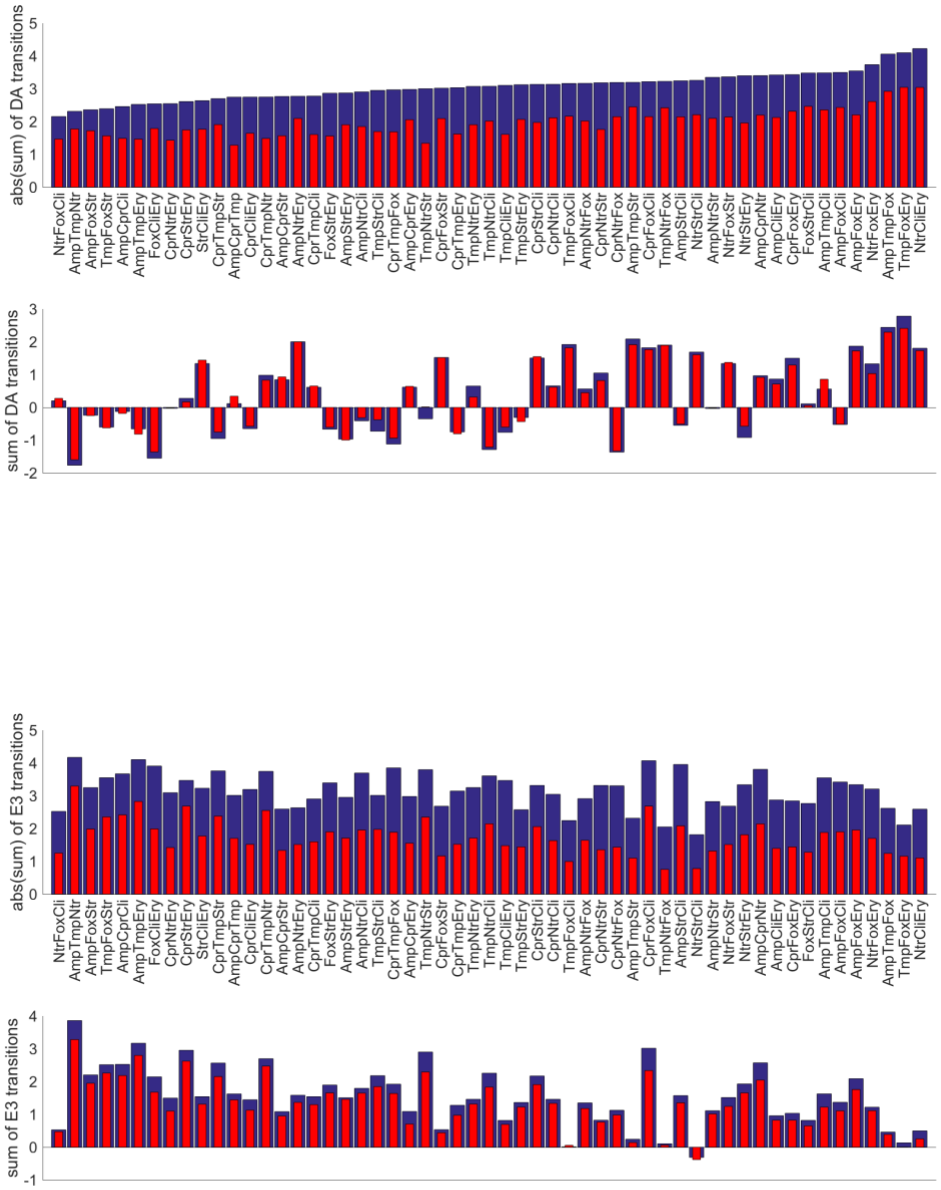

Increasing the dose of one drug can lead to no change, additive to synergy, or additive to antagonism (Figure 4-7). Again, the landscapes are not randomly scattered with different interaction types, but instead are composed of local areas of synergy or antagonism. Transitions between different interaction types are generally buffered by a region of additivity, or what we call "smooth".

Figure 4-7 Transition trajectory of three-way *DA* interaction versus doses grouped by transition category. From antagonism at dose index 1 (green) to antagonism (199), additivity (556), and synergy (110) at dose index 6, from additivity (gray) to antagonism (413), additivity (1885), and synergy (679), and from synergy (red) to antagonism (13), additivity (32), and synergy (28). Error bars are s.e.m.

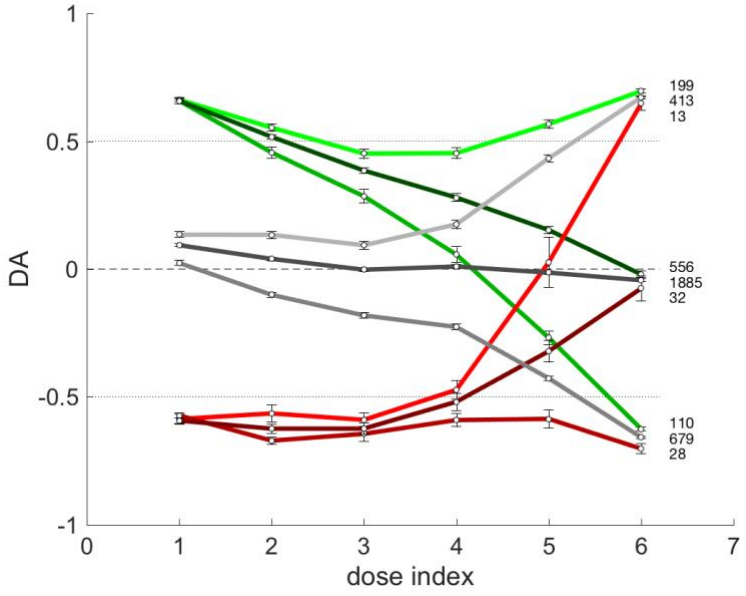

Pairwise interactions contribute most to net three-way interactions. Emergent three-way interactions are not predicted by pairwise interactions.

For each three-drug combination, we calculated three-way net (*DA3*), pairwise net (*DA2*), and three-way emergent (*E3*) interaction for drug-dose combinations with a third drug at low, intermediate, and high concentrations (dose indices 2, 4, and 6). For all three doses, the mean of the three pairwise *DA2* correlates strongly with three-way *DA3* (Spearman's ρ = 0.793, Figure 4-8a). Surprisingly, *DA3* and *E3* show *no correlation* (Spearman's ρ = -0.094, Figure 4-8b), but *E3* and pairwise *DA2* exhibit a slightly anti-correlated pattern (Spearman's ρ = -0.384, Figure 4-8c). A more synergistic mean pairwise *DA2* thus predicts a more synergistic three-way *DA3*, which is to be expected because the pairwise interactions are included in the three-way *DA3*.

Figure 4-8 Comparisons of three-way interactions to pairwise interactions. For each three-drug combination, we calculated three-way net (*DA*), pairwise net (*DA*), and three-way emergent (*E3*) interaction metrics for all possible drug pairs and doses with the third drug at low, intermediate, and high concentrations (dose indices 2, 4, and 6). The relationship between the three-way *DA* at dose index 6 and the mean of the three pairwise *DAs* at the same doses shows a strong positive correlation (Spearman's ρ = 0.793), whereas this correlation is absent between *E3* and three-way *DA*, as well as between *E3* and the mean pairwise *DA*. Together, this suggests that the *E3* interactions emerge independently of the pairwise interactions. The pairwise interactions surprisingly are negatively correlated with the emergent three-way interactions. *DA* and *E3* are evaluated at a high dose (dose index 6), and markers are colored according to the three-way *DA* value for antagonism (green), additivity (gray), and synergy (red). Three-way *DA* and *E3* are calculated for one drug at dose index 6 and the other two drugs at all dose combinations. The three pairwise *DA* components are calculated with one of the three drugs concentrations at zero. The mean pairwise-*E3* correlation for synergy alone is ρ = –0.619.

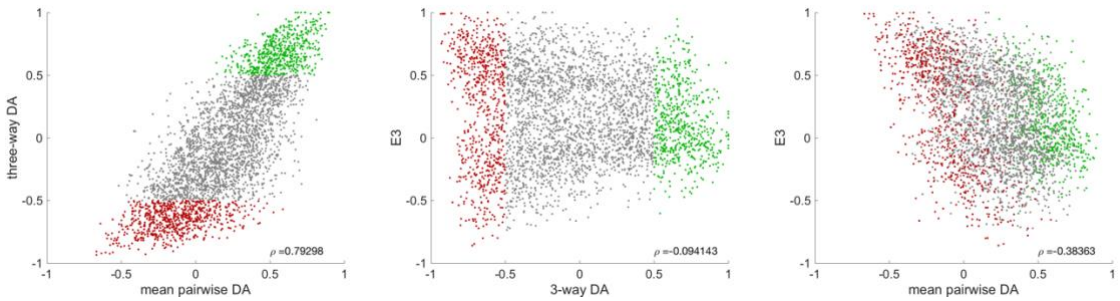

We also note that synergistic three-way *DA3* (red points) interactions can be driven by synergistic *E3* while the pairwise *DA2* are antagonistic (Figure 4-9).

Figure 4-9 Correlations between the mean pairwise *DA* and *E3*. Interactions are antagonistic (green), additive (gray), and synergistic (red) for three-way *DA*. There is a particularly strong correlation between mean pairwise *DA* and *E3* for synergisitic interactions.

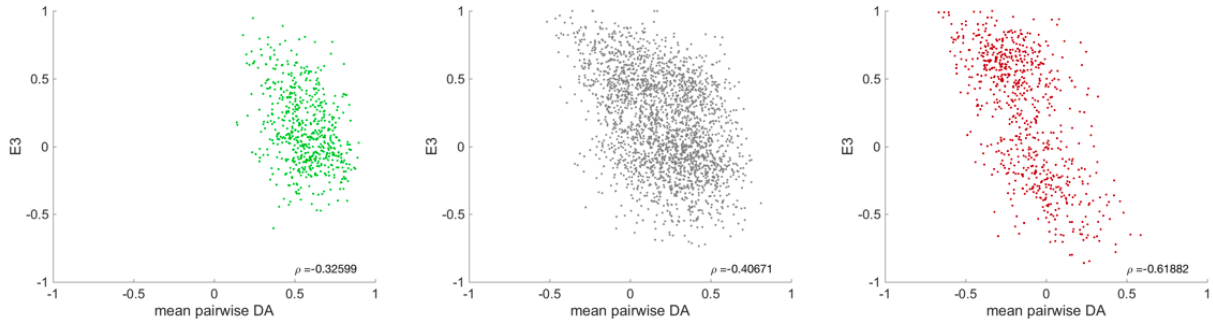

Conversely, *E3* can remain predominantly antagonistic when both the mean of the three-pairwise interactions and the three-way *DA3* are synergistic. This effect is likely to result from low fitness at high doses that can cause large deviations in *DA* and *E3*. The correlations between pairwise *DA*, three-way *DA*, and *E3* are similar for both low and intermediate doses of the third drug (dose indices 2 and 4) (Figure 4-10).

Figure 4-10 Correlations between pairwise *DA*, three-way *DA*, and *E3* using dose index 2 (top row) and dose 4 (bottom row). This is similar to the correlation using dose 6 (Figure 4-8).

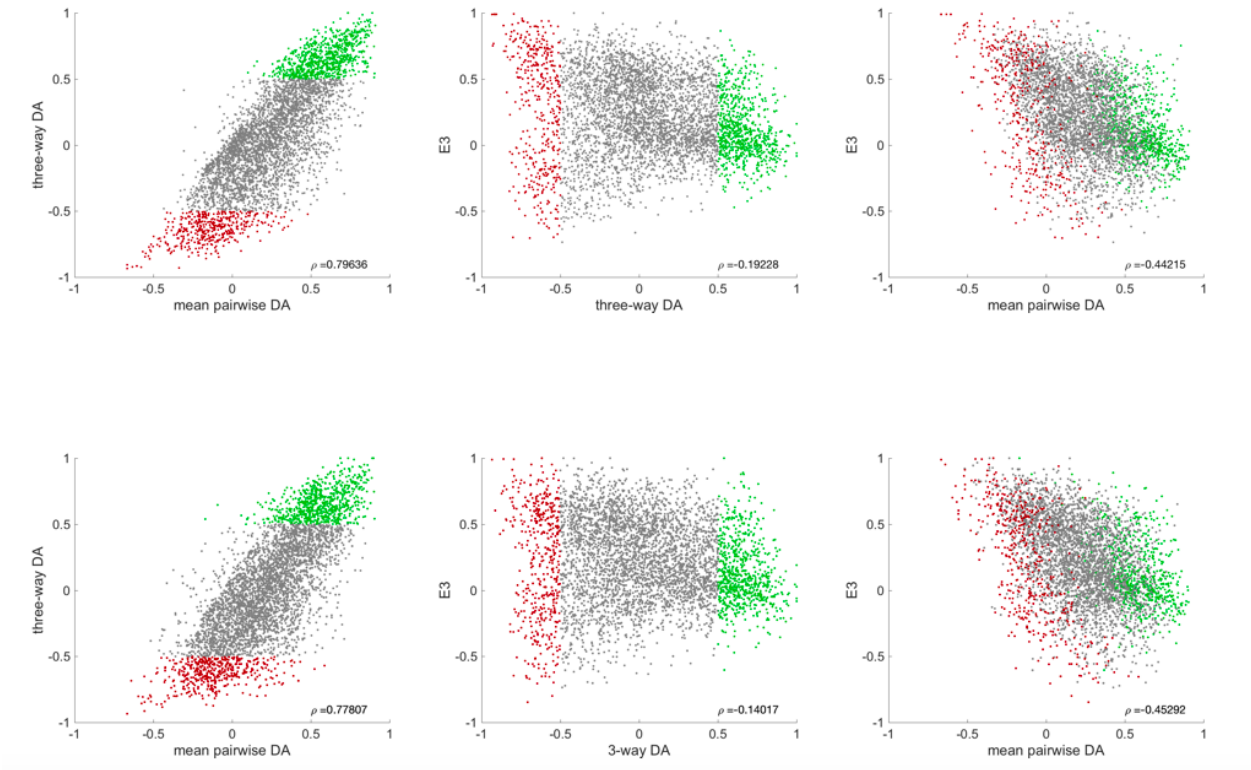

4.4 Discussion

To quantify the effect of dose on drug interactions, we measured fitness of a pathogenic strain of *E. coli* subjected to all possible 3-drug combinations of eight antibiotics across a gradient of doses for each drug. To visualize the high-dimensional interaction space of our data, we introduced the interaction landscape that displays quantitative measures of interactions as a function of the interacting components. We provide evidence that different environmental conditions (*i.e.*, drug concentrations) can change drug interaction type and thus lead to dose-dependent interactions. But within a smaller dose space, interaction types are more consistent, and this gives rise to locally synergistic or antagonistic regions. We also showed these transitions are smooth, rarely going from synergy directly to antagonism or vice versa. Instead, transitions first pass through the intermediate type of additivity (no interaction) as they pass from antagonism to synergy or from synergy to antagonism. This is the opposite of what one might expect with "smoothing" the data. Smoothing could average over additive regions and make the transitions go straight from synergistic to antagonistic, which would then be interpreted as sharp transition. The interaction landscapes give a direct and intuitive view of how the environmental space of combined drug doses affects the efficacy of drugs in combination. This representation is analogous to other maps of underlying control variables onto one dependent variable, such as genotype-fitness maps [155-157], genotype-phenotype maps [158, 159], and phenotype-fitness maps [160-162]. It is also similar to the analysis of a reaction norm in an ecological sense, since a typical dose response curve for a single drug describes the growth pattern across one concentration gradient. In addition, we expect our approach can be usefully applied or complementary to other systems or studies

related to toxins, pollution, stressors, genetic interactions, or environmental heterogeneity [163-166].

Our results lead to two insights that should aid future studies of drug combinations. First, within our interaction landscapes, there are large, clearly delineated subspaces that correspond to specific types of drug interactions. These subspaces often occur at high or low concentrations of the combined drugs. Conclusions can therefore be made with less information than is needed for fitness landscapes by mapping the boundaries between these different subspaces and by understanding how the magnitude of the interactions change when moving toward or away from a boundary. Moreover, these subspaces suggest simple methods for predicting regions of positive or negative evolutionary pressures on subpopulations of treated cells (*e.g.*, selecting for or against resistance) and could have profound implications for choosing effective drug-dose combinations as well as intelligent drug treatments. Second, because there are transitions across the landscape that go between these subspaces of interaction type, synergistic combinations identified with only one dose regime [63, 141, 144, 148] can be antagonistic when used or prescribed at a different dose regime. Such a reversal could have detrimental impact on clinical decisions and scientific studies. For example, in Figure 4-1c, an interaction type of antagonism at one set of doses ([ERY]= 125 μM, [AMP] = 0.39 μM, and [CLI] = 7.81 μM) changes to synergy at another set of doses ([ERY] = 125 μM, [AMP] = 6.25 μM, and [CLI] = 125 μM). Understanding how drugs interact in a dose-specific way will help to avoid conflicting results and potentially detrimental antagonistic combinations being applied in the wrong setting [167, 168]. Importantly, fluctuating drug dosages could be used to create fluctuating selection pressures for cell populations. Indeed, evolutionary dynamics of a population can change drastically in changing environments [169, 170] and fluctuating environments can lead to higher levels of genetic diversity and biodiversity [171],

evolution of generalist over specialist species [33], and other evolutionary and ecological phenomena. To assess whether this picture of drug interactions as strongly dose dependent goes beyond these particular drugs for this specific strain of *E. coli*, other drugs or other organisms need to be explicitly examined. Further detailed data and identification of general patterns across bacterial strains or drugs will contribute to better methods for predictions and might aid the understanding of the underlying mechanisms of these complex interactions, which is currently lacking.

Zimmer *et al*. [148]proposed a model that predicts higher-order interactions at a full range of doses based only on pairwise interactions at low doses. We find component pairwise interactions are the largest contributor to overall net interactions, suggesting the approach of Zimmer *et al.* may be frequently useful but with one important caveat that it does not apply to emergent interactions. Specifically, we show emergent interactions are independent of pairwise interactions and conclude that higher-order *emergent* interactions are not easily predictable or understood using the framework of Zimmer *et al*. That is, for most of the three-drug combinations, the pairwise *DA2* is a reasonable predictor of three-way net interaction (*DA*3), but it does not correlate well with or usefully predict *E3*. Moreover, even *net* synergistic three-way *DA3* is not always predictable from component pairwise interactions. Nevertheless, it still is more correlated with *E3*, demonstrating that the net interaction arises from the emergent part as opposed to its lower-order components. For such cases, inferences based on the Zimmer *et al.* model can be especially misleading. This critical distinction appears to be absent from the literature, possible because previous studies on dose-dependent interactions have been conducted with either limited numbers of drug combinations, with drugs at fixed doses, or have analyzed interactions with methods that do not at all between distinguish net versus emergent interactions. Our study remedies both the lack of data

and missing analysis for emergent interactions for dose dependency. Crucially, our studies examine emergent interactions, rather than interactions arising solely from deviations from additivity.

Finally, we acknowledge that examining the whole-drug space for three-drug combinations can be extremely time consuming and expensive. An intriguing recent work by Cokol *et al.* [172] sampled data that correspond to a portion of our interaction landscape in order to infer the interaction type based on the Loewe additivity model in which it is assumed that a drug cannot interact with itself [173]. However, this methodology requires that the interactions be uniform throughout the entire interaction space, such that the contours stay either concave or convex across all doses. That is, the Cokol *et al.* framework assumes that there is no dose dependency— meaning no transitions between subspaces of interaction types. In contrast, our study using Bliss Independence models—which applies to single-dose measurements and makes no assumptions about dose dependency—shows that drug interactions generally are strongly affected by dose when we look at the entire interaction landscape. These fundamental discrepancies between the Bliss and Loewe models are also observed in two-drug interactions [174]. Future work to understand the meaning of these differences, which are intricately connected to the domain of Bliss versus Loewe models, are therefore greatly needed.

The advantage of our framework is its ability to disentangle the overall net interactions from higher-order emergent interactions that require component drugs to predict and to understand. Indeed, intuiting and thus understanding the complexity of drug interactions is aided by our introduction of interaction landscapes along with our results that regional synergy and antagonism are buffered by additivity and transition smoothly between interaction types. Our results explicitly demonstrate and highlight the independence of higher-order interactions from pairwise pieces and

urges the careful consideration and evaluation of any predictive approach for studying how higher-order interactions depend on lower-order components [175, 176].

Such insight is needed because combinatorial therapy is an extremely common practice in complex, chronic diseases such as hypertension, infectious disease, and cancer [177, 178], and because it could be strategically valuable and informative for preventing the evolution of resistance. Visualization and analysis of multi-dimensional interaction data is a challenge faced by an increasing number of disciplines as experimental advances for collecting big data continue to grow. By combining our large dataset with a rigorous theoretical framework to quantify both net and emergent interactions, our approach enables new insights via the detection and quantification of how multi-drug interaction landscapes are structured from low to high doses or for small or large numbers of drugs.

4.5 Acknowledgements

We thank Nina Singh and Cynthia White for comments on the manuscript. We thank Bryan France, Jackie Song, and Bobby Tofig for the laboratory assistance.

CHAPTER 5

Fitness landscapes across environmental gradients reveal changes in the direction and magnitude of epistasis

5.1 Introduction

The vision of evolution as a hill climbing process, introduced by Sewall Wright, has motivated numerous studies on how organisms move up to higher fitness peaks in a mountainous fitness landscape [179, 180]. The concept of the fitness landscape has since been widely used to visualize genotype-fitness relationships, and to understand and even predict evolutionary dynamics [156, 180-184]. The ability to make accurate predictions varies tremendously depending on the topology of the fitness landscapes, including such characteristics as the number of fitness peaks, the area of low fitness between peaks or fitness valley, and the smoothness and ruggedness of the landscapes [181, 185-188].

The ruggedness of the fitness landscape is caused by epistatic interactions [189, 190]. Epistasis describes the dependence between genes and their genetic background, or gene-gene interaction (GxG), and is extremely pervasive, because genes do not function in isolation [181]. It can also reveal functional organization and biological modularity of gene-gene interaction networks [62, 191]. Ruggedness obscures the fitness consequence of specific genes or mutations, and limit the predictability regarding which evolutionary path an organism is likely to take [181, 185, 192-194]. For example, the fitness cost of antibiotic resistance mutations can be alleviated by compensatory mutations, which are essential for the persistence of costly mutations in an antibiotic-free environment, where the selective pressure is relieved [195, 196]. This would result

in a rugged landscape caused by epistasis between resistance mutations and compensatory mutations [195, 196]. Thus, epistasis can drastically shape the accessibility of adaptive trajectory of mutations and facilitate or constrain evolution [197-199].

Compensatory mutations can be one solution to cross a fitness valley, by which an indirect evolutionary trajectory is taken [200]. Another proposed solution to crossing a valley involves the non-static nature of fitness landscapes [201]. Environmental perturbations can give rise to both quantitative and qualitative changes, such as changes in peak height, or cases where a peak emerges or submerges. This may allow populations to traverse through a fitness valley, or move away from a local fitness peak, but through a different landscape topology. Thus, a fluctuating environment may reveal an otherwise maladaptive path in rugged landscapes, enable evolutionary rescue, and prevent the population from being trapped in an evolutionary dead-end [201, 202].

Understanding epistatic interactions require understanding how changing environments affect these interactions. Some intriguing recent studies have shown how the structures and features of fitness landscapes can be profoundly different based on different environments [156, 170, 182, 183, 203, 204]. But environmental changes are not always abrupt or acute—they can be gradual and subtle. For example, antibiotic concentration gradients are present in soils and hospitals, and across organs and tissues in treated patients. In fact, environmental heterogeneity in the case of bacterial exposure to antibiotics has been proposed to be an important mechanism of resistance evolution [205, 206]. Yet there have been few studies that focus on the dynamics of this phenomenon, and understanding the changes in fitness landscapes across environmental gradients. Our study is designed to examine such changes in fitness landscapes by quantifying the structural differences and specifically answering the question of whether it is the extent of environmental

change or the type of environmental change that contribute to the difference in fitness landscape that we observe.

Here we analyze empirical fitness landscapes with a set of *Escherichia coli* mutants exposed to a range of concentration gradients from 15 different antibiotics. These concentration gradients mimic fluctuating environments either temporally, such as the degradation of antibiotics over time, or spatially, where the antibiotics in the environment are not distributed homogeneously. We use a suite of quantitative methods to analyze the general features, with emphasis on epistasis and landscape ruggedness. We find significantly positive epistasis among five deleterious mutations in our reference environment, where no antibiotics is added. We show overall ruggedness decreases as fitness decreases in some antibiotic gradients. But the change of ruggedness varies by rate and direction in smaller concentration ranges, or by different antibiotics. The structural changes of fitness landscapes are difficult to predict, with the appearance and disappearance of local fitness peaks being caused both by changing the type and concentration of antibiotics. Finally, pairwise epistasis changes both in sign and magnitude from a more rugged to a less rugged landscape, in contrast to higher-order epistasis which almost never changes in sign. Tuning the level of environmental stress can drive different signs of pairwise epistasis (from negative epistasis to positive or vice versa) that either promote specialization by more efficiently purging less fit genotypes or maintaining genetic variation as a potential strategy to combat environmental fluctuations.

5.2 Materials and Methods

Bacterial Strains

We used a collection of *Escherichia coli*, with a total of 32 strains, which has all possible combinations of five mutations (Table 5-1) that were the first to be substituted during a long-term evolution experiment [22] and were initially used in a previous study on epistasis between beneficial mutations [157] The ancestral strain was an *E. coli* B clone, a commonly used laboratory strain for many microbial experimental evolutionary studies [207, 208].

Table 5-1. Five mutations of *E. coli* used in the study.

Gene or gene region	***Abbreviation***	***Type of mutation***	***Gene Description***	***Binary code***
rbs	r	SNP	Ribose catabolism	10000
topA	t	SNP	Topoisomerase I	01000
spoT	s	SNP	Stringent response regulator	00100
glmUS	g	Insertion (1bp)	Cell wall biosynthesis	00010
pykF	p	SNP	Pyruvate kinase	00001

Culture and growth condition

We used LB broth (10 g/L tryptone, 5 g/L yeast extract, and 10 g/L NaCl per liter) for cultivating and maintaining *E. coli* strains. The strains were originally evolved in Davis minimal broth with 0.025 g glucose per liter [209]. For each strain, a single colony was inoculated into 2 mL of LB and grown for 24 hours. Following the incubation, the culture was mixed with 2 mL of 50% glycerol and 50 μL aliquots of the mixture were used to generate bacterial cell stocks with 25% glycerol for storing at -80°C. Each experiment was started with a thawed aliquot stock by inoculating 20 μL into 2 mL of LB media. The culture was incubated at 37°C until it reached

exponential growth phase (an OD of 0.5) and diluted to maintain 10^4 cells per experimental condition.

Experimental design

We subjected all strains to a range of concentrations of antibiotics to create a gradually changing environment. The concentration gradients were established with 20 steps of 2-fold dilutions of a single antibiotic (Table 5-2). Antibiotics used include erythromycin (ERY), ampicillin (AMP), clindamycin (CLI), streptomycin (STR), nitrofurantoin (NTR), cefoxitin (FOX), and trimethoprim (TMP), all from Sigma (St Louis, Mo), and ciprofloxacin (CPR) from MP Biomedicals (Santa Ana, Ca). All antibiotics were dissolved in 100% DMSO (Sigma) except for STR which was dissolved in 50% DMSO, due to limited solubility in 100% DMSO. The following preparations were completed with automated liquid handling system in the Molecular Screening Shared Resources facility at UCLA. A 20-step two-fold serial dilution was prepared for each antibiotic with starting concentration at 100x the experimented concentrations (or the starting concentration in Table 5-2) of 70 μL in DMSO, filled into a 384-well source plate. Meanwhile, 25 μL of LB per well were prefilled into a second 384-well plates using the Multidrop 384 (Thermo Scientific). Next, 500 nL from the source plate were delivered into the prefilled plate using the Biomek FX (Beckman Coulter) with a pin tool (V&P Scientific). Then, 25 μL of bacteria inoculum was added to each well to reach a final 50 μL per well with 1% DMSO. Each plate included negative controls (media alone), vehicle controls (media with 1% DMSO), and positive controls (media with 1% DMSO and cells). The plates were incubated at 37°C with OD_{595} measurement for cell density at 12 and 24 hours. A total of 38,400 wells were screened for each of the 32 strains in 300 distinct environments with 4 replicates.

Table 5-2 List of antibiotics used in the study.

Antibiotic	*Abbreviation*	*Maximum concentration (mM)*	*Minimum concentration (nM)*	*Molecular weight (g/mol)*	*IC50* (μM)*
Erythromycin	ERY	3	5.722	733.93	12.3
Clindamycin	CLI	3	5.722	461.44	1499
Levofloxacin	LVX	0.25	0.048	361.37	0.24
Ciprofloxacin	CPR	0.25	0.048	385.82	0.06
Chloramphenicol	CHL	1	1.907	445.18	153
Tetracycline	TET	1	1.907	444.43	0.41
Doxycycline	DOX	1	1.907	512.94	0.96
Nitrofurantoin	NTR	1	1.907	238.16	-
Piperacillin	PIP	1	1.907	539.54	0.76
Spectinomycin	SPT	1	1.907	367.00	384.4
Cefoxitin	FOX	1	1.907	449.43	1.37
Ampicillin	AMP	1	1.907	371.39	1.55
Trimethoprim	TMP	1	1.907	290.32	0.58
Sulfamonomethoxine	SLF	1	1.907	280.30	121.6
Amikacin	AMK	0.125	0.238	585.60	23.45

Epistasis

Epistasis between pairs of mutations are calculated as

$\varepsilon = \log10(W_0W_{AB}/W_AW_B)$

where W_0 is the fitness without either mutation, W_A is the fitness with mutation A, W_B is the fitness with mutation B, and W_{AB} is the fitness of the population with both mutations. This results in negative epistasis ($\varepsilon < 0$) when the double-mutant has lower fitness than the non-epistatic expectation (i.e., $W_0W_{AB} < W_AW_B$), and positive epistasis ($\varepsilon < 0$) when the combined effect of the two mutations yields a higher than expected fitness [210].

Extending the pairwise epistasis to epistasis with *N* mutations is generalized to the following form [157]:

$\varepsilon = \log10(W_0W_{AB \ldots N} / W_AW_B \ldots W_N)$

Ruggedness

Peaks, i.e., genotypes with higher fitness than all their one-mutant neighbors, can be used as a proxy for landscape ruggedness [211]. The more rugged a landscape, the more peaks it will generally have, whereas a smooth landscape will have just a single peak. To compare the ruggedness among different landscapes, we count the average number of peaks within all subgraphs of size four. That is, if a landscape has more than four loci, then every four-locus subgraph is constructed and the number of peaks is counted. We use the number of peaks because it is an intuitive measure of how rugged a landscape is, but emphasize that the number of peaks has been shown to correlate with other, less intuitive measures of landscape ruggedness such as the steps of adaptive walks to reach a peak that also reflect the relative contribution of epistasis [211]. In a smooth landscape with a single peak, the ruggedness is 1.

5.3 Results

Significant antagonistic epistasis in a rugged fitness landscape was observed for the antibiotic-free environment.

Our control, or reference environment was defined as growth in rich media (LB broth). The choice of LB broth allowed us to examine a broader range of antibiotic concentrations since bacterial growth with antibiotics are generally higher in rich media than it is in minimal media. As a result, the effects of all five single mutations, evolved in minimal media, were no longer beneficial but deleterious, except for one (*pyfK*) that remained nearly neutral (Fig 5-1a.). The observed fitness landscapes (Fig 5-1a.) were profoundly rugged, with a ruggedness of 3.4. The ruggedness is measured by counting the average number of peaks within all subgraphs of size four.

Therefore, the maximal ruggedness would be 8, in subgraphs of 4 genotypes. In a smooth landscape, ruggedness would be 1. We also calculated the overall epistasis of the antibiotic-free environment to be antagonistic with a positive mean at 0.265. An epistasis of 1 means the observed fitness for genotypes with more than one mutation was 10 times higher than expected compared to a null model of no epistasis. An epistasis of 0.265 means the observed fitness is approximately 1.84 times higher than expected, which is very large.

Figure 5-1 The observed fitness landscape in an antibiotic-free environment is highly rugged due to significant antagonistic epistasis. a. Observed fitness landscape of the reference (antibiotic-free) environment, the number of mutations is plotted on the x-axis and fitness is on the y-axis. Fitness is plotted as the average of four experimental replicates. b. Expected fitness landscape of the reference environment, calculated using a multiplicative null model of epistasis by taking the product of individual fitness effects of the relevant mutations.

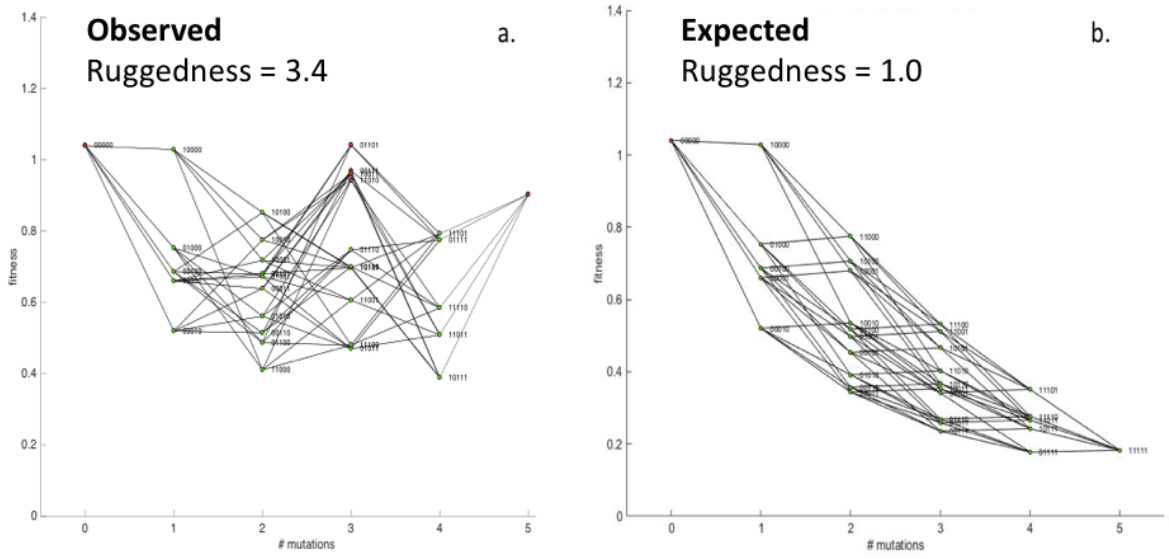

Ruggedness of fitness landscape generally decreases as environment gets more stressful.

We compared how fitness landscapes change over a concentration gradient, with the focus on ruggedness. Overall, the fitness of all genotypes decreases with increasing amount of antibiotics,

leading to different fitness distributions and distinct topology of fitness landscapes at each concentration step (Figure 5-2).

Figure 5-2 The landscape topology and fitness distribution are drastically different with different concentrations of a single antibiotic. The fitness landscape is plotted with the number of mutations on the x-axis and fitness on the y-axis. The fitness distribution of all genotypes for each landscape is shown on the right. Ciprofloxacin (CPR) is added in each condition at 0.006144 μM (low antibiotic dose), 0.012288 μM (intermediate antibiotic dose), and 0.024576 μM (high antibiotic dose).

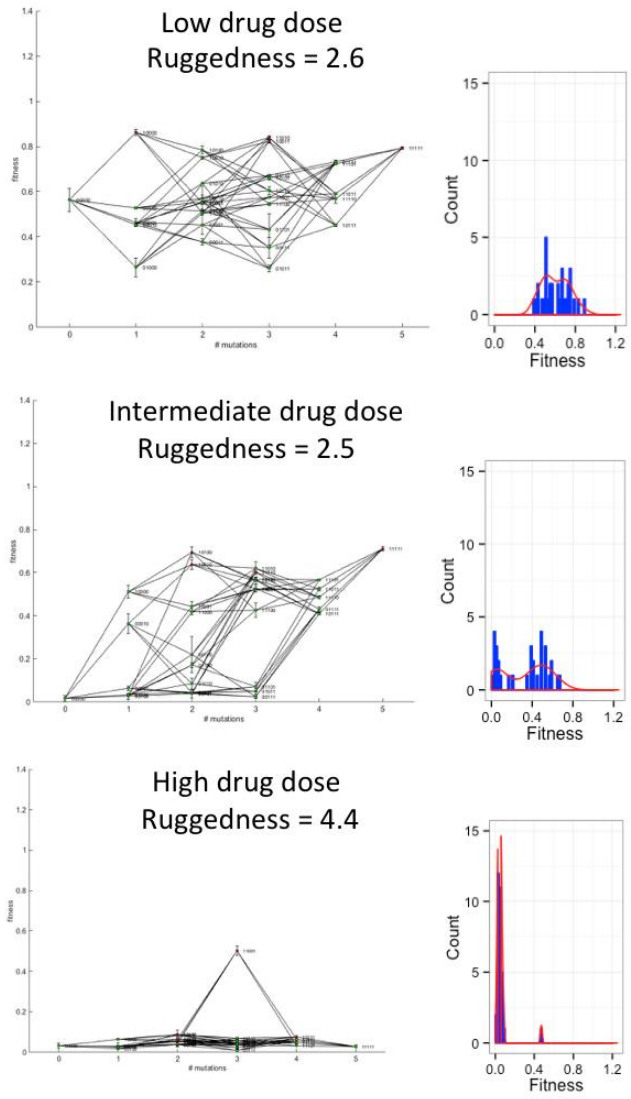

Among all 15 tested gradients, in general, ruggedness decreases when environments become increasingly stressful (Figure 5-3). However, with low amounts of antibiotics, ruggedness tends to fluctuate. In the case of SPT, CHL, and SLF, ruggedness is strikingly constant before a sharp decrease. For TMP and CPR, the drop is not as drastic, but ruggedness decreases overall. For CLI and ERY, we note a slight increase in ruggedness before the drop. We also see an opposite trend for FOX and AMP, where ruggedness seems to increase with increasing antibiotic concentrations, following the plateau. As the environment continues to become lethal and fitness landscapes flatten, the rugosity of the landscape becomes lower although the landscape can still exhibit ruggedness with multiple lower, local fitness peaks. These fitness peaks shift in an environmental gradient. For example, genotype 10010 emerged as a peak at sub-lethal concentrations, but as the concentrations decreased to a residual level, the peak disappeared (Figure 5-4). In comparison, genotype 11111 appears as a local fitness peak and remained as a peak through a much wider concentration gradient (Figure 5-4).

Figure 5-3 Ruggedness generally decreases when environments become more stressful. Each panel shows the change of ruggedness over a 20-step 2-fold concentration gradient for a specific antibiotic. A local regression model is used to fit the data, with the shaded area showing the 95% confidence interval.

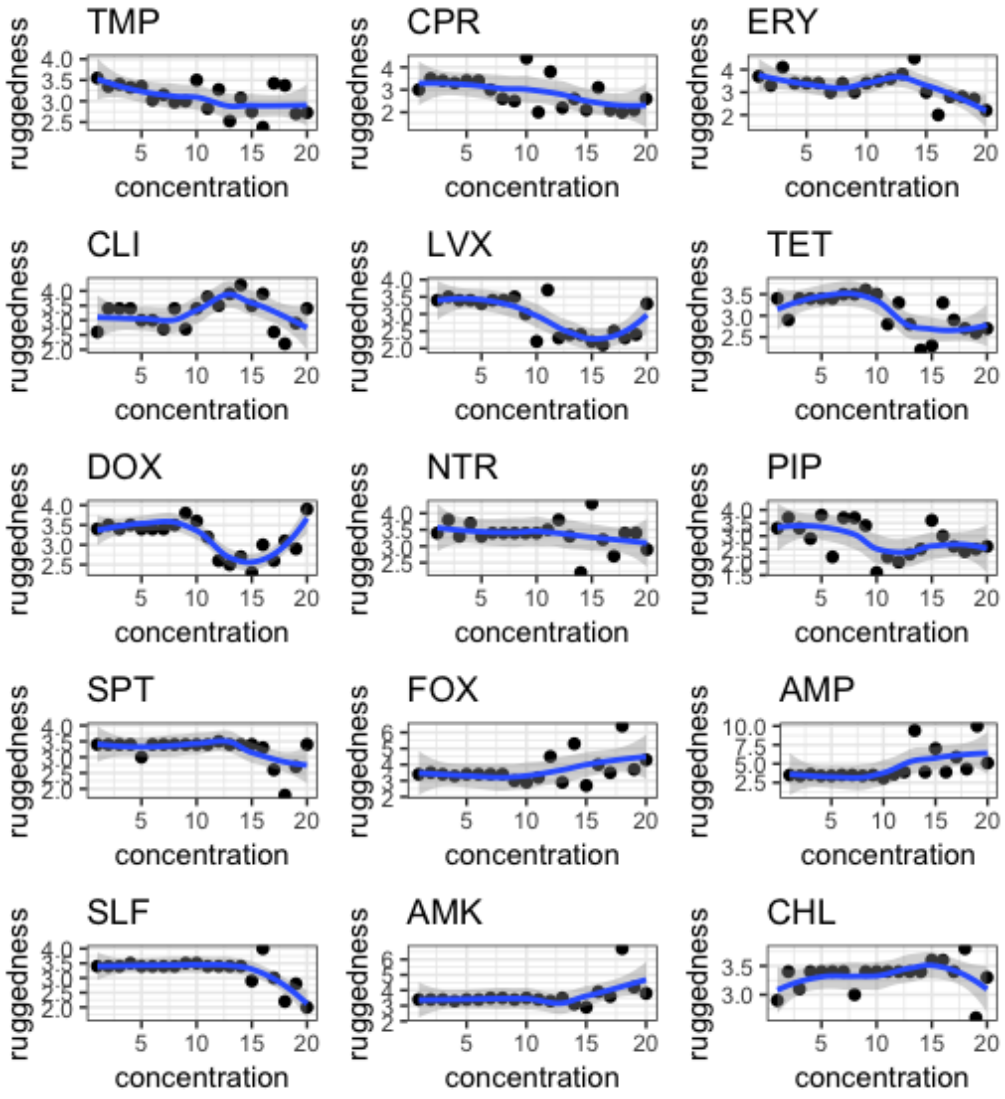

Figure 5-4 The appearance or disapperance of fitness peaks are concentration dependent. CPR is serially diluted of 2 fold at each step. Each row corresponds to a concentration of CPR , arranged from highest to lowest, gray for lethal concentrations where the mean fitness is less than 0.1, green for sub-lethal concentrations, and blue for antibiotic concentrations with no measurable fitness effect. The genotypes are aligned on the x axis. A presence of a bar indicates the corresponding genoytpe is a local maximum or fitness peak.

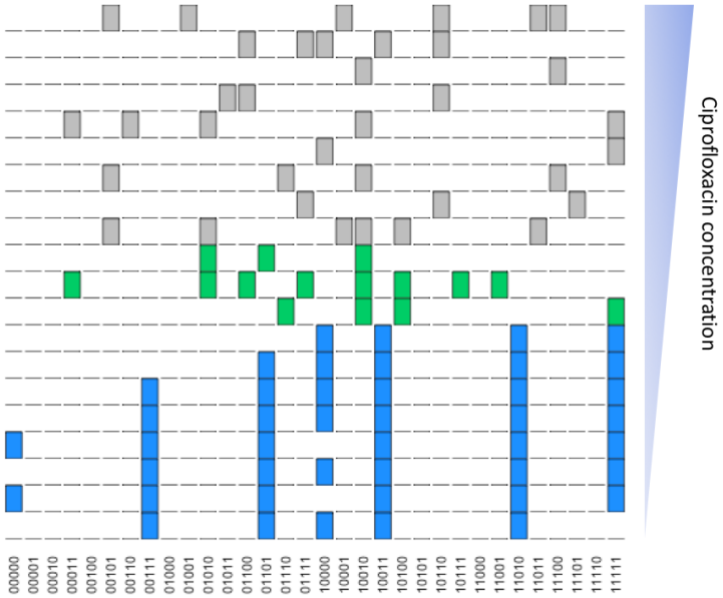

As ruggedness decreases, pairwise epistasis switches sign, where higher-order epistasis almost always changes in magnitude only.

Since ruggedness is caused by epistasis, we next set out to compare epistasis between the most and the least rugged landscapes in each concentration gradients. We calculate epistasis with any number of mutations (from 2 to 5) and the wild-type is always defined as the genotype with none of the five mutations. Among the 15 different gradients, 11 of the most rugged landscapes are associated with a higher antibiotic concentration (a more stressed environment) than the least rugged landscape. The four exceptions are NTR, FOX, AMP, and AMK. The higher rugged landscapes for these 4 cases and TMP also have some genotypes with zero fitness value. Therefore,

the epistasis was not concluded and excluded for the figure. For all the other antibiotics, we show the ratio of epistasis between a high rugged and low rugged landscape for all possible combinations of the 5 mutations and group them by epistasis order (Figure 5-5). In general, epistasis at all orders is higher in a more rugged compared to a less rugged landscape. For pairwise epistasis, we see some ratio with a negative value, indicating a change in the sign of epistasis. For epistasis beyond pairwise (3, 4 and 5 way), we rarely see a change in the sign, but only change in the magnitude.

Figure 5-5 From a high rugged to low rugged landscape over each antibiotic gradient, pairwise epistasis changes sign, while higher order epistasis almost always changes in magnitude. Each panel shows one specific gradient, with the ratio of epistasis between a high-rugged to low-rugged landscape. In each panel, a total of 26 epistatic interactions from all possible combinations of 5 mutations is shown. The interactions are grouped of by the number of mutations or the epistasis order, indicated by the number at the top of each box. The dotted line is added for a ratio of 1 for no change.

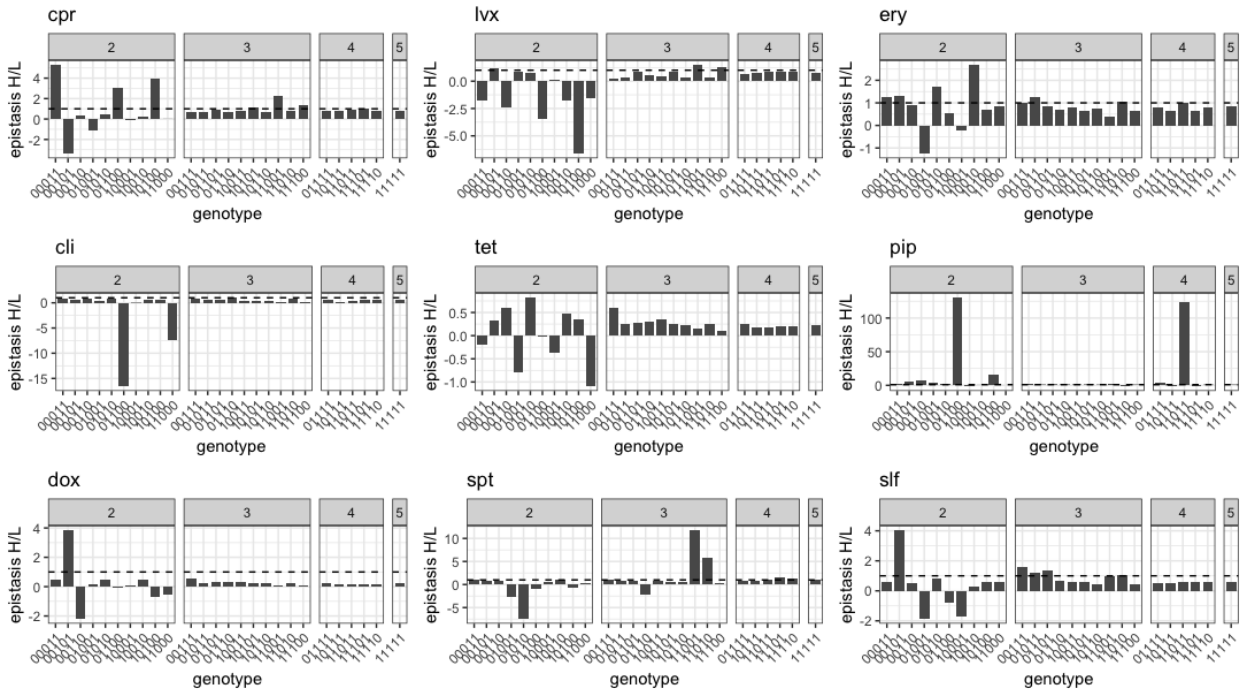

The switch in the sign of pairwise epistasis from a high rugged landscape to a low rugged landscape is specific to a single mutation.

To take a closer look at the change in sign of pairwise interaction, we choose LVX as a representative, where we see the most sign changes (6 out of 10 pairwise) (Figure 5-6). We also included the change of pairwise interactions for all the remaining drugs in the supplemental information (Figure 5-7). The switch in epistasis sign does not seem to be consistently in one direction (i. e. from negative to positive or vice versa), from a high rugged to low rugged landscape. Three out of the six sign changes are from negative in a high-rugged landscape to positive in a low-rugged landscape. All three cases involve the same mutation, namely *topA* (which encodes a type of topoisomerase that relaxes DNA supercoiling) where the single mutant is more fit than the wild-type at the concentration for higher ruggedness. The rest of the three switches is from positive epistasis in a more rugged landscape to negative in a less rugged landscape. Two of them involves the mutation of *spoT*, which encodes a key enzyme in the stringent response that is first recognized in starved bacterial cells. The third case of sign switching directions is an exception in the sense that it does not involve *spoT*, but despite the difference in sign, the change is less significant from 0.08 to -0.051 (Figure 5-6).

Figure 5-6 Pairwise epistasis switches sign from a high rugged landscape to low rugged landscape, over the concentration gradient of LVX. All ten possible pairwise epistasis from 5 single mutations is shown. Every single mutation is listed by the first letter of the gene for simplicity. The color and the exact value for each pairwise epistasis are shown for comparison.

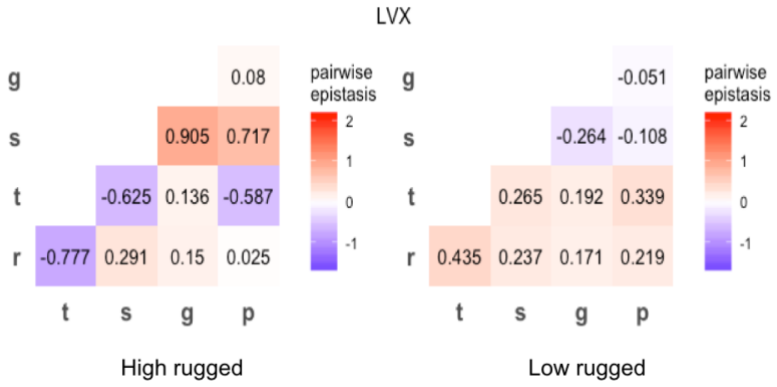

Figure 5-7 Pairwise epistasis switches directions from a high rugged landscape to low rugged landscape, over the concentration gradient of various drugs. All ten possible pairwise epistasis from 5 single mutations is shown. Every single mutation is listed by the first letter of the gene for simplicity. The color and the exact value for each pairwise epistasis are shown for comparison.

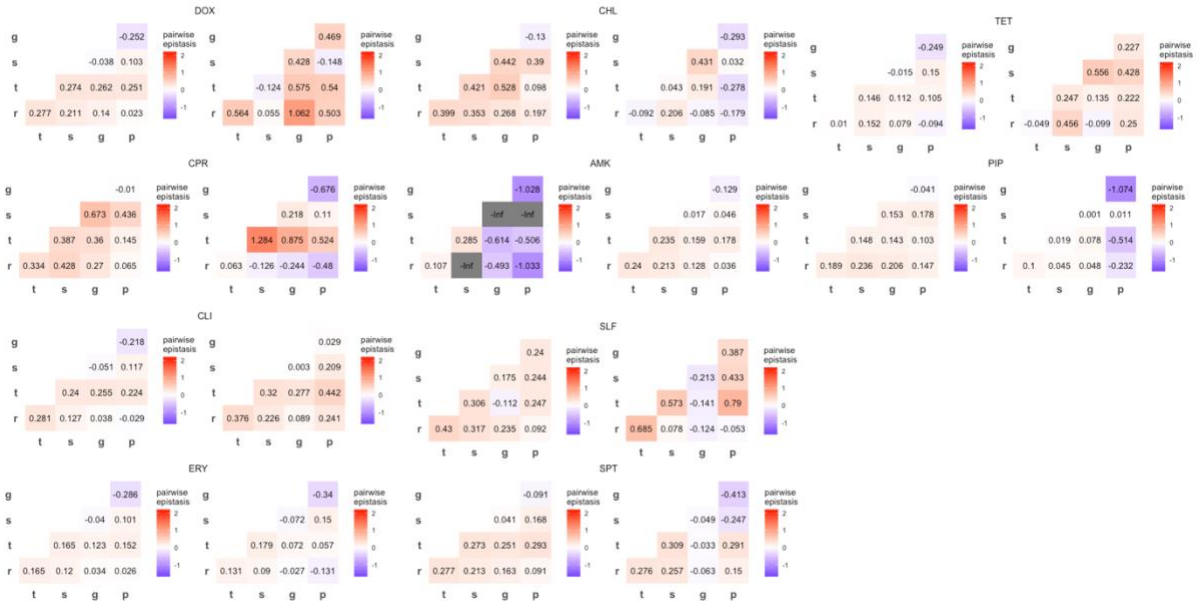

5.4 Discussion

Through a suite of quantitative analyses of fitness landscapes, we examined the changes of landscape topology upon gradual fluctuations of various environmental gradients. Not surprisingly, the degree of structural change depends on the magnitude of environmental fluctuations. As the environments get increasingly stressful, the fitness of all genotypes decreased towards zero. Some genotypes are more sensitive in that their fitness approached zero faster, leading to a regional collapse of the fitness landscapes, meaning the landscapes typically do not collapse in a whole but in parts first. The ruggedness of the landscapes generally decreases with the fitness decrease over a large gradient, although the rate and direction of change are specific to the stressor (antibiotic). Along with the change of ruggedness, the underlying change of epistasis is complex. Particularly,

pairwise epistasis changes frequently in both the magnitude and sign, where higher order epistasis almost never changes in sign and only change in magnitude. Moreover, the sign switches of pairwise epistasis typically involves the drastic fitness difference of a single mutation from one antibiotic concentration to another. Our results suggest epistasis can be a potential force to drive different evolutionary strategies between promoting specialization with positive pairwise epistasis and maintaining genetic variation with negative pairwise epistasis.

In recent years, technological advances in molecular biology such as genetic manipulations and sequencing have made empirical work on fitness landscapes possible. Many studies have revealed general patterns including the significance and pervasiveness of epistasis and its environmental dependency [156, 157, 170, 180, 181, 183, 185, 203]. Environmental change is one of the most important stochastic factors that affect evolution. Therefore, to understand or even predict the process of evolution through the lens of the fitness landscape requires considering the environmental change. Here we are motivated by the question of how much environmental change needs to be considered, whether it is the extent of change or the type of change that matters.

A recent study on multi-environment fitness landscapes of a tRNA gene of yeast compared the fitness correlation between an optimal growth environment and three perturbed environments with cold, heat and oxidative stress [183]. The fitness of mutants in each environment was generally well correlated, with similar fitness landscape across the examined conditions. But the difference in correlation appeared to be hierarchical, depending on the extent of environmental variation. For example, fitness correlation was much higher between the cold-stressed and reference environment than it was between a cold-stressed and heat-stressed condition. Another study from Matsui *et al.* also noted the magnitude of environmental effect on gene interaction was dependent on the severity of environmental perturbation [212]. Other studies on fitness landscapes

of antibiotic resistance genes in bacteria have shown dramatically different landscapes with different antibiotics (environments) or the concentrations of antibiotics (degree of environmental fluctuations) [170, 203]. Mira *et al.* concluded that the effect of changing the concentration of an antibiotic could have an equally large effect as that from changing the type of antibiotic [203]. Our study shows that when comparing fitness landscapes across various environments, the magnitude of environmental change is crucial for the amount of change we observe in bacterial populations.

One interpretation of the decrease of ruggedness as environments get more stressful is that there is a relaxed evolutionary constraint, where fitness landscapes have a smaller number of local maxima. Therefore, more genotypes can be connected in a path that leads to the highest fitness endpoint available. Meanwhile, the relaxed constraint also means that one genotype would be less committed in a path to any specific peak. A previous study has extensively analyzed the landscapes of a transcription factors from different eukaryotic species using their binding affinity [213]. The authors showed the number of peaks and the types of epistasis were directly related to the navigability of landscapes, which may have been an important mechanism to generate variation and innovation of transcriptional regulation [213]. Moreover, the magnitude of epistasis with any number of mutations generally is lower in a less rugged landscape, which is not surprising, since epistasis causes ruggedness.

Although the pairwise epistasis often changes in sign, epistasis at higher-orders almost always only changes in magnitude. This could be explained by how genes or mutations are organized genetically or biochemically. In general, the order of action of genes in a regulatory hierarchy governs the phenotypic effect of epistatic mutations [214]. Disabling two genes in genetically compensatory pathways can lead to synthetic lethality [215], while disabling two genes in the same linear biochemical pathway can have a much more modest effect [214]. Weinreich *et*

al. assessed the influence of this principle by examining 16 published, biological fitness landscapes [216]. They found that on average the effects of epistasis declined with the order of epistasis. Another example is a study from Palmer *et al.* where seven mutations in the dihydrofolate reductase gene in *E. coli* that confer resistance to trimethoprim were examined [217]. They showed that adding a third-order interaction did not create more pathways or peaks than the number of distinct peaks generated by pairwise sign epistasis [217]. The significance and prevalence of higher order interactions have been controversial with some studies showing compelling results on increasingly frequent higher order interactions with increasing interacting components [218], while other studies show a pattern of diminishing return [219]. We suspect these differences probably arise from different biological systems or the mathematical frameworks used to quantify interactions.

The change in sign of pairwise epistasis can have profound evolutionary consequences. For example, in the environment of LVX where ruggedness is high, *topA* is the fittest single mutant. The gene *topA* in *E. coli* encodes for topoisomerase I, which is responsible for relaxing negative supercoiling of the DNA by causing single-stranded DNA breaks [220]. The antibiotic LVX acts by inhibiting topoisomerase type II (also known as DNA gyrase) and type IV, and therefore impairs the replication, transcription, recombination, and repair of DNA [221]. Resistance to LVX or other fluoroquinolones typically involves mechanisms to alter the structure of the targeted topoisomerases so the antibiotics can no longer bind to their targets or the binding affinity is reduced [221]. Although *topA* is not a direct target, some studies show it could be the subject of selection for fluoroquinolone resistance [222]. The exact mechanism of resistance from non-targeted genes is not fully understood [222]. It is possible that mutations in genes that control supercoiling, such as *topA* and *fis,* can impact the evolutionary flexibility of cell due to the overall

changes in chromosome structure [222]. This could explain the fitness advantage that we observe for *topA* mutant when CPR and LVX are added.

When a secondary mutation is paired with *topA*, they tend to interact synergistically, where the combined fitness is smaller than expected. As a result, the double mutants could be removed from the population more efficiently because they are much less fit than expected with no epistasis. In the context of antibiotic resistance evolution, the synergistic epistasis at the specific antibiotic concentration would promote the specialization of *topA* mutant, while driving other genotypes extinct. This type of dose specialization aided by epistasis can be an important mechanism of resistance evolution.

When the environment gets more stressful—that is, at higher antibiotic concentrations—the fitness of *topA* mutant decreases to a similar level as the other mutations, and pairwise epistasis that involves *topA* switches signs, from negative to positive. Here the fitness of a double mutant is greater than expected based on the fitness effects of the two single mutants. This is therefore an antagonistic epistasis between two deleterious mutations, which is prevalent in our dataset and common in some studies with bacteria [223-225].

A previous study has suggested the mechanism for such antagonistic epistasis of deleterious mutations. Researchers used an error-prone DNA polymerase of *Salmonella* where deleterious mutations could accumulate randomly [226]. They found an increased expression of heat shock chaperones, namely DnaK and GroEL, in their evolved lineages, that have been shown to assist in the folding of proteins with damaged confirmation [227]. Experimentally-induced overproduction of GroEL further rescued the fitness decrease. For bacterial population that experience constant environmental fluctuations, it might be advantageous to maintain genetic variation where a genotype may be less fit in one environment but more fit in another [228].

For deleterious mutations, negative (synergistic) epistasis is proposed to be advantageous in purging those mutations [229-231], when the fitness reduction is greater with the combination of deleterious mutations than expected based on their individual effects. This is a critical premise for the mutational deterministic hypothesis which postulates that high recombination rates are maintained due to synergistic epistasis where deleterious mutations can be removed more efficiently [232]. From simpler genomes of RNA viruses to more complex multicellular eukaryotes, epistasis tends to transition from antagonistic to synergistic [225, 233]. In bacteria, *E. coli* was shown to exhibit roughly equal amounts of synergistic and antagonistic epistasis by measuring the individual and combined pairwise effects on fitness of mutations in recombinant genotypes [234]. Here we show that environmental differences can be a force that drives the change between synergistic epistasis that purges mutations and antagonistic epistasis that could help maintain genetic variation.

Our work can help explain adaptation in a heterogeneous environment, by examining the changes in fitness landscapes across various environmental gradients. Since concentration gradients of antibiotics is likely ubiquitous from natural soil environment [235] to human tissues and organs [236]. Spatial heterogeneity has been proposed to play a role in the emergence and maintenance of genetic diversity and antibiotic resistance evolution [206, 237-245]. Our findings on the changes in fitness landscape topology and the underlying differences in ruggedness and epistasis interaction provide empirical evidence for a potential strategy for bacterial populations to combat environmental fluctuations or persist in a heterogeneous environment.

5.5 Acknowledgements

We thank Tim Cooper for gifting us the bacterial strains. We thank Mauricio Cruz-Loya, Natalie Lozano, and Nina Singh for helpful comments and discussion on the manuscript. We thank Jackie Song and Bobby Tofig for laboratory assistance.

REFERENCES

1. Isaak, D.J., S.J. Wenger, and M.K. Young, *Big biology meets microclimatology: defining thermal niches of ectotherms at landscape scales for conservation planning.* Ecological Applications, 2017. **27**(3): p. 977-990.
2. Ackerly, D.D., *Community assembly, niche conservatism, and adaptive evolution in changing environments.* International Journal of Plant Sciences, 2003. **164**(S3): p. S165-S184.
3. Ricklefs, R.E., *A comprehensive framework for global patterns in biodiversity.* Ecology letters, 2004. **7**(1): p. 1-15.
4. Ricklefs, R.E., *Evolutionary diversification and the origin of the diversity–environment relationship.* Ecology, 2006. **87**(sp7): p. S3-S13.
5. Chase, J.M., *Stochastic community assembly causes higher biodiversity in more productive environments.* Science, 2010. **328**(5984): p. 1388-1391.
6. Hoffmann, A.A. and P.A. Parsons, *Evolutionary genetics and environmental stress*. 1991: Oxford University Press.
7. Cahill, A.E., et al., *How does climate change cause extinction?* Proceedings of the Royal Society B: Biological Sciences, 2013. **280**(1750): p. 20121890.
8. Adams, H.D., et al., *Temperature sensitivity of drought-induced tree mortality portends increased regional die-off under global-change-type drought.* Proceedings of the national academy of sciences, 2009. **106**(17): p. 7063-7066.

9. KOEHN, R.K. and B.L. BAYNE, *Towards a physiological and genetical understanding of the energetics of the stress response.* Biological Journal of the Linnean Society, 1989. **37**(1-2): p. 157-171.

10. Freedman, B., *Ecological effects of environmental stressors*. 2015.

11. Costantini, D., *Oxidative stress in ecology and evolution: lessons from avian studies.* Ecology letters, 2008. **11**(11): p. 1238-1251.

12. Rothschild, L.J. and R.L. Mancinelli, *Life in extreme environments.* Nature, 2001. **409**(6823): p. 1092-1101.

13. Rampelotto, P.H., *Extremophiles and extreme environments.* Life (Basel, Switzerland), 2013. **3**(3): p. 482-485.

14. Lim, J.Y., J. Yoon, and C.J. Hovde, *A brief overview of Escherichia coli O157:H7 and its plasmid O157.* Journal of microbiology and biotechnology, 2010. **20**(1): p. 5-14.

15. Prevention, C.f.D.C.a. *Antibiotic resistance threats in the United States, 2013*. 2013.

16. Jacoby, R., et al., *The Role of Soil Microorganisms in Plant Mineral Nutrition-Current Knowledge and Future Directions.* Frontiers in plant science, 2017. **8**: p. 1617-1617.

17. Adesemoye, A., H. Torbert, and J. Kloepper, *Increased plant uptake of nitrogen from 15N-depleted fertilizer using plant growth-promoting rhizobacteria.* Applied Soil Ecology, 2010. **46**(1): p. 54-58.

18. The Human Microbiome Project, C., et al., *Structure, function and diversity of the healthy human microbiome.* Nature, 2012. **486**: p. 207.

19. Sekirov, I., et al., *Gut Microbiota in Health and Disease.* Physiological Reviews, 2010. **90**(3): p. 859-904.

20. Vuong, H.E., et al., *The Microbiome and Host Behavior.* Annual Review of Neuroscience, 2017. **40**(1): p. 21-49.

21. Chen, X., et al., *Metabolic engineering of Escherichia coli: a sustainable industrial platform for bio-based chemical production.* Biotechnology advances, 2013. **31**(8): p. 1200-1223.

22. Lenski, R.E., et al., *Long-Term Experimental Evolution in Escherichia coli. I. Adaptation and Divergence During 2,000 Generations.* The American Naturalist, 1991. **138**(6): p. 1315-1341.

23. O'Malley, M.A., *The Experimental Study of Bacterial Evolution and Its Implications for the Modern Synthesis of Evolutionary Biology.* Journal of the History of Biology, 2018. **51**(2): p. 319-354.

24. Crick, F., et al., *General nature of the genetic code for proteins.* 1961.

25. Jacob, F. and J. Monod, *Genetic regulatory mechanisms in the synthesis of proteins.* Journal of molecular biology, 1961. **3**(3): p. 318-356.

26. Atwood, K.C., L.K. Schneider, and F.J. Ryan, *Periodic selection in Escherichia coli.* Proceedings of the National Academy of Sciences of the United States of America, 1951. **37**(3): p. 146.

27. Barrick, J.E. and R.E. Lenski, *Genome dynamics during experimental evolution.* Nature Reviews Genetics, 2013. **14**(12): p. 827.

28. Clarke, P.H., *Experiments in microbial evolution.* 1978.

29. Stearns, S.C., *Hoffman, A. A. and Parsons, P. A. 1991. Evolutionary Genetics and Environmental Stress. Oxford University Press. paper .ix + 284 pp., illus. ISBN: 0-19-854081-7.* Journal of Evolutionary Biology, 1994. **7**(5): p. 634-635.

30. Meyers, L.A. and J.J. Bull, *Fighting change with change: adaptive variation in an uncertain world.* Trends in Ecology & Evolution, 2002. **17**(12): p. 551-557.

31. Kohanski, M.A., et al., *A Common Mechanism of Cellular Death Induced by Bactericidal Antibiotics.* Cell, 2007. **130**(5): p. 797-810.

32. Cho, H., T. Uehara, and Thomas G. Bernhardt, *Beta-Lactam Antibiotics Induce a Lethal Malfunctioning of the Bacterial Cell Wall Synthesis Machinery.* Cell, 2014. **159**(6): p. 1300-1311.

33. Gilchrist, G.W., *Specialists and generalists in changing environments. I. Fitness landscapes of thermal sensitivity.* The American Naturalist, 1995. **146**(2): p. 252-270.

34. Csonka, L.N. and A.D. Hanson, *PROKARYOTIC OSMOREGULATION: Genetics and Physiology.* Annual Review of Microbiology, 1991. **45**(1): p. 569-606.

35. Sharma, U.K. and D. Chatterji, *Transcriptional switching in Escherichia coli during stress and starvation by modulation of σ70 activity.* FEMS Microbiology Reviews, 2010. **34**(5): p. 646-657.

36. Levy, S.B., *Active efflux mechanisms for antimicrobial resistance.* Antimicrobial Agents and Chemotherapy, 1992. **36**(4): p. 695.

37. Paulsen, I.T., et al., *A family of Gram-negative bacterial outer membrane factors that function in the export of proteins, carbohydrates, drugs and heavy metals from Gram-negative bacteria.* FEMS Microbiology Letters, 1997. **156**(1): p. 1-8.

38. Begic, S. and E.A. Worobec, *Regulation of Serratia marcescens ompF and ompC porin genes in response to osmotic stress, salicylate, temperature and pH.* Microbiology, 2006. **152**(2): p. 485-491.

39. Kaprelyants, A.S. and D.B. Kell, *Dormancy in stationary-phase cultures of Micrococcus luteus: flow cytometric analysis of starvation and resuscitation.* Appl. Environ. Microbiol., 1993. **59**(10): p. 3187-3196.

40. Bada, J.L. and A. Lazcano, *Some like it hot, but not the first biomolecules.* Science, 2002. **296**(5575): p. 1982-1983.

41. Braun, D. and A. Libchaber, *Thermal force approach to molecular evolution.* Physical Biology, 2004. **1**(1): p. P1.

42. Daniel, I., P. Oger, and R. Winter, *Origins of life and biochemistry under high-pressure conditions.* Chemical Society Reviews, 2006. **35**(10): p. 858-875.

43. Hazen, R.M., et al., *High pressure and the origin of life.* Journal of Physics: Condensed Matter, 2002. **14**(44): p. 11489.

44. Stetter, K.O., *Hyperthermophiles in the history of life.* Philosophical Transactions of the Royal Society B: Biological Sciences, 2006. **361**(1474): p. 1837-1843.

45. Schwartzman, D. and C. Lineweaver, *The hyperthermophilic origin of life revisited*. 2004, Portland Press Limited.

46. Åkerfelt, M., R.I. Morimoto, and L. Sistonen, *Heat shock factors: integrators of cell stress, development and lifespan.* Nature reviews Molecular cell biology, 2010. **11**(8): p. 545.

47. De, A.M., *Heat shock proteins: facts, thoughts, and dreams.* Shock (Augusta, Ga.), 1999. **11**(1): p. 1-12.

48. Lindquist, S., *The heat-shock response.* Annual review of biochemistry, 1986. **55**(1): p. 1151-1191.

49. Richter, K., M. Haslbeck, and J. Buchner, *The heat shock response: life on the verge of death.* Mol Cell, 2010. **40**(2): p. 253-66.

50. D'Costa, V.M., et al., *Antibiotic resistance is ancient.* Nature, 2011. **477**(7365): p. 457.

51. Dinh, T., I.T. Paulsen, and M.H. Saier, Jr., *A family of extracytoplasmic proteins that allow transport of large molecules across the outer membranes of gram-negative bacteria.* Journal of bacteriology, 1994. **176**(13): p. 3825-3831.

52. Battesti, A., N. Majdalani, and S. Gottesman, *The RpoS-mediated general stress response in Escherichia coli.* Annual review of microbiology, 2011. **65**: p. 189-213.

53. Gruber, T.M. and C.A. Gross, *Multiple sigma subunits and the partitioning of bacterial transcription space.* Annual Reviews in Microbiology, 2003. **57**(1): p. 441-466.

54. Somorin, Y., et al., *The general stress response is conserved in long-term soil-persistent strains of Escherichia coli.* Appl. Environ. Microbiol., 2016. **82**(15): p. 4628-4640.

55. Mondal, S., et al., *Impact of P-Site tRNA and antibiotics on ribosome mediated protein folding: studies using the Escherichia coli ribosome.* PLoS One, 2014. **9**(7): p. e101293.

56. Vabulas, R.M., et al., *Protein folding in the cytoplasm and the heat shock response.* Cold Spring Harbor perspectives in biology, 2010. **2**(12): p. a004390.

57. Cardoso, K., et al., *DnaK and GroEL are induced in response to antibiotic and heat shock in Acinetobacter baumannii.* Journal of medical microbiology, 2010. **59**(9): p. 1061-1068.

58. Loughman, K., et al., *Temperature-dependent gentamicin resistance of Francisella tularensis is mediated by uptake modulation.* Frontiers in microbiology, 2016. **7**: p. 37.

59. Rodríguez-Verdugo, A., B.S. Gaut, and O. Tenaillon, *Evolution of Escherichia coli rifampicin resistance in an antibiotic-free environment during thermal stress.* BMC evolutionary biology, 2013. **13**(1): p. 50.

60. Goltermann, L., L. Good, and T. Bentin, *Chaperonins fight aminoglycoside-induced protein misfolding and promote short-term tolerance in Escherichia coli.* Journal of Biological Chemistry, 2013. **288**(15): p. 10483-10489.

61. Poole, K., *Stress responses as determinants of antimicrobial resistance in Gram-negative bacteria.* Trends in microbiology, 2012. **20**(5): p. 227-234.

62. Segrè, D., et al., *Modular epistasis in yeast metabolism.* Nature Genetics, 2005. **37**(1): p. 77-83.

63. Yeh, P., A.I. Tschumi, and R. Kishony, *Functional classification of drugs by properties of their pairwise interactions.* Nat Genet, 2006. **38**(4): p. 489-94.

64. Bliss, C., *The toxicity of poisons applied jointly.* Annals of applied biology, 1939. **26**(3): p. 585-615.

65. Datsenko, K.A. and B.L. Wanner, *One-step inactivation of chromosomal genes in Escherichia coli K-12 using PCR products.* Proceedings of the National Academy of Sciences, 2000. **97**(12): p. 6640.

66. Zaslaver, A., et al., *A comprehensive library of fluorescent transcriptional reporters for Escherichia coli.* Nature methods, 2006. **3**(8): p. 623.

67. Rodriguez-Verdugo, A., B.S. Gaut, and O. Tenaillon, *Evolution of Escherichia coli rifampicin resistance in an antibiotic-free environment during thermal stress.* BMC Evol Biol, 2013. **13**: p. 50.

68. Mingeot-Leclercq, M.-P., Y. Glupczynski, and P.M. Tulkens, *Aminoglycosides: activity and resistance.* Antimicrobial agents and chemotherapy, 1999. **43**(4): p. 727-737.

69. Chopra, I. and M. Roberts, *Tetracycline antibiotics: mode of action, applications, molecular biology, and epidemiology of bacterial resistance.* Microbiol. Mol. Biol. Rev., 2001. **65**(2): p. 232-260.

70. Yamanaka, K., *Cold shock response in Escherichia coli.* Journal of molecular microbiology and biotechnology, 1999. **1**(2): p. 193-202.

71. Goldstein, E. and K. Drlica, *Regulation of bacterial DNA supercoiling: plasmid linking numbers vary with growth temperature.* Proceedings of the National Academy of Sciences, 1984. **81**(13): p. 4046-4050.

72. Mizushima, T., et al., *Increase in negative supercoiling of plasmid DNA in Escherichia coli exposed to cold shock.* Molecular microbiology, 1997. **23**(2): p. 381-386.

73. Niu, P., et al., *Overexpressed heat shock protein 70 protects cells against DNA damage caused by ultraviolet C in a dose-dependent manner.* Cell stress & chaperones, 2006. **11**(2): p. 162.

74. VanBogelen, R.A. and F.C. Neidhardt, *Ribosomes as Sensors of Heat and Cold Shock in Escherichia coli.* Proceedings of the National Academy of Sciences, 1990. **87**(15): p. 5589-5593.

75. Bhatti, A., et al., *High temperature induced antibiotic sensitivity changes in Pseudomonas aeruginosa.* Microbios, 1999. **97**(387): p. 103-115.

76. Wang, N., K. Yamanaka, and M. Inouye, *CspI, the Ninth Member of the CspA Family ofEscherichia coli, Is Induced upon Cold Shock.* Journal of bacteriology, 1999. **181**(5): p. 1603-1609.

77. Chadwick, L.E. and H. Rahn, *Temperature Dependence of Rattling Frequency in the Rattlesnake, Crotalus v. viridis.* Science, 1954. **119**(3092): p. 442-443.

78. Ali, R.M., *The influence of suspension density and temperature on the filtration rate of Hiatella arctica.* Marine biology, 1970. **6**(4): p. 291-302.

79. Bennett, A.F., *The thermal dependence of lizard behaviour.* Animal behaviour, 1980. **28**(3): p. 752-762.

80. Lynch, M. and W. Gabriel, *Environmental tolerance.* The American Naturalist, 1987. **129**(2): p. 283-303.

81. Huey, R.B. and J.G. Kingsolver, *Evolution of thermal sensitivity of ectotherm performance.* Trends in Ecology & Evolution, 1989. **4**(5): p. 131-135.

82. Savage, V.M., et al., *Effects of body size and temperature on population growth.* The American Naturalist, 2004. **163**(3): p. 429-441.

83. Ohlberger, J., et al., *Temperature-related physiological adaptations promote ecological divergence in a sympatric species pair of temperate freshwater fish, Coregonus spp.* Functional Ecology, 2008. **22**: p. 501-508.

84. Somero, G., *The physiology of climate change: how potentials for acclimatization and genetic adaptation will determine 'winners' and 'losers'.* Journal of Experimental Biology, 2010. **213**(6): p. 912-920.

85. Fenberg, P.B., et al., *Exploring the universal ecological responses toclimate change in a univoltine butterfly.* Journal of animal ecology, 2016. **85**(3): p. 739-748.

86. Beaugrand, G., et al., *Reorganization of North Atlantic marine copepod biodiversity and climate.* Science, 2002. **296**(5573): p. 1692-1694.

87. Angilletta, M.J., et al., *Coadaptation: a unifying principle in evolutionary thermal biology.* Physiol Biochem Zool, 2006. **79**(2): p. 282-294.

88. Parmesan, C., *Ecological and evolutionary responses to recent climate change.* Annual review of ecology, evolution, and systematics, 2006. **37**: p. 637-669.

89. Angilletta, M.J., *Thermal adaptation: a theoretical and empirical synthesis*. 2009, Oxford Scholarship Press.

90. Buckley, L.B. and R.B. Huey, *How Extreme Temperatures Impact Organisms and the Evolution of their Thermal Tolerance.* Integr Comp Biol, 2016. **56**(1): p. 98-109.

91. Padfield, D., et al., *Rapid evolution of metabolic traits explains thermal adaptation in phytoplankton.* Ecology Letters, 2016. **19**(2): p. 133-142.

92. Russell, N.J. and S.P. Sandercock, *The regulation of bacterial membrane fluidity by modification of phospholipid fatty acyl chain length.*, in *Membrane Fluidity* 1980, Humana Press.

93. Mansilla, M.C., et al., *Control of Membrane Lipid Fluidity by Molecular Thermosensors.* Journal of bacteriology, 2004. **186**(20): p. 6681-6688.

94. Maeda, K., et al., *Effect of temperature on motility and chemotaxis of Escherichia coli.* Journal of bacteriology, 1976. **127**(3): p. 1039-1046.

95. Paulick, A., et al., *Mechanism of bidirectional thermotaxis in Escherichia coli.* elife, 2017. **6:e26607**.

96. Liao, H., T. Mackenzie, and R. Hageman, *Isolation of a thermo- stable enzyme variant by cloning and selection in a thermophile.* Proceedings of the National Academy of Sciences, 1986. **84**: p. 576-580.

97. Takami, H., et al., *Thermoadaptation trait revealed by the genome sequence of thermophilic Geobacillus kaustophilus.* Nucleic Acids Res, 2004. **32**(21): p. 6292-303.

98. Chen, Z., et al., *Mechanisms of thermal adaptation and evolutionary potential of conspecific populations to changing environments.* Mol Ecol, 2018. **27**(3): p. 659-674.

99. Mayer, M.P., and Bukau, B., *Hsp70 chaperones: cellular functions and molecular mechanism.* Cell. Mol. Life Sci, 2005. **62**: p. 670-684.

100. Gaitan-Espitia, J.D., et al., *Variation in thermal sensitivity and thermal tolerances in an invasive species across a climatic gradient: lessons from the land snail Cornu aspersum.* PLoS One, 2013. **8**(8): p. e70662.

101. Dell, A.I., S. Pawar, and V.M. Savage, *Systematic variation in the temperature dependence of physiological and ecological traits.* Proceedings of the National Academy of Sciences, 2011. **108**(26): p. 10591-10596.

102. Reed, T.E., D.E. Schindler, and R.S. Waples, *Interacting effects of phenotypic plasticity and evolution on population persistence in a changing climate.* Conserv Biol, 2011. **25**(1): p. 56-63.

103. Thomas, M.K., et al., *Temperature-nutrient interactions exacerbate sensitivity to warming in phytoplankton.* Global change biology, 2017. **23**: p. 3269-3280.

104. Deutsch, C.A., et al., *Impacts of climate warming on terrestrial ectotherms across latitude.* Proceedings of the National Academy of Sciences, 2008. **105**(18): p. 6668-6672.

105. Martin, T.L. and R.B. Huey, *Why "suboptimal" is optimal: Jensen's inequality and ectotherm thermal preferences.* Am Nat, 2008. **171**(3): p. E102-18.

106. Amarasekare, P. and V. Savage, *A framework for elucidating the temperature dependence of fitness.* Am Nat, 2012. **179**(2): p. 178-91.

107. Cruz-Loya, M., et al., *Stressor interaction networks suggest antibiotic resistance coopted from stress responses to temperature.* ISME, 2018. **In press**.

108. Briere, J.-F., et al., *A Novel Rate Model of Temperature-Dependent Development for Arthropods.* Environmental Entomology, 1990. **28**(1): p. 22-29.

109. Salvatier, J., T.V. Wiecki, and C. Fonnesbeck, *Probabilistic programming in Python using PyMC3.* PeerJ Preprints, 2016.

110. Kucukelbir, A., et al., *Automatic differentiation variational inference.* The Journal of Machine Learning Research, 2017. **18**(1): p. 430-474.

111. Cruz-Loya, M., et al., *Stressor interaction networks suggest antibiotic resistance co-opted from stress responses to temperature.* ISME J, 2019. **13**(1): p. 12-23.

112. Vabulas, R.M., et al., *Protein folding in the cytoplasm and the heat shock response.* Cold Spring Harb Perspect Biol, 2010. **2**(12): p. a004390.

113. VanBogelen, R.A. and F.C. Neidhardt, *Ribosomes as sensors of heat and cold shock in Escherichia coli.* Proc Natl Acad Sci U S A, 1990. **87**(15): p. 5589-93.

114. Hofmann, S., et al., *Translation suppression promotes stress granule formation and cell survival in response to cold shock.* Mol Biol Cell, 2012. **23**(19): p. 3786-800.

115. Sinha, A.K., et al., *Replication arrest is a major threat to growth at low temperature in Antarctic Pseudomonas syringae Lz4W.* Mol Microbiol, 2013. **89**(4): p. 792-810.

116. Lewis, K., *Persister cells, dormancy and infectious disease.* Nat Rev Microbiol, 2007. **5**(1): p. 48-56.

117. Mitchell, S.M., et al., *pH and temperature effects on the hydrolysis of three beta-lactam antibiotics: ampicillin, cefalotin and cefoxitin.* Sci Total Environ, 2014. **466-467**: p. 547-55.

118. Loughman, K., et al., *Temperature-Dependent Gentamicin Resistance of Francisella tularensis is Mediated by Uptake Modulation.* Front Microbiol, 2016. **7**: p. 37.

119. Segrè, D., et al., *Modular epistasis in yeast metabolism.* Nat Genet, 2005. **37**(1): p. 77-83.

120. Greulich, P., et al., *Growth-dependent bacterial susceptibility to ribosome-targeting antibiotics.* Molecular Systems Biology, 2015. **11**(3): p. 796-796.

121. Mingeot-Leclercq, M.P., Y. Glupczynski, and P.M. Tulkens, *Aminoglycosides: activity and resistance.* Antimicrob Agents Chemother, 1999. **43**(4): p. 727-37.

122. Brennan, G. and S. Collins, *Growth responses of a green alga to multiple environmental drivers.* Nature Climate Change, 2015. **5**(9): p. 892-897.

123. Huey, R.B. and J.G. Kingsolver, *Variation in universal temperature dependence of biological rates.* Proceedings of the National Academy of Sciences, 2011. **108**(26): p. 10377-8.

124. Rohr, J.R., et al., *The complex drivers of thermal acclimation and breadth in ectotherms.* Ecol Lett, 2018. **21**(9): p. 1425-1439.

125. MacFadden, D.R., et al., *Antibiotic resistance increases with local temperature.* Nature Climate Change, 2018. **8**(6): p. 510-514.

126. Gautam, R., et al., *Modeling the effect of seasonal variation in ambient temperature on the transmission dynamics of a pathogen with a free-living stage: example of Escherichia coli O157:H7 in a dairy herd.* Prev Vet Med, 2011. **102**(1): p. 10-21.

127. Mermel, L.A., J.T. Machan, and S. Parenteau, *Seasonality of MRSA infections.* PLoS One, 2011. **6**(3): p. e17925.

128. Lorenz, M.G. and W. Wackernagel, *Bacterial gene transfer by natural genetic transformation in the environment.* Microbiol Rev, 1994. **58**(3): p. 563-602.

129. Walsh, T.R., et al., *Dissemination of NDM-1 positive bacteria in the New Delhi environment and its implications for human health: an environmental point prevalence study.* The Lancet Infectious Diseases, 2011. **11**(5): p. 355-362.

130. Molnar, P.K., et al., *Metabolic approaches to understanding climate change impacts on seasonal host-macroparasite dynamics.* Ecol Lett, 2013. **16**(1): p. 9-21.

131. Harvell, C.D., et al., *Climate Warming and Disease Risks for Terrestrial and Marine Biota.* Science, 2002. **296**(5576): p. 2158-2162.

132. Manchado, E., et al., *A combinatorial strategy for treating KRAS-mutant lung cancer.* Nature, 2016. **534**(7609): p. 647-651.

133. Komarova, N.L. and C.R. Boland, *Calculated treatment.* Nature, 2013. **499**: p. 291.

134. McManus, M., et al., *Early Combination Antiretroviral Therapy Limits Exposure to HIV-1 Replication and Cell-Associated HIV-1 DNA Levels in Infants.* PloS one, 2016. **11**(4): p. e0154391-e0154391.

135. Autran, B., et al., *Positive Effects of Combined Antiretroviral Therapy on CD4+T Cell Homeostasis and Function in Advanced HIV Disease.* Science, 1997. **277**(5322): p. 112.

136. Taddei, S., *Combination Therapy in Hypertension: What Are the Best Options According to Clinical Pharmacology Principles and Controlled Clinical Trial Evidence?* American Journal of Cardiovascular Drugs, 2015. **15**(3): p. 185-194.

137. Kullar, R., et al., *When sepsis persists: a review of MRSA bacteraemia salvage therapy.* Journal of Antimicrobial Chemotherapy, 2015. **71**(3): p. 576-586.

138. Liu, C., et al., *Clinical Practice Guidelines by the Infectious Diseases Society of America for the Treatment of Methicillin-Resistant Staphylococcus aureus Infections in Adults and Children.* Clinical Infectious Diseases, 2011. **52**(3): p. e18-e55.

139. Cokol, M., et al., *Systematic exploration of synergistic drug pairs.* Molecular Systems Biology, 2011. **7**(1): p. 544.

140. Fuentes-Hernandez, A., et al., *Using a Sequential Regimen to Eliminate Bacteria at Sublethal Antibiotic Dosages.* PLOS Biology, 2015. **13**(4): p. e1002104.

141. Hegreness, M., et al., *Accelerated evolution of resistance in multidrug environments.* Proc Natl Acad Sci U S A, 2008. **105**(37): p. 13977-81.

142. Wood, K.B., et al., *Uncovering scaling laws to infer multidrug response of resistant microbes and cancer cells.* Cell Rep, 2014. **6**(6): p. 1073-1084.

143. Ocampo, P.S., et al., *Antagonism between bacteriostatic and bactericidal antibiotics is prevalent.* Antimicrob Agents Chemother, 2014. **58**(8): p. 4573-82.

144. Yeh, P.J., et al., *Drug interactions and the evolution of antibiotic resistance.* Nat Rev Microbiol, 2009. **7**(6): p. 460-6.

145. Singh, N. and P.J. Yeh, *Suppressive drug combinations and their potential to combat antibiotic resistance.* J Antibiot (Tokyo), 2017. **70**(11): p. 1033-1042.

146. Park, M., M. Nassar, and H. Vikalo, *Bayesian Active Learning for Drug Combinations.* IEEE Transactions on Biomedical Engineering, 2013. **60**(11): p. 3248-3255.

147. Wang, H., et al., *Mechanism-Independent Optimization of Combinatorial Nanodiamond and Unmodified Drug Delivery Using a Phenotypically Driven Platform Technology.* ACS Nano, 2015. **9**(3): p. 3332-3344.

148. Zimmer, A., et al., *Prediction of multidimensional drug dose responses based on measurements of drug pairs.* Proc Natl Acad Sci U S A, 2016. **113**(37): p. 10442-7.

149. White, D.B., et al., *Nonlinear Response Surface and Mixture Experiment Methodologies Applied to the Study of Synergism.* Biometrical Journal, 2004. **46**(1): p. 56-71.

150. Meletiadis, J., et al., *Concentration-dependent synergy and antagonism within a triple antifungal drug combination against Aspergillus species: analysis by a new response surface model.* Antimicrob Agents Chemother, 2007. **51**(6): p. 2053-64.

151. O'Shaughnessy, E.M., et al., *Antifungal interactions within the triple combination of amphotericin B, caspofungin and voriconazole against Aspergillus species.* J Antimicrob Chemother, 2006. **58**(6): p. 1168-76.

152. Santos, J.R., et al., *Dynamic interaction between fluconazole and amphotericin B against Cryptococcus gattii.* Antimicrob Agents Chemother, 2012. **56**(5): p. 2553-8.

153. Weiss, A., et al., *Rapid optimization of drug combinations for the optimal angiostatic treatment of cancer.* Angiogenesis, 2015. **18**(3): p. 233-44.

154. Tekin, E., et al., *Enhanced identification of synergistic and antagonistic emergent interactions among three or more drugs.* J R Soc Interface, 2016. **13**(119).

155. Aguilar-Rodríguez, J., J.L. Payne, and A. Wagner, *A thousand empirical adaptive landscapes and their navigability.* Nature ecology & evolution, 2017. **1**(2): p. 0045.

156. Flynn, K.M., et al., *The environment affects epistatic interactions to alter the topology of an empirical fitness landscape.* PLoS Genet, 2013. **9**(4): p. e1003426.

157. Khan, A.I., et al., *Negative epistasis between beneficial mutations in an evolving bacterial population.* Science, 2011. **332**(6034): p. 1193-1196.

158. Fontana, W. and P. Schuster, *Shaping space: the possible and the attainable in RNA genotype-phenotype mapping.* J Theor Biol, 1998. **194**(4): p. 491-515.

159. Wagner, G.P. and J. Zhang, *The pleiotropic structure of the genotype-phenotype map: the evolvability of complex organisms.* Nat Rev Genet, 2011. **12**(3): p. 204-13.

160. Szendro, I.G., et al., *Predictability of evolution depends nonmonotonically on population size.* Proc Natl Acad Sci U S A, 2013. **110**(2): p. 571-6.

161. Østman, B., A. Hintze, and C. Adami, *Critical properties of complex fitness landscapes.* arXiv preprint arXiv:1006.2908, 2010.

162. Bull, J.J., R.H. Heineman, and C.O. Wilke, *The phenotype-fitness map in experimental evolution of phages.* PLoS One, 2011. **6**(11): p. e27796.

163. Braberg, H., et al., *Quantitative analysis of triple-mutant genetic interactions.* Nature protocols, 2014. **9**(8): p. 1867-1881.

164. Kuzmin, E., et al., *Systematic analysis of complex genetic interactions.* Science (New York, N.Y.), 2018. **360**(6386): p. eaao1729.

165. Bleuven, C. and C.R. Landry, *Molecular and cellular bases of adaptation to a changing environment in microorganisms.* Proc Biol Sci, 2016. **283**(1841).

166. Sherlock, G. and D.A. Petrov, *Seeking Goldilocks During Evolution of Drug Resistance.* PLOS Biology, 2017. **15**(2): p. e2001872.

167. Mira, P.M., et al., *Rational design of antibiotic treatment plans: a treatment strategy for managing evolution and reversing resistance.* PLoS One, 2015. **10**(5): p. e0122283.

168. Wicha, S.G., et al., *A general pharmacodynamic interaction model identifies perpetrators and victims in drug interactions.* Nature communications, 2017. **8**(1): p. 2129-2129.

169. Bell, G. and A. Gonzalez, *Adaptation and evolutionary rescue in metapopulations experiencing environmental deterioration.* Science, 2011. **332**(6035): p. 1327-30.

170. Ogbunugafor, C.B., et al., *Adaptive landscape by environment interactions dictate evolutionary dynamics in models of drug resistance.* PLoS computational biology, 2016. **12**(1): p. e1004710.

171. Carja, O., U. Liberman, and M.W. Feldman, *Evolution in changing environments: modifiers of mutation, recombination, and migration.* Proc Natl Acad Sci U S A, 2014. **111**(50): p. 17935-40.

172. Cokol, M., et al., *Efficient measurement and factorization of high-order drug interactions in Mycobacterium tuberculosis.* Sci Adv, 2017. **3**(10): p. e1701881.

173. Loewe, S., *The problem of synergism and antagonism of combined drugs.* Arzneimittelforschung, 1953. **3**(6): p. 285-90.

174. Doern, C.D., *When does 2 plus 2 equal 5? A review of antimicrobial synergy testing.* Journal of clinical microbiology, 2014. **52**(12): p. 4124-4128.

175. Rothschild, D., et al., *Linear Superposition and Prediction of Bacterial Promoter Activity Dynamics in Complex Conditions.* PLOS Computational Biology, 2014. **10**(5): p. e1003602.

176. Wood, K., et al., *Mechanism-independent method for predicting response to multidrug combinations in bacteria.* Proceedings of the National Academy of Sciences, 2012. **109**(30): p. 12254.

177. Al-Lazikani, B., U. Banerji, and P. Workman, *Combinatorial drug therapy for cancer in the post-genomic era.* Nat Biotechnol, 2012. **30**(7): p. 679-92.

178. Moore, R.D. and R.E. Chaisson, *Natural history of HIV infection in the_era of combination antiretroviral therapy.* Aids, 1999. **13**(14): p. 1933-1942.

179. Wright, S., *The roles of mutation, inbreeding, crossbreeding, and selection in evolution.* Proc. 6th Int. Congress Genet., 1932. **1**: p. 356-366.

180. de Visser, J.A.G.M. and J. Krug, *Empirical fitness landscapes and the predictability of evolution.* Nat Rev Genet, 2014. **15**(7): p. 480-90.

181. de Visser, J.A.G.M., et al., *The utility of fitness landscapes and big data for predicting evolution.* Heredity, 2018. **121**(5): p. 401-405.

182. Fragata, I., et al., *The fitness landscape of the codon space across environments.* Heredity, 2018. **121**(5): p. 422-437.

183. Li, C. and J. Zhang, *Multi-environment fitness landscapes of a tRNA gene.* Nature Ecology & Evolution, 2018. **2**(6): p. 1025-1032.

184. Gorter, F.A., et al., *Local fitness landscapes predict yeast evolutionary dynamics in directionally changing environments.* Genetics, 2018. **208**(1): p. 307-322.

185. Ferretti, L., et al., *Evolutionary constraints in fitness landscapes.* Heredity, 2018. **121**(5): p. 466-481.

186. Fragata, I., et al., *Evolution in the light of fitness landscape theory.* Trends in Ecology & Evolution, 2019. **34**(1): p. 69-82.

187. Kondrashov, D.A. and F.A. Kondrashov, *Topological features of rugged fitness landscapes in sequence space.* Trends in Genetics, 2015. **31**(1): p. 24-33.

188. Crona, K., D. Greene, and M. Barlow, *The peaks and geometry of fitness landscapes.* Journal of Theoretical Biology, 2013. **317**: p. 1-10.

189. Van Cleve, J. and D.B. Weissman, *Measuring ruggedness in fitness landscapes.* Proceedings of the National Academy of Sciences, 2015. **112**(24): p. 7345-7346.

190. Phillips, P.C., *Epistasis - the essential role of gene interactions in the structure and evolution of genetic systems.* Nat Rev Genet, 2008. **9**(11): p. 855-67.

191. Tong, A.H.Y., et al., *Global mapping of the yeast genetic interaction network.* science, 2004. **303**(5659): p. 808-813.

192. Blount, Z.D., C.Z. Borland, and R.E. Lenski, *Historical contingency and the evolution of a key innovation in an experimental population of Escherichia coli.* Proceedings of the National Academy of Sciences, 2008. **105**(23): p. 7899.

193. Salverda, M.L.M., et al., *Initial mutations direct alternative pathways of protein evolution.* PLOS Genetics, 2011. **7**(3): p. e1001321.

194. Woods, R.J., et al., *Second-order selection for evolvability in a large Escherichia coli population.* Science, 2011. **331**(6023): p. 1433.

195. Andersson, D.I. and D. Hughes, *Antibiotic resistance and its cost: is it possible to reverse resistance?* Nature Reviews Microbiology, 2010. **8**: p. 260.

196. Böttger, E.C., et al., *Fitness of antibiotic-resistant microorganisms and compensatory mutations.* Nature Medicine, 1998. **4**: p. 1343.

197. Bonhoeffer, S., et al., *Evidence for positive epistasis in HIV-1.* Science, 2004. **306**(5701): p. 1547.

198. Rojas Echenique, J.I., et al., *Modular epistasis and the compensatory evolution of gene deletion mutants.* PLOS Genetics, 2019. **15**(2): p. e1007958.

199. Sailer, Z.R. and M.J. Harms, *High-order epistasis shapes evolutionary trajectories.* PLOS Computational Biology, 2017. **13**(5): p. e1005541.

200. Szamecz, B., et al., *The genomic landscape of compensatory evolution.* PLOS Biology, 2014. **12**(8): p. e1001935.

201. Steinberg, B. and M. Ostermeier, *Environmental changes bridge evolutionary valleys.* Science advances, 2016. **2**(1): p. e1500921-e1500921.

202. Taute, K.M., et al., *Evolutionary constraints in variable environments from proteins to networks.* Trends in Genetics, 2014. **30**(5): p. 192-198.

203. Mira, P.M., et al., *Adaptive landscapes of resistance genes change as antibiotic concentrations change.* Molecular Biology and Evolution, 2015. **32**(10): p. 2707-2715.

204. Bajić, D., et al., *On the deformability of an empirical fitness landscape by microbial evolution.* Proceedings of the National Academy of Sciences, 2018. **115**(44): p. 11286.

205. De Jong, M.G. and K.B. Wood, *Tuning spatial profiles of selection pressure to modulate the evolution of drug resistance.* Phys Rev Lett, 2018. **120**(23): p. 238102.

206. Fu, F., M.A. Nowak, and S. Bonhoeffer, *Spatial heterogeneity in drug concentrations can facilitate the emergence of resistance to cancer therapy.* PLoS Comput Biol, 2015. **11**(3): p. e1004142.

207. Chao, L., B.R. Levin, and F.M. Stewart, *A Complex Community in a Simple Habitat: An Experimental Study with Bacteria and Phage.* Ecology, 1977. **58**(2): p. 369-378.

208. Lenski, R.E. and B.R. Levin, *Constraints on the Coevolution of Bacteria and Virulent Phage: A Model, Some Experiments, and Predictions for Natural Communities.* The American Naturalist, 1985. **125**(4): p. 585-602.

209. Lenski, R.E., *Experimental Studies of Pleiotropy and Epistasis in Escherichia coli. I. Variation in Competitive Fitness Among Mutants Resistant to Virus T4.* Evolution, 1988. **42**(3): p. 425-432.

210. Østman, B., A. Hintze, and C. Adami, *Impact of epistasis and pleiotropy on evolutionary adaptation.* Proc Biol Sci., 2012. **279**(1727): p. 247-256.

211. Szendro, I.G., et al., *Quantitative analyses of empirical fitness landscapes.* Journal of Statistical Mechanics: Theory and Experiment, 2013. **2013**(01): p. P01005.

212. Matsui, T. and I.M. Ehrenreich, *Gene-Environment Interactions in Stress Response Contribute Additively to a Genotype-Environment Interaction.* PLOS Genetics, 2016. **12**(7): p. e1006158.

213. Aguilar-Rodríguez, J., J.L. Payne, and A. Wagner, *A thousand empirical adaptive landscapes and their navigability.* Nature Ecology & Evolution, 2017. **1**: p. 0045.

214. Avery, L. and S. Wasserman, *Ordering gene function: the interpretation of epistasis in regulatory hierarchies.* Trends in Genetics, 1992. **8**(9): p. 312-316.

215. Ma, X., A.M. Tarone, and W. Li, *Mapping Genetically Compensatory Pathways from Synthetic Lethal Interactions in Yeast.* PLOS ONE, 2008. **3**(4): p. e1922.

216. Weinreich, D.M., et al., *The Influence of Higher-Order Epistasis on Biological Fitness Landscape Topography.* Journal of Statistical Physics, 2018. **172**(1): p. 208-225.

217. Palmer, A.C., et al., *Delayed commitment to evolutionary fate in antibiotic resistance fitness landscapes.* Nature communications, 2015. **6**: p. 7385-7385.

218. Tekin, E., et al., *Prevalence and patterns of higher-order drug interactions in Escherichia coli.* npj Systems Biology and Applications, 2018. **4**(1): p. 31.

219. Chou, H.-H., et al., *Diminishing Returns Epistasis Among Beneficial Mutations Decelerates Adaptation.* Science, 2011. **332**(6034): p. 1190.

220. Tse-Dinh, Y.-C. and R.K. Beran, *Multiple promoters for transcription of the Escherichia coli DNA topoisomerase I gene and their regulation by DNA supercoiling.* Journal of Molecular Biology, 1988. **202**(4): p. 735-742.

221. Drlica, K. and X. Zhao, *DNA gyrase, topoisomerase IV, and the 4-quinolones.* Microbiology and Molecular Biology Reviews, 1997. **61**(3): p. 377.

222. Redgrave, L.S., et al., *Fluoroquinolone resistance: mechanisms, impact on bacteria, and role in evolutionary success.* Trends in Microbiology, 2014. **22**(8): p. 438-445.

223. Trindade, S., et al., *Positive epistasis drives the acquisition of multidrug resistance.* PLoS genetics, 2009. **5**(7): p. e1000578-e1000578.

224. Silva, R.F., et al., *Pervasive Sign Epistasis between Conjugative Plasmids and Drug-Resistance Chromosomal Mutations.* PLOS Genetics, 2011. **7**(7): p. e1002181.

225. Sanjuán, R. and S.F. Elena, *Epistasis correlates to genomic complexity.* Proceedings of the National Academy of Sciences, 2006. **103**(39): p. 14402.

226. Maisnier-Patin, S., et al., *Genomic buffering mitigates the effects of deleterious mutations in bacteria.* Nature Genetics, 2005. **37**: p. 1376.

227. Sigler, P.B., et al., *Structure and function in GroEL-mediated protein folding.* Annual Review of Biochemistry, 1998. **67**(1): p. 581-608.

228. Elena, S.F. and J.A.G.M. de Visser, *Environmental stress and the effects of mutation.* Journal of biology, 2003. **2**(2): p. 12-12.

229. Barton, N.H., *Mutation and the evolution of recombination.* Philosophical transactions of the Royal Society of London. Series B, Biological sciences, 2010. **365**(1544): p. 1281-1294.

230. Kondrashov, A.S., *Deleterious mutations as an evolutionary factor: 1. The advantage of recombination.* Genetical Research, 1984. **44**(2): p. 199-217.

231. Kondrashov, A.S., *Selection against harmful mutations in large sexual and asexual populations.* Genetical Research, 1982. **40**(3): p. 325-332.

232. Hartfield, M. and P.D. Keightley, *Current hypotheses for the evolution of sex and recombination.* Integrative Zoology, 2012. **7**(2): p. 192-209.

233. Sanjuán, R. and M.R. Nebot, *A Network Model for the Correlation between Epistasis and Genomic Complexity.* PLOS ONE, 2008. **3**(7): p. e2663.

234. Elena, S.F. and R.E. Lenski, *Test of synergistic interactions among deleterious mutations in bacteria.* Nature, 1997. **390**(6658): p. 395-398.

235. Cycoń, M., A. Mrozik, and Z. Piotrowska-Seget, *Antibiotics in the Soil Environment—Degradation and Their Impact on Microbial Activity and Diversity.* Frontiers in Microbiology, 2019. **10**(338).

236. Nix, D.E., et al., *Antibiotic tissue penetration and its relevance: impact of tissue penetration on infection response.* Antimicrobial agents and chemotherapy, 1991. **35**(10): p. 1953-1959.

237. Habets, M.G.J.L., et al., *The effect of population structure on the adaptive radiation of microbial populations evolving in spatially structured environments.* Ecology Letters, 2006. **9**(9): p. 1041-1048.

238. Ponciano, J.M., et al., *Evolution of Diversity in Spatially Structured Escherichia coli Populations.* Applied and Environmental Microbiology, 2009. **75**(19): p. 6047.

239. Greulich, P., B. Waclaw, and R.J. Allen, *Mutational Pathway Determines Whether Drug Gradients Accelerate Evolution of Drug-Resistant Cells.* Physical Review Letters, 2012. **109**(8): p. 088101.

240. Hermsen, R., J.B. Deris, and T. Hwa, *On the rapidity of antibiotic resistance evolution facilitated by a concentration gradient.* Proceedings of the National Academy of Sciences, 2012. **109**(27): p. 10775.

241. Kepler, T.B. and A.S. Perelson, *Drug concentration heterogeneity facilitates the evolution of drug resistance.* Proceedings of the National Academy of Sciences, 1998. **95**(20): p. 11514.

242. Moreno-Gamez, S., et al., *Imperfect drug penetration leads to spatial monotherapy and rapid evolution of multidrug resistance.* Proceedings of the National Academy of Sciences, 2015. **112**(22): p. E2874.

243. Zhang, Q., et al., *Acceleration of Emergence of Bacterial Antibiotic Resistance in Connected Microenvironments.* Science, 2011. **333**(6050): p. 1764.

244. Baym, M., et al., *Spatiotemporal microbial evolution on antibiotic landscapes.* Science, 2016. **353**(6304): p. 1147-1151.

245. De Jong, M.G. and K.B. Wood, *Tuning Spatial Profiles of Selection Pressure to Modulate the Evolution of Drug Resistance.* Physical review letters, 2018. **120**(23): p. 238102-238102.